Université des Sciences et Technologies de Lille

Laboratoire de Mécanique de Lille (UMR 8107)

Année: 2007-2008 **N° d'ordre:4159**

THESE

Pour obtenir le grade de

Docteur de l'Université des Sciences et Technologies de Lille

Discipline : Génie Civil

Présentée et soutenue publiquement par

Yan ZHANG

le 30 Janvier 2008

Modélisation du comportement élastoplastique d'une pâte cimentaire soumise à la dégradation chimique

JURY

M. Frédéric SKOCZYLAS, Ecole Centrale de Lille	**Président**
M. Dariusz LYDZBA, Professeur, Université de technologie de Wroclaw, Pologne	**Rapporteur**
M. Dashnor HOXHA, Professeur, Université d'Orléans	**Rapporteur**
M. Nicolas BURLION,Professeur, Polytech'Lille-USTL	**Examinateur**
M. Ismaïl YURTDAS, Maître de conférences, Université de Reims	**Examinateur**
M. Jianfu SHAO, Professeur, Polytech'Lille-USTL	**Directeur de Thèse**

A Bin YAO

A mes parents

Remerciements

Je souhaite tout d'abord remercier Jian-Fu SHAO, mon directeur de thèse, pour m'avoir fait confiance dans ce travail, pour ses conseils, pour le temps qu'il m'a consacré et pour la simplicité de son contact.

Monsieur Frédéric SKOZYLAS m'a fait l'honneur de présider mon jury. Qu'il trouve ici l'expression de toute ma gratitude. Messieurs Dariusz LYDZBA et Dashnor HOXHA ont accepté la tache ardue d'être rapporteurs de ce travail. Je les en remercie sincèrement. Je remercie tout autant Messieurs Nicolas BURLION et Ismaïl YURTDAS pour avoir pris part au jury en tant qu'examinateurs.

Mes remerciements s'adressent à Monsieur Michel STANISLAS, directeur du Laboratoire Mécanique de Lille, qui m'a accueilli au sein du laboratoire.

J'adresse également tous mes remerciements à l'ensemble du personnel de l'Ecole Polytechnique Universitaire de Lille et du Laboratoire de Mécanique de Lille pour son soutien moral et matériel qui m'a permis de mener à bien ce travail.

Enfin, j'exprime toute ma gratitude à mes collègues et amis pour leurs encouragements et leurs attentions lors de la réalisation de ce travail.

Table of Contents

Résumé

Dans cette thèse, nous présentons une modélisation numérique du comportement élastoplastique d'une pâte de ciment soumise à la dégradation chimique.

Une courte synthèse bibliographique est d'abord présentée sur la composition minéralogique, la chimie, le comportement mécanique de base, les mécanismes de dégradation chimique et le couplage chimie-mécanique des matériaux cimentaires en général et de la pâte de ciment en particulier.

En se basant sur cette synthèse et des données expérimentales, un modèle de comportement élastoplastique est ensuite formulé dans le chapitre 2, pour des pâtes de ciment soumises essentiellement à des contraintes de compression. Deux mécanismes de déformations plastiques sont identifiés, liés respectivement au cisaillement déviatorique et à la compaction des pores. En définissant la dégradation chimique par une variable d'endommagement chimique, les propriétés élastiques et plastiques sont affectées par cet endommagement. Les essais mécaniques effectués sur des échantillons sains et chimiquement dégradés sont simulés par le modèle proposé.

La détermination de la cinétique de l'endommagement chimique est abordée dans le chapitre 3. En se basant sur un modèle phénoménologique de la lixiviation chimique, la cinétique de l'endommagement chimique est contrôlée par le processus de diffusion des ions calcium dans la solution interstitielle. La concentration en calcium de la solution interstitielle est alors considérée comme la variable d'état chimique. La variation de la teneur en calcium dans la matrice solide et celle de la porosité sont reliées à la concentration en calcium en fluide par la courbe d'équilibre thermodynamique. La méthode des éléments finis est utilisée par la résolution numérique de l'équation de diffusion généralisée.

Le modèle proposé est enfin étendu pour inclure l'endommagement mécanique par microfissuration afin de décrire le comportement fragile des matériaux cimentaires. Un exemple d'application du modèle à une structure soumise à la dégradation chimique est présenté.

Mot clés :

Dégradation chimique, endommagement mécanique, matériaux cimentaire, plasticité, lixiviation de calcaire, couplage chemo-mécanique

Abstract

This thesis presents elastoplastic modelling of cement-based materials coupled with chemical degradation and mechanical damage. The emphasis is put on cement paste subjected to compressive stresses.

A short literature review is first presented on the mineralogical composition, chemical degradation mechanisms, basic mechanical behaviour and chemical-mechanical coupling.

Based on this analyses and a series of experimental data obtained from uncoupled and coupled tests, an elastoplastic constitutive model coupled with chemical damage is first formulated. Two plastic mechanisms are taken into account; respectively related to deviatoric shearing and pore collapse. The chemical damage is identified as relative variation of porosity. Elastic and plastic properties are affected by chemical damage. Numerical simulations are compared with experimental data and good agreements have been obtained.

The evolution of the chemical damage has been described by the generalized diffusion equation which is based on the mass balance equation and a phenomenological chemistry model. We have used finite element method to solve the generalized diffusion equation. Coupled chemical-mechanical tests have been simulated by the proposed model and we have also obtained satisfactory concordance.

An extension of the model is finally proposed by including mechanical damage due to microcracks in order to describe brittle responses of material under tensile stresses and low confining pressures. An example of application to structural analysis with chemical degradation is presented. It has been shown that the proposed model describes correctly the main features of the mechanical behaviours of cement-based materials at different stress conditions with chemical degradation.

Key words:

Chemical degradation, mechanical damage, cement paste, plasticity, calcium leaching, chemo-mechanical coupling

General introduction

Cement-based materials are largely used in different engineering constructions. Stability analysis of these structures requires the understanding and modelling of mechanical behaviours under complex multi-axial loading conditions. Extensive experimental investigations and various constitutive models have been developed on cement-based materials. Their basic mechanical behaviour can be characterized by coupled plastic deformation and damage, depending on applied stresses. Both micromechanical and phenomenological approaches are available to describe mechanical responses of cement-based materials and structures.

However, in many situations, cement-based materials are subjected not only to mechanical loading but also to chemical degradation when they are in contact with aggressive environment such as rain, water, acid fluids. More recently, in the framework of sustainable development, it is of great concerns of storage and sequestration of toxic residual fluids and gas such as CO_2 and H_2S. It is clear that the durability analysis of structures requires the identification and modelling of long term behaviour of cement-based materials undergoing chemical attacks. For this purpose, a lot of research efforts have been contributed to experimental investigations and numerical modelling of chemical degradation. The main topics cover the identification of chemical degradation mechanism and its kinetics, and the determination of chemical degradation effects on short and long term mechanical behaviour of cement-based materials.

It is now known that the chemical degradation of cement-based materials is essentially controlled by two processes, the dissolution of different hydrate phases and diffusion of dissolved species inside interstitial fluid. The chemical dissolution mainly concerns Portland and $C-S-H$ phases, which provide macroscopic mechanical cohesion and strength of materials. The kinetics of chemical degradation is influenced by microstructure (compositions) of materials, chemical nature and temperature of aggressive solution, as well as fluid pressure gradient. On the effects on mechanical behaviour, chemical degradation induces an increase of material porosity, and affects elastic and plastic properties, and transport properties (diffusivity, permeability). Different chemistry models have been proposed to describe the process of chemical degradation. Based on these models, coupled chemo-mechanical models have been developed to describe mechanical responses of chemically degraded cement-based materials. However, so far, most of models focused on brittle behaviour of concrete structures exhibiting mechanical damage and chemical degradation. In one class of applications, such as the sequestration of residual gas in geological reservoirs, cement paste is used as isolation barrier for confinement capacity of reservoir. Therefore, it is useful for study chemical degradation effects on mechanical behaviour of the cement paste. Due to its high porosity, the mechanical behaviour of cement paste is mainly dominated by plastic deformation under compressive stresses with significant volumetric compaction. There is a strong dependency on confining pressure. Brittle responses with material softening are observed only under very low confining pressures and tensile stresses.

The main objective of this work is to develop a coupled chemo-mechanical model for porous cement-paste under compression-dominated conditions.

In the first chapter, a short summary will be presented on the composition and microstructure of cement-based materials, together with basic mechanisms of chemical degradation and consequences of mechanical behaviours of these materials. The emphasis will be put on the experimental background for the modelling of chemical degradation.

The second chapter will be devoted to constitutive modelling of mechanical behaviour of cement paste. Based on experimental data on a typical cement paste, a new elastoplastic model will be proposed. Two complementary plastic mechanisms will be taken into account: plastic shearing under deviatoric stress and volumetric compaction due to pore collapse. Comparing experimental data obtained respectively on sound and chemical degraded materials, we will identify the effects of chemical degradation on the elastic and plastic properties of material. An internal variable is introduced to represent chemical degradation state. In this stage, mechanical damage due to microcracks is first neglected by putting the emphasis to ductile responses of cement paste.

In the third chapter, the evolution of chemical damage will be addressed. Based on a simplified phenomenological chemistry model, the calcium concentration in interstitial solution is used as a state variable to characterize chemical leaching process. The kinetics of chemical leaching is controlled by the diffusion of dissolved calcium ions in interstitial solution governed by generalized Fick's law. Based on the thermodynamic equilibrium curve, we will determine variation of porosity, diffusivity and chemical damage.

In the last chapter, the proposed model will be extended to modelling of brittle responses of cement paste under tensile loading or compressive loading with low confining pressure. We will introduce two damage variables, mechanical damage by microcracks and chemical damage due to dissolution to characterize the degradation of cement paste. A simplified criterion will be proposed to describe mechanical damage. The developed model will be used to predict materials responses in laboratory tests. An example of application to chemo-mechanical analysis of structures will also be presented.

Chapter 1: Summary of chemical-mechanical coupling in cement-based materials

1.1 Introduction

During the last decades, many experimental investigations and analytical and numerical studies have been devoted to durability analysis of cement-based materials. The cement-based material, under attack of environmental aggressive conditions (rain, sea water, drying and wetting, frost and thaw, acid fluids), undergo modification of microstructure and degradation of mechanical and hydraulic properties. Modeling of long term durability of these materials is primordial in many engineering applications. In this chapter, we propose to give a short bibliographic summary of previous works on the chemical-mechanical coupling in cement-based materials, with an emphasis on cement paste.

1.2 Composition and microstructure of cement paste

The cement paste which forms the binding matrix for all cementitious materials, is the resulting product of the chemical reaction between cement and water, a reaction commonly referred to as hydration. In an Ordinary Portland Cement (OPC), four components are regarded as the major constituents, these are: tricalcium silicates, C_3S, dicalcium silicates, C_2S, tricalcium aluminates, C_3A, and tetracalcium aluminum ferrites, C_4AF. The hydration of Portland cement is composed of the hydration of silicates and aluminates. They form the most important part of the microstructure of a cement paste.

The hydration of silicates, C_3S and C_2S produces the same products, named Calcium-Silicate-Hydrates (C-S-H) and Calcium Hydroxide (CH). On the other hand, the hydration of the tricalcium aluminates, C_3A leads to formation of AFm phases.

Finally, the hydration of tetracalcium aluminum ferrites C_4AF is very similar to the hydration of C_3A except for the slower kinetics.

From the chemical reactions that occur during hydration, it is readily understood that the resulting solid, the hardened cement paste, is a multiphase composite material. It consists of the hydration products of the different cement phases and residues of unhydrated cement particles, in addition to water filling the pores. Table 1-1 shows a typical mineralogical composition together with their relative volumetric proportions found in Portland cements.

Table 1-1: Typical mineralogical composition in Portland cements (Neville, 1995)

Mineralogical Phase	Volume %	Crystallinity	Morphology	Dimensions
CSH	50-70	Very Poor	Unresolved	10 – 100 nm
CH	15-20	Very Good	Solid Hexagonal	10 - 100 um
Ettringite	1-5	Fair-Good	Solid Slender needles	10 x 0.5 um
AFm	1-5	Good	Solid Thin hexagonal plates	1 x 1 x 0.1 um

From this table, we can see the complex heterogeneous nature of cement paste. The reaction products manifest themselves in a range of length scales from the nanometer scale to the millimeter scale. In mortar and concrete, sands and aggregates are further included in the mix system. The scale of heterogeneity increases up to the macroscopic decimeter scale. In order to the comprehensively address the multiscale properties of cementitious materials, tentative investigations have been recently performed in order to determine mechanical properties of cement-based material at different length scale (Heukamp 2003). For instance, a three level microstructure for cement based composite materials was introduced by Constantinides and Ulm and is presented in Table 1-2 (Constantinides, 2006). Based on the characterization of constituents at each level, there is a tentative to find macroscopic behavior using homogenization techniques. However, this is still a very open issue, which is beyond the scope of the work.

Table 1-2: Intrinsic properties of cement paste and mortar constituents (Constantinides, 2006)

Level	Composite	Density kg/m^3	Elastic modulus GPa
I	C-S-Ha	1910	21.7
	C-S-Hb	2100	29.4
II	CH	2240	35-40
	Ettringite	1750	130-150
	Calcium Aluninate	2000	140-160
III	Aggregate Sandstone	2650	60-80

1.3 Chemistry of cement paste

The cement paste is a porous medium saturated by an interstitial solution essentially composed of alkaline ions C_a^{++}, OH^- and characterized by a basic pH generally higher than 12.5, and air.

In natural state, there is equilibrium between the hydrates of cement paste and interstitial ions. This equilibrium can be characterized by an experimental curve giving the relationship between the $\mathrm{C_aO/SiO_2}$ ratio in solid matrix and calcium concentration in interstitial solution C_a^{++}, as shown in Fig. 1-1. The ratio evolves with the composition of interstitial solution in contact with the solid.

We can see that when the concentration C_a^{++} decreases, there is a rapid diminution of the ratio $\mathrm{C_aO/SiO_2}$ (from 2.5 to 1.5) associated with the dissolution of Portland $\mathrm{C_a(OH)_2}$. Then the ratio $\mathrm{C_aO/SiO_2}$ decreases more slowly until reaching a value close to 1. This second phase corresponds to the dissolution of C-S-H phases. Finally, for a concentration of C_a^{++} from 2 to 1 mmol/l, the ratio C_aO/SiO_2 varies from 1 to 0.3 leading to complete dissolution calcium in solid phase. The evolution of calcium concentration C_a^{++} in interstitial solution allows the characterization of chemical state of cement paste.

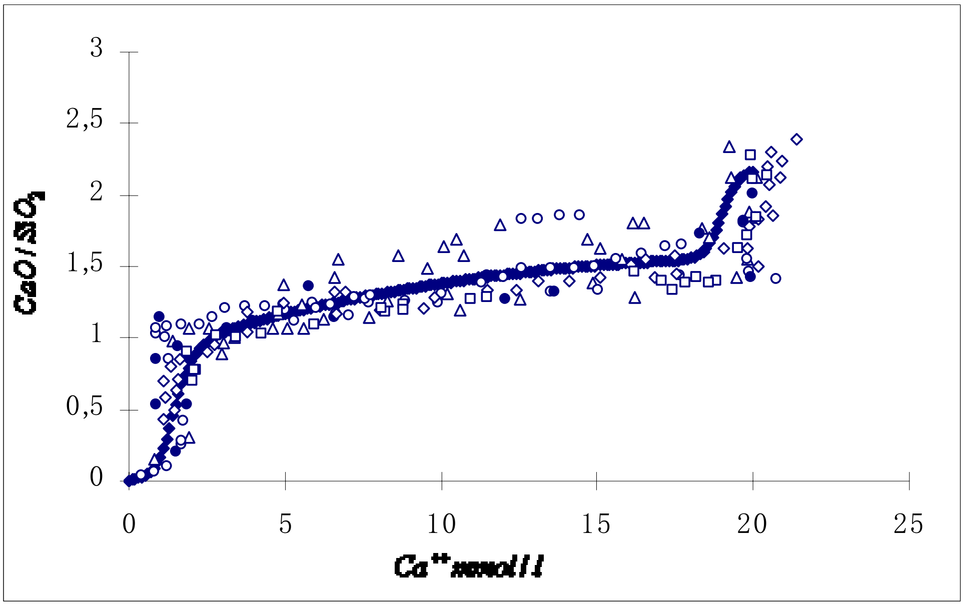

Figure 1-1: Equilibrium curve giving relationship between C/S ratio and C_a^{++} in interstitial solution (Berner, 1992). Data collected from pure C_3S paste and cement paste (Gérard, 1996)

1.4 Diffusion

As shown above, the diffusion process in pore solution is an essential phenomenon in the determination of kinetics of chemical degradation, and then in the durability analysis of cement-based materials.

The porosity of cement-based materials is generally very complex. The size of pores may vary from 1 nm to 1 mm. Usually, there exist two classes of pores:

- Inter-plates pores in $C-S-H$, of small size (in order of nm), which may occupy 25% of $C-S-H$ volume;

- Capillary pores, from 300 nm to 800 nm ; which constitute the connected porosity generating macroscopic permeability of material.

The origins of porosity may be the porosity of cement paste depending on the ratio (w/c), the porosity of interfaces between aggregates and matrix, and porosity due to microcracks.

In the context of modeling the coupling between mechanical degradation and mechanical deformation, we are mainly interested in the diffusion of calcium ions in pores. In most cases of chemical degradation of cement-based materials, the transport by diffusion of aggressive agents occurs either in liquid and gas phases. In the first case, the aggressive agents penetrate through interstitial liquid; this is the case of degradation by sea water, rain and other liquid species. In the second case, the aggressive gas penetrates through the air or interstitial liquid, such as the gas of degradation by $\mathrm{CO_2}$.

The penetration of species C inside porous medium, without interaction with other phenomena, is governed by the classic Fick's law:

$$\vec{\Phi} = \overline{\overline{D}}.\vec{\nabla} C \tag{1-1}$$

$\vec{\Phi}$ is the flux vector, $\overline{\overline{D}}$ the tensor of diffusion coefficients. Making use of masse balance, the kinetics of penetration is described by the following diffusion equations:

$$\frac{\partial C}{\partial t} = \mathrm{div}(\overline{\overline{D}}.\vec{\nabla} C) \tag{1-2}$$

The solution of the above equation leads to a kinetics law of the specie in terms of $\sqrt{t}$. In the case of dissolution of solid calcium, the phase change has to be taken into account in the mass balance equation. This feature is discussed in chapter 3.

1.5 Chemical degradation of cement paste

The chemical degradation of cement paste discussed in this work is limited to the dissolution of solid calcium by aggressive solution. In natural environment, the chemical dissolution par aggressive water is a basic fundamental degradation phenomenon. The aggressive water, in contact with cement paste, induces gradients of calcium concentration between exterior solution and interstitial solution of cement-based material. These gradients generate diffusion of alkaline ions (N_a^+, K^+, C_a^{++}, OH^-) from interstitial solution to the outside of material volume. As aforementioned, the hydrates of cement-based material are in thermodynamic equilibrium with the interstitial solution. The diffusion of alkaline ions to the outside breaks this equilibrium and causes the dissolution of hydrates. According to the equilibrium curve, the crystals of Portland are first dissolved. When all the Portland phase is completely leached, the equilibrium of system is controlled by C-S-H phases, which are also partially subjected to decalcification. When the calcium concentration C_a^{++} becomes less than a certain limit value (about 2 mmol/l), all the C-S-H phases are dissolved. The material, composed essentially of remaining gel of silicate, has no more any material cohesion.

The kinetics of degradation by pure water is generally very slow. It is not convenient for the characterization of chemical degradation effects on mechanical and transport properties of cement-based materials. Indeed, laboratory tests with very long duration are required. In order to obtain rapid degradation of material, various acceleration techniques have been proposed, including:

- Reinforced transportation of ions by application of fluid pressure or electric field;
- Increase of temperature of solution;
- Use of more aggressive solution; the increase of concentration gradient between interstitial solution and environmental allows significant acceleration

of degradation kinetics. For example, we can use solution with low pH. Further, the presence of acid ions in the aggressive solution can also significantly increase the solubility of hydrates of cement paste; for instance, the used of nitrate ammonium solution and H_2S solution.

The solution has been largely used in the degradation of cement-based materials. Indeed, the strongly aggressive and leaching property of nitrate ammonium ($\mathrm{NH_4NO_3}$) recommend its wide use, as an accelerating factor, in the chemical degradation of cement-based materials (Scheneider, 1992; Carde, 1996; Tognazzi, 1998). The typical chemical reaction between the nitrate ammonium ($\mathrm{NH_4NO_3}$) and cement paste are expressed as follows:

$$C_a(OH)_2 \rightarrow C_a^{++} + 2OH^- \tag{1-3a}$$

$$NH_4NO_3 \rightarrow NH_4^+ + NO_3^- \tag{1-3b}$$

$$C_a^{++} + 2OH^- + 2NH_4^+ + 2NO_3^- \leftrightarrow C_a(NO_3) + 2H_2O + 2NH_3 \tag{1-3c}$$

Table 1-3: examples of leaching kinetics in typical cement-based materials data collected by Le Bellego (2001)

Reference	Aggressive solution	material	W/C	Kinetics $a = X_d / \sqrt{t}$ (mm/$\sqrt{\text{day}}$)
Adenot (1992)	Pure water	Cement paste	0.4	0.120
Delagrave (1996)	Pure water	Cement paste	0.25	0.083
			0.25+6% SF	0.052
			0.45	0.287
			0.45+6% SF	0.188
Carde (1996)	Pure water	mortar	0.5	0.125
	$\mathrm{NH_4NO_3}$ (437g/l)			1.31

Tongnazzi (1998)	Pure water	mortar	0.4	0.14
	NH_4NO_3 (480g/l)			2

According to Carde (1996), there is close similarities between pure water and nitrate ammonium (NH_4NO_3) in terms of dissolution of Portland, decalcification of $C-S-H$ and general form the kinetics of degradation with time. Indeed, various experimental data have shown that it is possible to define an empirical law in terms of $\sqrt{t}$ to obtain an approximate estimation of depth of degraded zone, that is $X_d = a\sqrt{t}$. In this way, the parameter a (mm/$\sqrt{\text{day}}$) characterizes the kinetics of chemical degradation for each situation. In Table 1-3, we show some examples of chemical leaching kinetics for typical cement-based materials.

During the leaching process, the dissolution front can be well characterized by the pH indicator. The pH value in the pore solution of cementitious materials is higher than 12.5 while acid solution like ammonium nitrate has a small pH value which is inferior to 7. Therefore, indicator like phenolphthalein can be used to distinguish between the sound zone and the degraded zone. Note that phenolphthalein turns from colorless in acidic solutions to pink in basic solutions with the transition occurring around pH 9.

1.6 Mechanical behavior of cement-based material

Mechanical behaviors of cement-base materials depend on several factors: W/C ratio, porosity, aggregates forms and properties, saturation condition, temperature and loading condition.

Under tensile stress, cement-based materials generally exhibit elastic-brittle responses as shown in Fig. 1-2. Damage by growth of microcracks is the main mechanism of inelastic deformation and failure. Elastic properties are significantly affected by microcracks. Macroscopic failure of material is issued from coalescence of localization of microcracks.

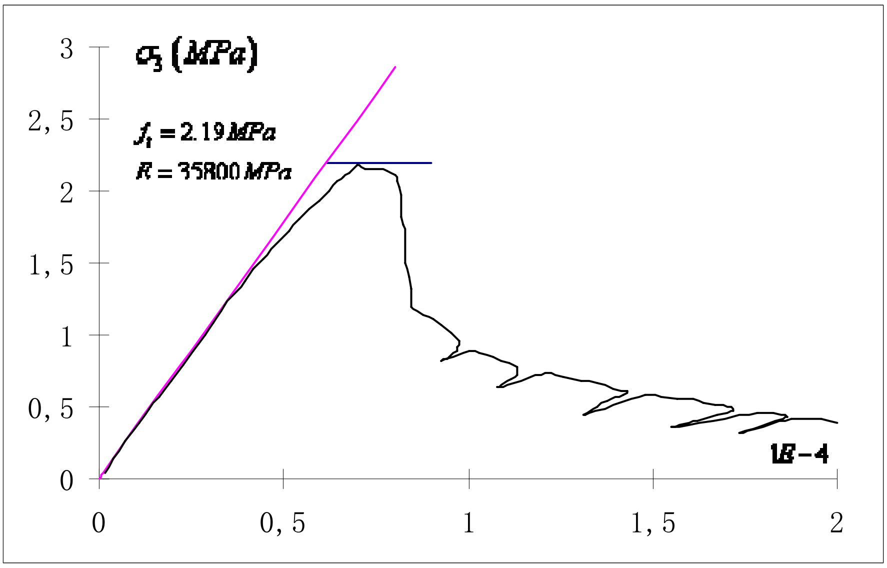

Figure 1-2: Typical mechanical response of cement paste under uniaxial tension (Terrien, 1980)

However, under compressive stresses, the mechanical behavior of cement-paste materials strongly depends on confining pressure. Under low confining pressures, one obtains elastic brittle behavior like under tensile stress. Thus, the mechanical strength of material is significantly different between compression and tension. There is a transition from brittle to ductile behavior with the increase of confining pressure. Under high confining pressures, the mechanical behavior of cement-based materials is characterized by coupled plastic damage. Damage by microcracks affects both elastic and plastic properties. Another important feature is the transition from plastic volumetric compressibility to dilation. Further the plastic volumetric dilation and opening of microcracks may also affect transport properties (diffusion, permeability).

We are concerned by chemical effects on mechanical properties. One of most important consequences of chemical leaching is the increase of porosity. Therefore, it is useful to consider influences of porosity on mechanical properties of cement-based materials. Generally, the mechanical strength and elastic modulus decrease with the increase of porosity. Two representative results are shown on Fig. 1-3 and 1-4 (Feldman and Beaudoin, 1974).

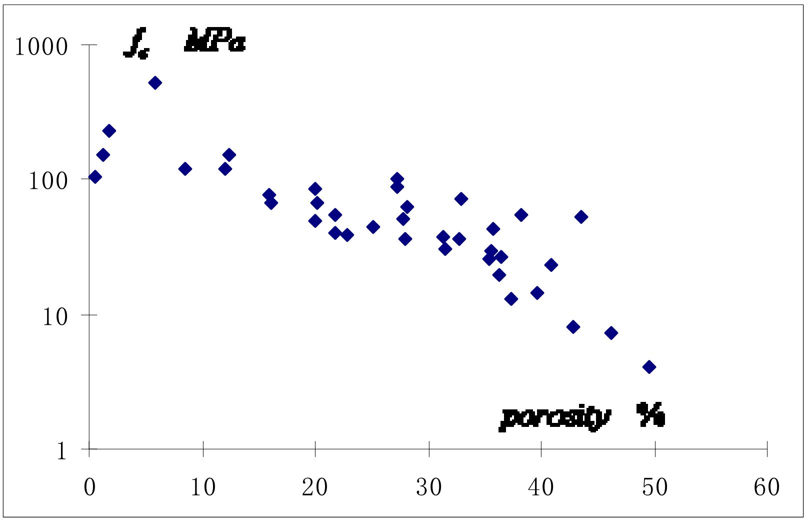

Figure 1-3: Variation of uniaxial compression strength with porosity

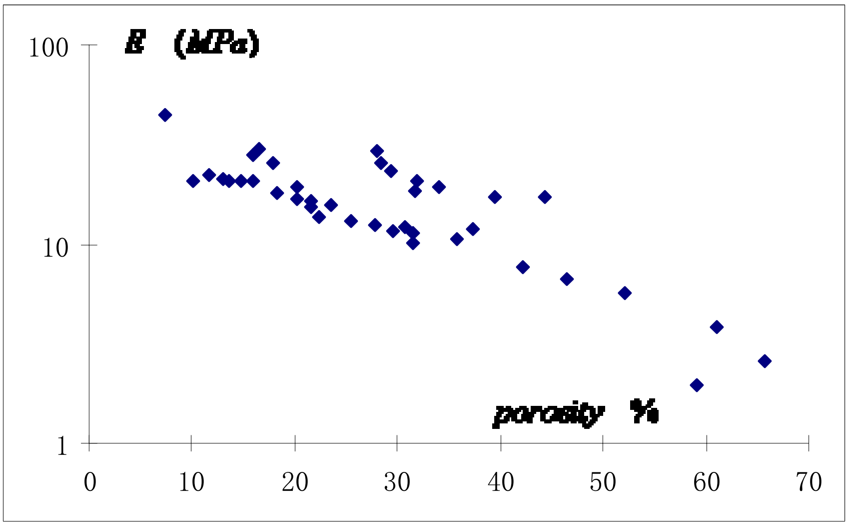

Figure 1-4: Variation of elastic modulus with porosity

1.7 Modeling of chemical degradation

In the recent twenty years, a series of research works have been carried out on experimental characterization and numerical modeling of chemical degradation of cement-based materials. The main attention was given to the understanding of mechanisms of degradation and the determination of constitutive law. Mention here some representative works (Adenot, 1992 ; Carde et al, 1997; Gérard et al, 1996; Tognazzi, 1998; Le Bellégo et al, 2003; Ulm et al, 2003; Torrenti et al, 1998. etc.). Most experimental data suggest that the chemical degradation is controlled by two processes: dissolution of solid hydrates and diffusion of calcium ions. However, the characteristic time of dissolution is generally much shorter than that of diffusion. Theoretical analyses and phenomenological models (Adenot 1992; Buil et al.1990; Gerard 1996, Mainguy et al. 2000) have been proposed.

Two different approaches have been proposed:

- The discrete mineral model, in which the diffusion of all types of hydration products with distinct chemical equilibria is considered. This approach was put into practice by Adenot (1992), who considered 12 mineral phases and their corresponding fronts in a 1-D diffusion setting. Being anchored in the physical chemistry of cement-based materials, tracing the mechanical consequences of the leaching of all individual minerals would be a difficult task.
- The simplified dissolution model in which only the diffusion of calcium ions C_a^{++} is taken into account (Buil et al., 1990; Gérard, 1996). The equilibrium formulation is continuous and based on the Berner's curve. This approach was largely used and leads to very good leaching predictions. This approach will be adopted in this work. The detailed presentation of the simplified chemical model will be given in chapter 3.

1.8 Modeling of chemical-mechanical coupling

Modeling of chemical-mechanical coupling is based on the characterization of chemical degradation effects on mechanical properties of cement-based materials, such as elastic stiffness and failure strength. Based on relevant experimental results, different coupled chemo-mechanical models have been developed for cement paste, mortar and concrete, for instance, Adenot et al. (1992), Gérard et al. (1996), Torrenti et al.(1998), Ulm et al.(1999), Mainguy et al.(2000), Le Bellego et al.(2003),Kuhl et al.(2004), among others.

All these models are based on a phenomenological chemistry model. In most cases, the simplified chemical degradation model is used based on the thermodynamic equilibrium between the calcium concentration in the solid phase and in the liquid phase. Only the calcium concentration in interstitial solution, C_a^{++}, is used as the state variable of chemical degradation. As mentioned above, the present simplified approach avoids considering all the elementary chemical mechanisms and focuses on the evolution of one variable only. From this calcium concentration, the evolutions of porosity, the diffusivity and the mechanical properties due to calcium leaching are determined by different empirical relations. Some representative chemo-mechanical models can be summarized as follows:

- Elastic-damage models coupled with chemical damage for concrete (Gérard et al., 1996, Le Bellego, 2001, Kuhl et al., 2004 and others). This class of models essentially focuses the description of brittle behavior of concrete subjected to mechanical loading and chemical degradation. Two internal variables, respectively to represent mechanical damage by microcracks and chemical damage by dissolution, are used. The evolution of mechanical damage is controlled by a suitable damage criterion. And the chemical damage is governed by the generalized diffusion equations.
- Elastoplastic model coupled with chemical degradation; this class of models addresses the description of ductile behavior of cement-based materials (Pietruszczak et al., 2005; Ulm et al., 2001; Lydzba et al., 2006; etc). The chemical damage is described in the same way. It consists then in the determination of coupling between chemical damage and elastic and plastic properties, for instance variations of material cohesion, frictional coefficient and plastic hardening laws with chemical damage.
- Micromechanical analyses (Heukamp, 2003; Ulm et al, 2003; Lydzba et al., 2006); these models are based on homogenization techniques of representative volume element (RVE). The cement-based materials are considered as heterogeneous materials. Base on relevant analyses of mechanism at relevant microscopic scales, macroscopic behavior of homogenized medium are deduced.

Chapter 2: Mechanical modeling of cement paste and effects of chemical degradation

In this chapter, basic mechanical behaviour of cement paste and influence of chemical degradation will be studied. After a summary of experimental data, an elastoplastic model coupled with both mechanical and chemical damage will be formulated. However, the emphasis will be put on plastic behaviour of cement paste under compression-dominated stresses. Therefore, the mechanical damage is first neglected. We will present then procedure of parameters identification. Finally, the proposed model will be used to simulate typical laboratory tests performed both on sound and chemically degraded materials.

2.1 Summary of basic mechanical behavior of cement paste

A series of laboratory investigations have been performed in the LML (Laboratory of Mechanics of Lille) with technical and financial support of TOTAL Company. The material tested is an ordinary Portland cement paste. The samples were taken out off moulds after 24 hours and then the cement paste were cured for 27 days immerged in water at 90°C (Yurtdas et al., 2006). In order to study influences of chemical degradation on mechanical behaviour, two groups of samples were prepared. The first group was conserved in hot water until the test was performed. In the second group, the samples were immerged in nitrate ammonium (NH_4NO_3) solution with a concentration of $6\,\mathrm{mol/l}$ and a volume ratio of 1:10 until a quasi complete degradation state was obtained. The evolution of front of degraded zone was determined and it was observed that the evolution kinetics of degradation front verified in an approximate way the square root relation $x_d = a\sqrt{day}$. When the degradation front reached the centre of sample, this one was considered as completely degraded and mechanical test was performed.

Triaxial compression tests have been performed to characterize basic mechanical behavior of cement paste, respectively on sound and degraded samples. In order to have full saturation state in the sample, a constant pore pressure is prescribed during each test. Some representative results are shown in Fig. 2-1 to Fig. 2-6.

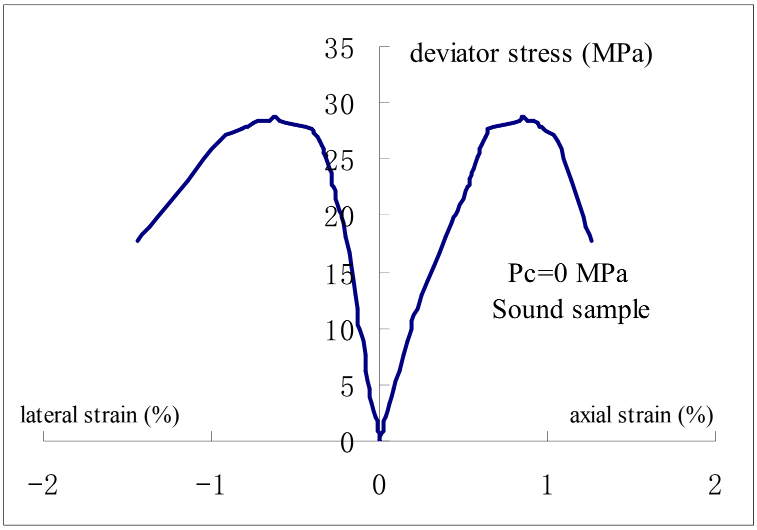

Figure 2-1: Stress strain curves of sound material in uniaxial compression test $P_c = 0\text{MPa}$

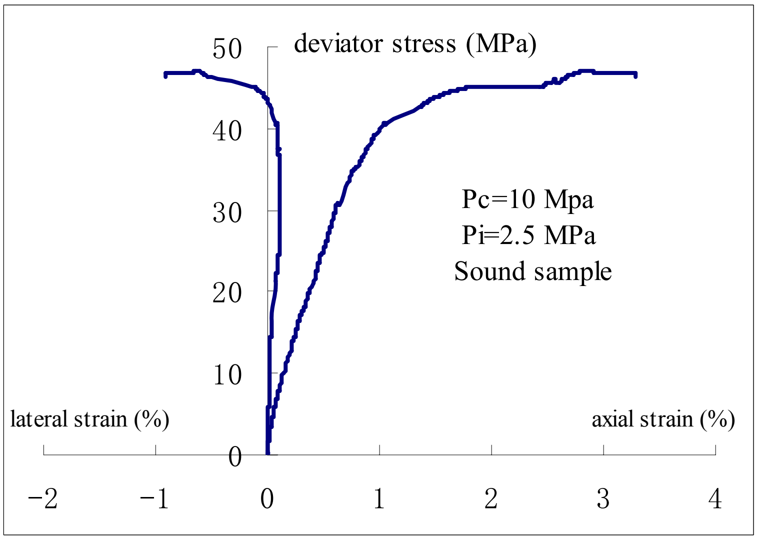

Figure 2-2: Stress strain curves of sound material in triaxial compression test with confining pressure $P_c = 10\text{MPa}$ and constant pore pressure $P_i = 2.5\text{MPa}$

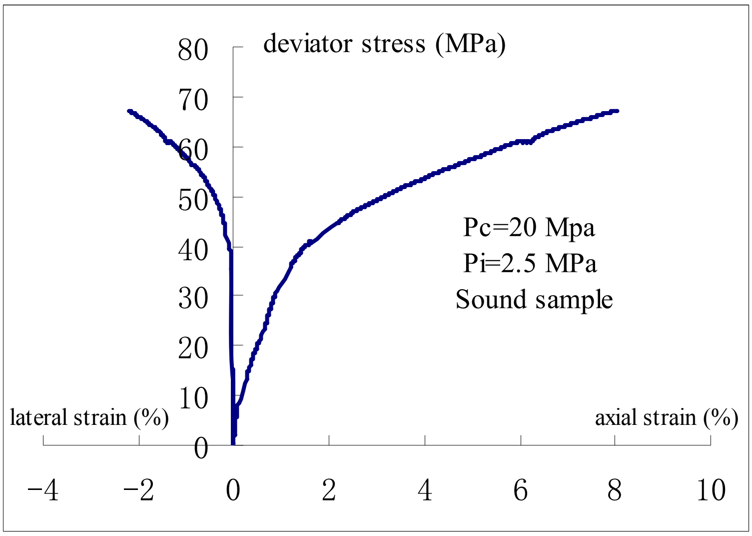

Figure 2-3: Stress strain curves of sound material in triaxial compression test with confining pressure $P_c = 20\text{MPa}$ and constant pore pressure $P_i = 2.5\text{MPa}$

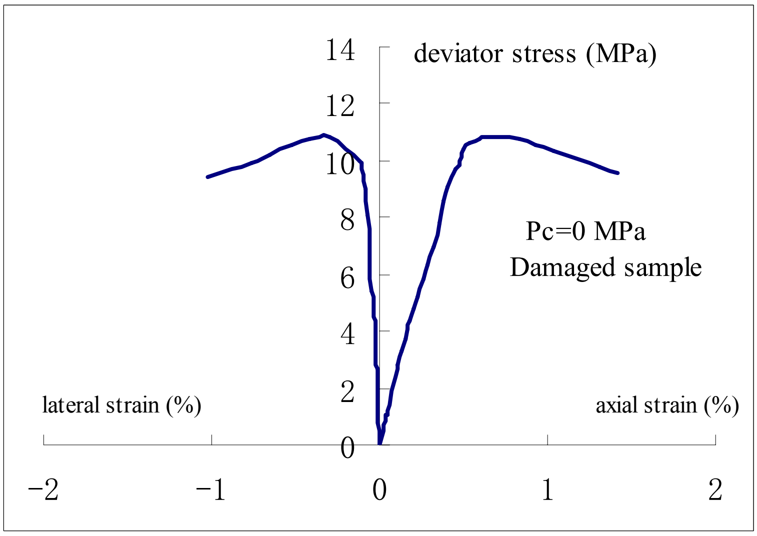

Figure 2-4: Stress strain curves of degraded material in uniaxial compression test $P_c = 0\text{MPa}$

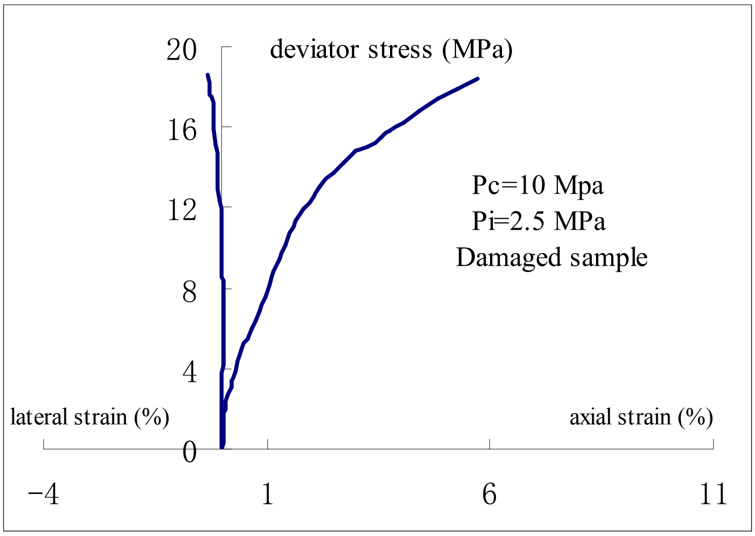

Figure 2-5: Stress strain curves of degraded material in triaxial compression test with confining pressure $P_c = 10\text{MPa}$ and constant pore pressure $P_i = 2.5\text{MPa}$

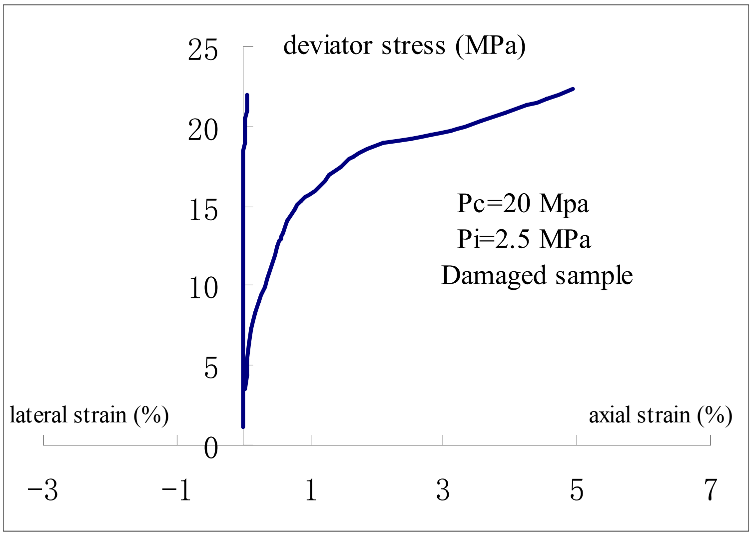

Figure 2-6: Stress strain curves of degraded material in triaxial compression test with confining pressure $P_c = 20\text{MPa}$ and constant pore pressure $P_i = 2.5\text{MPa}$

Based on the experimental data obtained from these laboratory tests, the main features of basic mechanical behaviour of cement paste under compression can be summarized as follows:

- The mechanical response of cement paste is clearly sensitive to confining pressure; under low confining pressure, one observes an elastic brittle behaviour accompanied by material softening phase in post peak region. When the confining pressure is higher, the cement paste exhibits an elastic plastic ductile response and material softening phase is not observed until the axial strain reaches a relatively high value.
- The mechanical behaviour of cement paste is similar to that of typical porous materials due to its high porosity (around 35%). Under deviatoric stress, the volumetric strain is essentially compressive. The volumetric compressibility is as important as the confining pressure is higher. The transition from compressibility to dilatancy is observed only at very low confining pressure.
- Comparing the results obtained from sound and degraded samples, one can see that the chemical degradation significantly affects mechanical responses of cement paste; the mechanical strength is drastically decreased and elastic properties are also affected.
- The mechanical response of cement paste under hydrostatic stress is composed of two phases (see Fig. 2-7); a quasi linear elastic phase and a pore collapse phase with increasing plastic volumetric compaction. The stress threshold for pore collapse is significant lower in degraded material than in sound material.
- The porosity of cement paste was measured in sound and degraded state (Yurtdas et al., 2006); the average increase of porosity is about 19% due to dissolution of solid calcium by aggressive fluid. This increase of porosity will be considered as chemical damage in the formulation of constitutive model with chemical degradation presented in the next section.

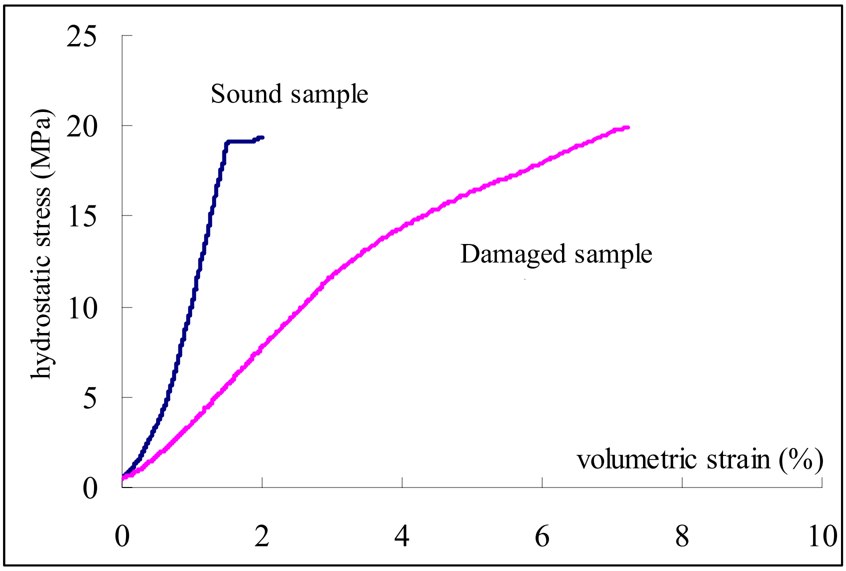

Figure 2-7: Hydrostatic stress and volumetric strain during hydrostatic compression test

2.2 Formulation of constitutive model coupled with chemical damage

In this section, we present the formulation of constitutive model for the description of mechanical behavior of cement paste by taking into account chemical degradation. This last one is directly related to chemical leaching of cement. However, the evolution of chemical damage is not discussed here. It will be determined together with chemical diffusion process in the next chapter.

2.2.1 General framework of constitutive model

Based on the experimental investigations summarized above, the mechanical behavior of cement paste can be described by an elastoplastic damage model. Two kinds of damage with different physical natures should be defined; mechanical damage due to microcracks in solid matrix and chemical damage due to dissolution of solid matrix leading to increase of cement paste porosity.

We assume isothermal conditions throughout this chapter. The principal phenomena to be taken into account are: elastic deformation defined by the elastic strain tensor ε_{ij}^{e} ; plastic deformation defined by the plastic strain tensor ε_{ij}^{p} ;

mechanical damage defined by the internal variable d_m and chemical damage defined by the internal variable d_c. Using the assumption of small strains, the total strain increment $d\varepsilon_{ij}$ is composed by an elastic part $d\varepsilon_{ij}^{e}$ and a plastic part $d\varepsilon_{ij}^{p}$. The assumption of small strain and displacement is adopted. The strain increment partition rule is applied:

$$d\varepsilon_{ij} = d\varepsilon_{ij}^{e} + d\varepsilon_{ij}^{p} \tag{2-1}$$

As mentioned above, we assume an isotropic behavior of cement-based material. The thermodynamic potential can be expressed as follows:

$$\Psi\left(\varepsilon^{e},\gamma^{p},d_m,d_c\right)=\frac{1}{2}(\varepsilon-\varepsilon^{p}):\mathbf{C}(d_m,d_c):(\varepsilon-\varepsilon^{p})+\Psi_p\left(\gamma_p,d_m,d_c)\right) \tag{2-2}$$

The fourth order tensor $\mathbf{C}$ is the elastic stiffness tensor of damaged material; the function Ψ_p represents the locked plastic energy in plastic hardening of damaged material. γ_p denotes the internal variable of plastic hardening. The standard derivation of the thermodynamic potential yields the state equation:

$$\boldsymbol{\sigma}=\frac{\partial\Psi}{\partial\boldsymbol{\varepsilon}^{e}}=\mathbf{C}(d_m,d_c):(\boldsymbol{\varepsilon}-\boldsymbol{\varepsilon}^{p}) \tag{2-3}$$

In the case of isotropic materials, following Hill's notation (see for instance Nemat-Nasser and Hori, 1993), the effective elastic stiffness tensor of damaged material reads in the general form:

$$\mathbf{C}\left(d_m,d_c\right)=2\mu(d_m,d_c)\mathbf{K}+3k(d_m,d_c)\mathbf{J} \tag{2-4}$$

$k(d_m,d_c)$ is the bulk modulus of the damaged material while $\mu(d_m,d_c)$ represents the shear modulus. The two isotropic symmetric fourth order tensors $\mathbf{J}$ and $\mathbf{K}$ are defined by:

$$\mathbf{J} = \frac{1}{3}\delta \otimes \delta \quad \text{and} \quad \mathbf{K} = \mathbf{I} - \mathbf{J} \tag{2-5}$$

in which δ denotes the second order unit tensor and $\mathbf{I} = \delta \underline{\overline{\otimes}} \delta$ is the symmetric fourth order unit tensor : $I_{ijkl} = \frac{1}{2}(\delta_{ik}\delta_{jl} + \delta_{il}\delta_{jk})$. Note that for any second order tensor $\boldsymbol{E}$, $\mathbf{J}:\mathbf{E} = \frac{1}{3}(tr\mathbf{E})\,\delta$ and $\mathbf{K}:\boldsymbol{E} = \boldsymbol{E} - \frac{1}{3}(tr\boldsymbol{E})\delta$ which are respectively the isotropic and deviatoric part of $\boldsymbol{E}$.

The thermodynamic force associated with the mechanical damage variable is given by:

$$Y_{dm} = -\frac{\partial \Psi}{\partial d_m} = -\frac{1}{2}(\varepsilon - \varepsilon^p):\mathbf{C}'(d_m, d_c):(\varepsilon - \varepsilon^p) - \frac{\partial \Psi_p(\gamma_p, d_m, d_c)}{\partial d_m} \tag{2-6}$$

The fourth order tensor $\mathbf{C}'(d_m, d_c)$ is the derivative of the elastic tensor with respect to the mechanical damage variable:

$$\mathbf{C}'(d_m, d_c) = \frac{\partial \mathbf{C}(d_m, d_c)}{\partial d_m} \tag{2-7}$$

The intrinsic mechanical dissipation must verify the following fundamental inequality:

$$\sigma : \dot{\varepsilon}^p + Y_{dm}\dot{d}_m \geq 0 \tag{2-8}$$

By defining a chemical potential for calcium ion transport within the pore space as a function of the gradient of the calcium ion concentration field, the chemical dissipation law can be defined (Ulm et al., 1999; Kuhl et al., 2004). The rate of dissipated energy associated with the chemical dissolution process is additively decomposed into a portion related to the transport of C_a^{++} ions and a portion related to chemical dissolution, whereby each part must be non-negative.

The rate form of the constitutive Eq. (2-3) can be easily written as:

$$\dot{\sigma} = \mathbf{C}(d_m, d_c) : (\dot{\varepsilon} - \dot{\varepsilon}^p) + \mathbf{C}'(d_m, d_c) : (\varepsilon - \varepsilon^p)\dot{d}_m + \mathbf{C}'^c(d_m, d_c) : (\varepsilon - \varepsilon^p)\dot{d}_c \qquad (2\text{-}9)$$

The fourth order tensor $\mathbf{C}'^c$ is the derivative of the elastic stiffness tensor with respect to the chemical damage variable. The dot denotes time derivative of variables (or incremental variation of variables in numerical computing procedure). The evolution of chemical damage is determined by the phenomenological chemistry model in the previous section. The constitutive modelling requires now to determine the evolution laws of mechanical damage and of the plastic strains.

The evolution of mechanical damage is determined by giving a pseudo-potential of dissipation. In the case of non-viscous dissipation, the damage evolution law is deduced from a damage criterion, which is a scalar valued function of the conjugated damage force (damage energy release), being written in the general form:

$$f_{dm}(Y_{dm}, d_m, d_c) = Y_{dm} - r(d_m, d_c) \leq 0 \qquad (2\text{-}10)$$

where $r(d_m, d_c)$ represents the damage energy release threshold at a given state of material damage. Note that due to chemo-mechanical coupling, the mechanical damage threshold may be dependent on the state of chemical damage due to change of connected porosity. Further, as the mechanical damage force Y_{dm} depends on chemical damage and plastic strains (see Eq. (2-6)), the evolution of damage criterion is clearly influenced by both chemical reaction and plastic deformation. By using the classic normal dissipation scheme, the mechanical damage evolution rate is determined.

In the case of non-viscous flow, the plastic strain rate is characterised through the determination of plastic yield function, plastic hardening law and plastic flow rule. For most cement-based materials, a non-associated plastic flow rule is generally needed in order to correctly describe plastic volumetric dilatancy and compressibility. In the modelling of plastic deformation coupled with chemical and mechanical damage, the plastic yield criterion and plastic potential should be respectively expressed by a scalar valued function of Cauchy stress tensor, the damage variables and the thermodynamic conjugate force associated with the internal hardening variable γ_p:

$$f(\boldsymbol{\sigma},\alpha_p,d_m,d_c)\leq 0 \tag{2-11}$$

$$g(\boldsymbol{\sigma},\alpha_p,d_m,d_c)\leq 0 \tag{2-12}$$

The plastic hardening function $\alpha_p(\gamma_p,d_m,d_c)$ is deduced by standard derivative of the thermodynamic potential:

$$\alpha_p(\gamma_p,d_m,d_c)=\frac{\partial\Psi(\boldsymbol{\varepsilon},\gamma_p,d_m,d_c)}{\partial\gamma_p} \tag{2-13}$$

The plastic flow rule and the unloading – unloading condition can be then determined using standard plastic consistency conditions. In the case of coupled evolution of plastic deformation and mechanical damage, both the damage and plasticity consistency conditions must be verified (Ju, 1988; Shao et al., 2006).

2.2.2 Definition of chemical damage

The cement paste is considered as a porous material composed of the connected pore space and cementitious skeleton (Kuhl et al. 2004) (Fig. 2-8). As previously mentioned, in the chemically sound cement paste, the solid constituents contained in the cementitious skeleton and the substances constituting the pore fluid are in a state of chemical equilibrium. Let us note, by ϕ_r the reference value of connected porosity of sound material. When the chemical equilibrium between the pore fluid and solid skeleton is broken due to the diminution of ion concentration in the pore fluid, more substances of skeleton are dissolved instantaneously. The dissociation of calcium ions from the solid skeleton during the chemical leaching process leads to the increase of pore space and thus the increase of total connected porosity. This porosity change is governed by the mass balance equation of calcium ions. The increase of porosity due to chemical leaching affects not only mechanical properties of cement-based material but also diffusion properties of calcium ions inside pore fluid. From the mechanical point of view, the increase of porosity due to chemical leaching can be considered as a damage process, which is described by a scalar valued chemical damage variable:

$$d_c = \phi - \phi_r \tag{2-14}$$

Taking into account calcium mass balance equation and chemical equilibrium relation as mentioned in Chapter 1, the chemical damage can be expressed in the following form:

$$d_c = \frac{M}{\rho}\left(S_{tot} - f\left(Ca^{++}\right)\right) \tag{2-15}$$

Where M and ρ are the average molar mass and density of calcium in the skeleton. S_{tot} denotes the total amount of calcium in solid skeleton.

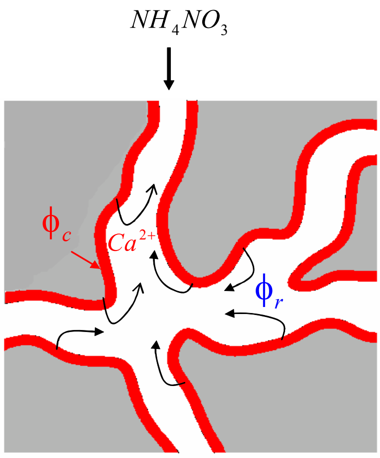

Figure 2-8: Increase of connected porosity due to calcium leaching process

The evolution of chemical damage is governed by diffusion process of calcium ions in pore fluid. The feature will be discussed in the next chapter together with initial and boundary conditions.

2.2.3 Specific model for cement paste under compression-dominated loading

Under compression-dominated stresses, the mechanical behavior of cement paste is essentially characterized by plastic deformation. Therefore, the mechanical damage due to microcracks will be neglected here. Thus, the thermodynamic potential for isotropic materials is reduced to the following form:

$$\psi\left(\varepsilon^e,\gamma^p,d_c\right)=\frac{1}{2}\left[k\left(d_c\right)\left(\varepsilon_v^e\right)^2+2\mu\left(d_c\right)e_{ij}^e e_{ij}^e\right]+\psi^p\left(\gamma^p,d_c\right) \tag{2-16}$$

where ε_v^e is elastic volumetric strain and e_{ij}^e are components of the elastic deviatoric strain tensor. The specific forms of the two functions $k\left(d_c\right)$ and $\mu\left(d_c\right)$ should be determined from relevant experimental data showing elastic degradation with chemical leaching. However, some theoretical estimates can be obtained from suitable micromechanics analysis, see for instance (Mura, 1987; Nemat-Nasser and Horri, 1993). In this work, we have adopted the general expressions of effective elastic properties of isotropic damaged materials issued from Mori-Tanaka scheme. The effective elastic properties of damaged material are expressed as follows:

$$k\left(d_c\right)=\frac{k_0}{1+\alpha_1 d_c} \quad \text{and} \quad \mu\left(d_c\right)=\frac{\mu_0}{1+\alpha_2 d_c} \tag{2-17}$$

where k_0 and μ_0 are the initial bulk modulus and shear modulus of undamaged material. Two parameters α_1 and α_2, which define the degradation of elastic properties by damage, can be identified from suitable experimental data. In the present study, the maximal chemical damage is estimated as 0.19. Using the experimental data on the bulk modulus and shear modulus of initial sound state and completely degraded state, the values of α_1 and α_2 can be easily calculated. Fig. 2-9 shows the evolution of bulk modulus and shear modulus versus chemical damage degree.

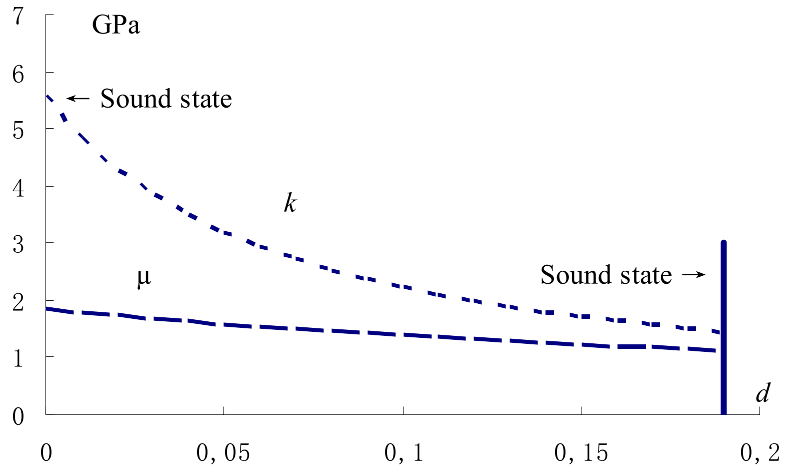

Figure 2-9: Evolutions of bulk modulus and shear modulus versus chemical damage in cement paste

2.2.4 Characterization of deviatoric plastic deformation

As aforementioned, the plastic deformation of cement paste, like that in most porous materials, can be characterized by two complementary plastic mechanisms: deviatoric mechanism and pore collapse mechanism. The deviatoric mechanism is common for frictional materials and motivated by shearing phenomenon under deviatoric stress. Classical yield functions are generally based on linear Mohr-Coulomb and Drucker-Prager type criteria. Material failure is represented as an ultimate state of plastic yielding. However, in cement paste material, we have mentioned that the plastic yielding condition is strongly sensitive to confining pressure. Linear yielding criteria are not suitable. In this work, inspired by the previous works by Pietruszczak et al. (1988) and Mohamad-Hussein and Shao (2007), we propose to use the following non linear form as the yield function of deviatoric plastic mechanism:

$$f_s = \left(\frac{q}{g(\theta) P_r} \right)^n + \alpha A \left(\frac{p - C}{P_r} \right) = 0 \qquad (2\text{-}18)$$

$$p = \frac{1}{3} tr\sigma \,,\ \ q = \sqrt{\frac{3}{2} S_{ij} S_{ij}} \,,\ \ S_{ij} = \sigma_{ij} - \frac{1}{3}\sigma_{kk}\delta_{ij}$$

where q denotes the deviatoric stress, S_{ij} are the components of the deviatoric stress tensor and p corresponds to the mean stress. The parameter C represents the cohesion (hydrostatic tension strength) of material and P_r is taken as a reference stress which is generally fixed to 1MPa. The function $g(\theta)$ is introduced to take into account influence of Lode angle on plastic flow. However, for the lack of relevant experimental data, this point is neglected in the present work by taking $g(\theta) = 1$. In this paper, the influence of Lode angle is not taken into account in the present version of model.

The function α in the yield function defines the plastic hardening law for the deviatoric plastic process. The generalized plastic distortion is generally used as the hardening variable frictional materials. For the studied material, as aforementioned, the softening behavior is observed only in very low confining pressures. For the sake of simplicity and putting the emphasis to chemical degradation, the material softening is not considered here. The material hardening is described by an increasing function of plastic distortion as follows:

$$\alpha = \alpha^0 + (1 - \alpha^0)\frac{\gamma_s}{B + \gamma_s} \tag{2-19}$$

where α^0 is the initial yield threshold, and B is a model's parameter controlling plastic hardening rate. The variable γ_s denotes the generalized plastic distortion, which is defined by:

$$d\gamma_s = \sqrt{\frac{2}{3} d_{ij}^s d_{ij}^s} \Big/ \chi_p \,,\ \ d_{ij}^s = \varepsilon_{ij}^s - \frac{1}{3}\varepsilon_{kk}^s \delta_{ij} \tag{2-20}$$

According to the experimental data of cement paste, we can observe that the plastic hardening depends strongly on the confining pressure. Therefore, we have introduced a regularizing coefficient χ_p in Eq. (2-20), which is a function of minor principal stress:

$$\chi_p = \exp\left(\beta \frac{\langle -\sigma_3 \rangle}{\mathrm{P_r}}\right) \tag{2-21}$$

where β is a model's parameter allowing taking into account influence of confining pressure on plastic hardening law. Note that the plastic hardening function α increases progressively during plastic flow and closes to the ultimate value defined by $\alpha \to 1$ when macroscopic failure is reached. The corresponding yield surface gradually closes up to the failure surface ($f_s \to F_s$) as illustrated in Fig. 2-10.

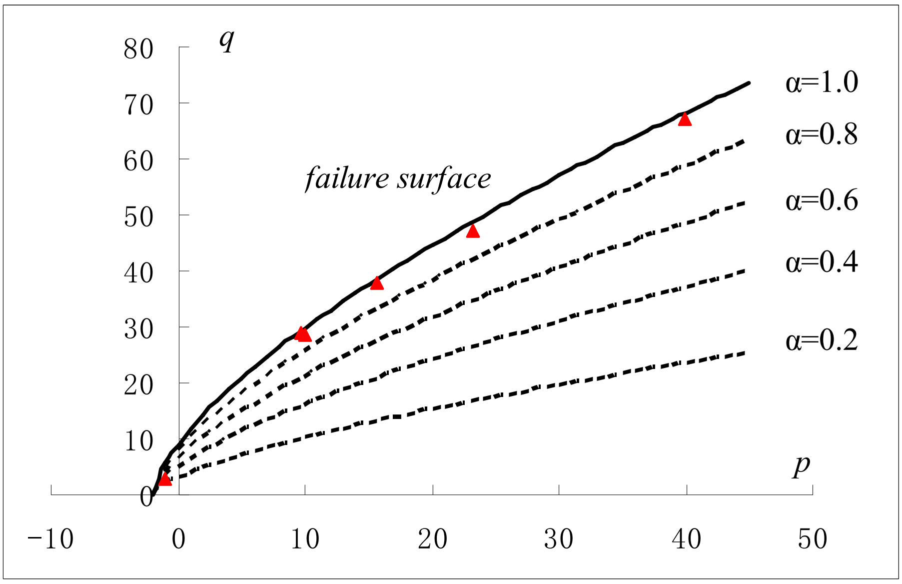

Figure 2-10: Evolution of yield surface with the plastic hardening variable α

Plastic potential:

In most frictional materials, plastic deformation under deviatoric stress exhibits a transition from volumetric compressibility to dilatancy. Non-associated plastic flow rules are generally necessary. This is also the case for the cement paste studied here. Inspired by the plastic model proposed by Pietruszczak et al. (1988) for concrete, the following plastic potential is used:

$$g_s = q + \eta\left(p - C\right)\ln\left(\frac{p-C}{I_0}\right) = 0 \tag{2-22}$$

The variable I_0 defines the intersection point between the potential surface and the axis p. The parameter η defines the transition boundary between compressibility and dilatancy in $q-p$ plane. While the stress points verify the condition $\partial g_s/\partial p$, the transition from plastic compressibility to dilatancy occurs. Based on experimental data, it is assumed that the transition boundary can be described by a linear function:

$$f_{c-d} = q - \eta\left(p - C\right) = 0 \tag{2-23}$$

Fig. 2-11 shows the illustration of the plastic potential surface in $p-q$ plan. We can clearly see volumetric compressibility and dilatancy zones depending on the current loading stress.

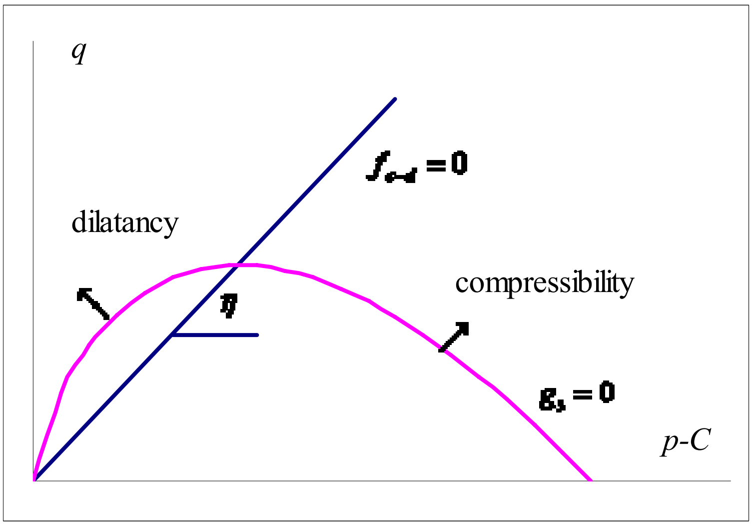

Figure 2-11: Illustration of the plastic potential surface

Plastic flow rule of deviatoric mechanism:

For the loading path where only the deviatoric plastic mechanism is activated, the plastic flow rule is written by:

$$d\varepsilon_{ij}^{s}=d\lambda^{s}\frac{\partial g_{s}}{\partial\sigma_{ij}} \tag{2-24}$$

$$\frac{\partial g_{s}}{\partial\sigma_{ij}}=\frac{\partial g_{s}}{\partial p}\cdot\frac{\partial p}{\partial\sigma_{ij}}+\frac{\partial g_{s}}{\partial q}\cdot\frac{\partial q}{\partial\sigma_{ij}}=\frac{1}{3}\eta\left[1+\ln\left(\frac{q-C}{I_{0}}\right)\right]\delta_{ij}+\frac{3}{2}\cdot\frac{S_{ij}}{p} \tag{2-25}$$

Considering the evolution of chemical damage, the plastic consistency condition can be expressed as:

$$df_{s}=\frac{\partial f_{s}}{\partial\sigma}:\dot{\sigma}+\frac{\partial f_{s}}{\partial\gamma^{p}}\dot{\gamma}^{p}+\frac{\partial f_{s}}{\partial d_{c}}\dot{d}_{c}=0 \tag{2-26}$$

The generalized plastic shear strain rate $\dot{\gamma}^{p}$ can be rewritten as:

$$\dot{\gamma}^{p}=\frac{\sqrt{\frac{2}{3}de_{ij}^{s}de_{ij}^{s}}}{\chi_{p}}=\dot{\lambda}^{s}\frac{\sqrt{\frac{2}{3}\boldsymbol{J}:\left(\frac{\partial g_{s}}{\partial\boldsymbol{\sigma}}\right):\boldsymbol{J}:\left(\frac{\partial g_{s}}{\partial\boldsymbol{\sigma}}\right)}}{\chi_{p}}=\dot{\lambda}^{s}\frac{h}{\chi_{p}} \tag{2-27}$$

$$J_{ijkl}=\frac{1}{2}\left(\delta_{ik}\delta_{jl}+\delta_{il}\delta_{jk}\right)-\frac{1}{3}\delta_{ij}\delta_{kl}\ ,\qquad h=\sqrt{\frac{2}{3}\boldsymbol{J}:\left(\frac{\partial g_{s}}{\partial\boldsymbol{\sigma}}\right):\boldsymbol{J}:\left(\frac{\partial g_{s}}{\partial\boldsymbol{\sigma}}\right)} \tag{2-28}$$

Therefore, the rate form of constitutive relations is determined as:

$$\dot{\sigma}=\boldsymbol{C}(d):\dot{\varepsilon}^{e}+\boldsymbol{C}':\varepsilon^{e}\dot{d}_{c} \tag{2-29}$$

Using the plastic flow rule, one obtains the plastic multiplier as follows:

$$\dot{\lambda}^{s}=\frac{\frac{\partial f_{s}}{\partial\boldsymbol{\sigma}}:\boldsymbol{C}(d):\dot{\varepsilon}+\left[\frac{\partial f_{s}}{\partial\boldsymbol{\sigma}}:\boldsymbol{C}':\varepsilon^{e}+\frac{\partial f_{s}}{\partial d_{c}}\right]\dot{d}_{c}}{\frac{\partial f_{s}}{\partial\boldsymbol{\sigma}}:\boldsymbol{C}(d):\frac{\partial g_{s}}{\partial\boldsymbol{\sigma}}-\frac{\partial f_{s}}{\partial\gamma^{p}}\frac{h}{\chi_{p}}} \tag{2-30}$$

2.2.5 Plastic pore collapse characterize

As we have mentioned, the plastic deformation caused by pore collapse mechanism represents an important phenomenon in porous materials such as cement and chalk. This mechanism takes an important role in many practice problems, such as oil reservoir engineering and concrete structure durability. Hydrostatic compression tests are generally used to characterize the pore collapse mechanism. Homand and Shao (2000) performed additional specific tests to characterize the evolution of yield surface during plastic hardening. Such tests for chalk can give guide to the choice of an appropriate plastic hardening law in cementitious materials. All tests have been performed on oil-saturated samples. The loading path in the conventional mean stress–deviatoric stress plane is composed of two phases. The samples are first subjected to a hydrostatic compression up to 25 MPa, which is higher than the initial pore collapse stress. A plastic hardening phase is thus induced in the samples. After this preliminary plastic hardening phase, the hydrostatic stress is unloaded to a chosen value (say 10, 14, 17 and 20 MPa). From this point, the previously plastically deformed sample is subjected to a triaxial compression test by increasing the axial stress. Yield stresses and eventually failure stresses are determined during the triaxial phase. The yield surface obtained after the hydrostatic preloading is compared to the initial yield surface (Fig. 2-12). We can see that the evolution of yield surface during plastic hardening can be characterized by an isotropic expansion of the elastic domain. Therefore, an isotropic plastic hardening law can be used. Another interesting feature of these results is that the failure stresses due to plastic shearing are not affected by the preliminary plastic hardening in pore collapse process. Indeed, the failure stresses obtained from two triaxial tests performed on preliminary plastically deformed samples with 10 and 14 MPa confining pressure are lined up with the failure stresses obtained from virgin samples. This result would suggest that the two plastic mechanisms could be considered as independent ones; the plastic hardening (expansion) of the cap yield surface for the pore collapse mechanism does not affect the yield surface for the plastic shear mechanism.

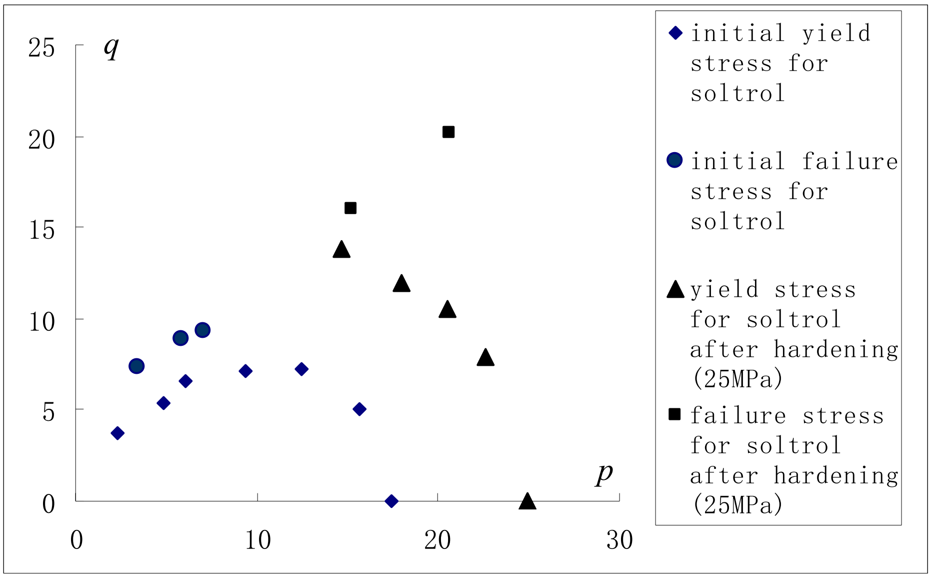

Figure 2-12: Evolution of yield surface of chalk during plastic hardening for oil saturated samples (Homand and Shao, 2000)

Yield function:

According to simplified schematization, the cement paste is idealized as a homogeneous porous material composed of a solid matrix and a connected porosity. It is firstly advisable to determine the criterion of plasticity of this material under compressive stresses. With this intention, one takes the criterion of plasticity proposed by Gurson (1977) as a starting point, and this criterion was used for metal porous materials subjected to tensile stresses. The deformation and the rupture of material are then determined by the evolution of the pores. This criterion was largely used and various versions were proposed for better describing the ductile rupture of porous materials. Recently, Leblond and Perrin (1990, 1996, 2000) showed micromechanical background for the criterion of Gurson. Indeed, the criterion of Gurson represents the exact solution of the macroscopic criterion of a porous media composed of a solid matrix obeying the Von-Mises perfect plasticity and of the spherical pores. According to this result, the macroscopic plasticity criterion depends on the plastic threshold of the solid matrix and macroscopic porosity. Various modifications of the yield surface were proposed for better corresponding to the experimental data, and describing plastic hardening law. Inspired by these works, we adopted the general form of the Gurson's criterion for the determination of yield function of pore collapse mechanism in cement paste. The following function is used:

$$f_c = \frac{q^2}{\overline{\sigma}^2} + 2\phi \cosh\left(q_2 \frac{3p}{2\overline{\sigma}} \right) - 1 - \phi^2 = 0 \tag{2-31}$$

The parameter q_2 is introduced to determine the geometrical form of the yield surface. In the initial Gurson's criterion, $q_2 = 1$. The introduction of this parameter is required so that the yield surface correctly reproduces the experimental data. $\overline{\sigma}$ denotes the plastic yield stress of solid matrix. The value of $\overline{\sigma}$ may vary with plastic deformation history. The variation of $\overline{\sigma}$ can be determined by plastic hardening law. ϕ is the total connected porosity used as an parameter of the model. In the present study, the cement paste is subjected to coupled mechanical loading and chemical degradation. There are two sources of variation of total porosity, one due to chemical leaching and another due to mechanical loading (compression or dilatancy). In general case, the variation of total porosity can be written as:

$$\dot{\phi} = \dot{\phi}_c + (1-\phi)\dot{\varepsilon}_{kk}^{p} = \dot{d}_c + (1-\phi)\dot{\varepsilon}_{kk}^{p} \tag{2-32}$$

Therefore, the evolution of total porosity is logically connected with chemical degradation in the pore collapse mechanism. Further, in general case, the porosity change due to mechanical loading, represented by the second term of Eq. (2-32) is much smaller than that induced by chemical damage.

Plastic hardening law:

In order to determine the pore collapse process, the result of hydrostatic compression tests is analyzed. In Fig. 2-13, we show typical stress - strain curve for porous cement paste. One observes first a quasi-linear and reversible phase, corresponding to the elastic compaction of porous skeleton. The slope of this linear phase gives the elastic compressibility modulus of material. When the hydrostatic stress exceeds to a certain limit, defined as the threshold of pore collapse, we have progressive irreversible compaction of pores produced by the progressive destruction of the initial porous structure. Unfortunately, the value of hydrostatic stress used in this test is not high enough, the results do not show a third phase generally observed in porous materials corresponding to progressive decrease of compaction rate due to increase of contact areas between grains.

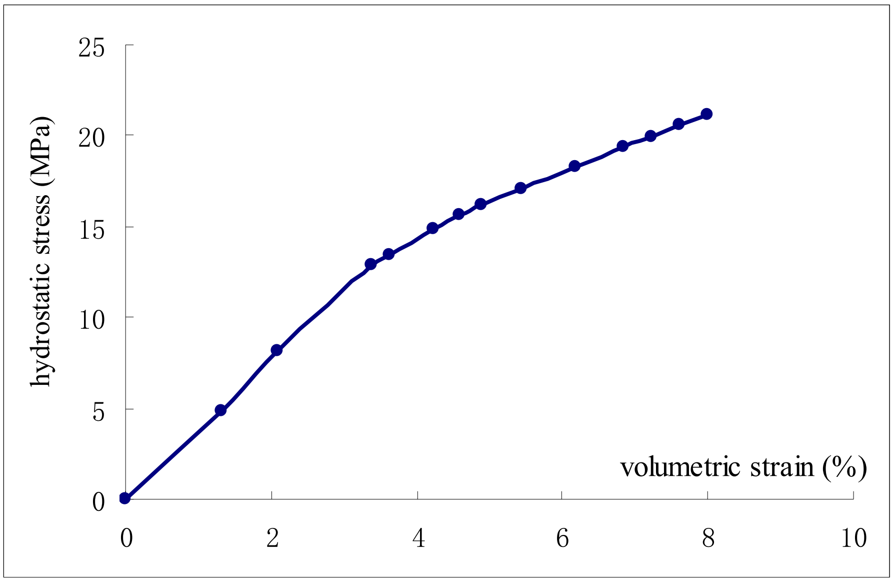

Figure 2-13: Hydrostatic compression test on chemically degraded cement paste

Based on the preceding considerations and the experimental data from hydrostatic compression test, the following hardening function is proposed:

$$\overline{\sigma} = \overline{\sigma}_0 \left[1 + a(-\varepsilon_v^c)^m e^{b(-\varepsilon_v^c)} \right] \tag{2-33}$$

where ε_v^c is the plastic volumetric strain due to pore collapse process, taken as the internal hardening variable. $\overline{\sigma}_0$ denotes the initial yield stress of the solid matrix. a, m and b are three parameters of the hardening law, which can be easily identified from a hydrostatic compression test.

Based on experimental data from cement paste and porous chalks, unlike in deviatoric plastic mechanism, an associated plastic flow rule is here used and we have the following plastic potential:

$$g_c = \frac{q^2}{\bar{\sigma}^2} + 2\phi \cosh\left(q_2^* \frac{3p}{2\bar{\sigma}} \right), \quad q_2^* = q_2 \tag{2-34}$$

Plastic flow rule for pore collapse mechanism:

For the loading path where only the pore collapse mechanism is activated, the plastic flow rule is written by:

$$d\varepsilon_{ij}^c = d\lambda^c \frac{\partial g_c}{\partial \sigma_{ij}} \tag{2-35}$$

$$\frac{\partial g_c}{\partial \sigma_{ij}} = \frac{\partial g_c}{\partial p} \cdot \frac{\partial p}{\partial \sigma_{ij}} + \frac{\partial g_c}{\partial q} \cdot \frac{\partial q}{\partial \sigma_{ij}} = q_2^* \frac{\phi}{\bar{\sigma}} \sinh\left(q_2^* \frac{3p}{2\bar{\sigma}} \right) \delta_{ij} + \frac{3}{\bar{\sigma}^2} S_{ij} \tag{2-36}$$

Considering the evolution of chemical damage, the plastic consistency condition can be expressed as:

$$df_c = \frac{\partial f_c}{\partial \sigma} : \dot{\sigma} + \frac{\partial f_c}{\partial \varepsilon_v^c} \dot{\varepsilon}_v^c + \frac{\partial f_c}{\partial \phi} (1-\phi) d\varepsilon_c^p + \frac{\partial f_c}{\partial d_c} \mathrm{d} d_c = 0 \tag{2-37}$$

The rate form of constitutive equations gives:

$$\dot{\sigma} = \boldsymbol{C}(d_c) : \dot{\varepsilon}^e + \boldsymbol{C}'(d_c) : \varepsilon^e \dot{d}_c \tag{2-38}$$

Taking consideration of flow rule and consistency condition, the plastic multiplier of pore collapse mechanism reads:

$$\dot{\lambda}^c = \frac{\dfrac{\partial f_c}{\partial \sigma} : \boldsymbol{C}(d) : \dot{\varepsilon} + \left[\dfrac{\partial f_c}{\partial \sigma} : \boldsymbol{C}' : \varepsilon^e + \dfrac{\partial f_c}{\partial d_c} \right] \dot{d}_c}{\dfrac{\partial f_c}{\partial \sigma} : C : \dfrac{\partial g_c}{\partial \sigma} - \dfrac{\partial f_c}{\partial \bar{\sigma}} \dfrac{\partial \bar{\sigma}}{\partial \varepsilon_v^c} tr\left(\dfrac{\partial g_c}{\partial \sigma} \right) - \dfrac{\partial f_c}{\partial \phi} (1-\phi) tr\left(\dfrac{\partial g_c}{\partial \sigma} \right)} \tag{2-39}$$

2.2.6 Coupling between two plastic mechanisms

During general loading history, the two plastic deformation mechanisms can be activated either separately or simultaneously. Four distinct constitutive domains can be identified.

- If f_c<0 and f_s<0, the applied stress state is fully inside the elastic domain or leads to an elastic unloading. No plastic flow occurs and we have: $d\lambda^c = 0$ and $d\lambda^s = 0$.
- If f_c=$0 \cup \dot{f}_c = 0$ but f_s<0, the pore collapse mechanism is activated while the plastic shear yield surface is not reached. The plastic multiplier $d\lambda^c > 0$ is determined by Eq. (2-39) and $d\lambda^s = 0$.
- If f_s=$0 \cup \dot{f}_s = 0$ but f_c<0, the plastic shearing mechanism is activated while the pore collapse yield surface is not reached. The plastic multiplier $d\lambda^s > 0$ is determined by Eq. (2.30) and $d\lambda^c = 0$.
- If f_s=$0 \cup \dot{f}_s = 0$ and f_c=$0 \cup \dot{f}_c = 0$, the two plastic deformation mechanisms are activated. The plastic multipliers $d\lambda^s > 0$ and $d\lambda^c > 0$ can be determined by the double consistency conditions:

$$\begin{cases} \dfrac{\partial f_s}{\partial \sigma} : C : \left(d\varepsilon - d\varepsilon^s - d\varepsilon^c \right) + \left[\dfrac{\partial f_s}{\partial \sigma} : C' : \varepsilon^e + \dfrac{\partial f_c}{\partial d_c} \right] \dot{d}_c + H_s d\lambda^s + H_{sc} d\lambda^c = 0 \\ \dfrac{\partial f_c}{\partial \sigma} : C : \left(d\varepsilon - d\varepsilon^s - d\varepsilon^c \right) + \left[\dfrac{\partial f_c}{\partial \sigma} : C' : \varepsilon^e + \dfrac{\partial f_s}{\partial d_c} \right] \dot{d}_c + H_c d\lambda^c + H_{cs} d\lambda^c = 0 \end{cases} \tag{2-40}$$

$$\begin{cases} \left[\dfrac{\partial f_s}{\partial \sigma}:C:\dfrac{\partial g_s}{\partial \sigma}-H_s\right]d\lambda^s+\left[\dfrac{\partial f_s}{\partial \sigma}:C:\dfrac{\partial g_c}{\partial \sigma}-H_{sc}\right]d\lambda^c \\ \qquad =\dfrac{\partial f_s}{\partial \sigma}:C:d\varepsilon+\left[\dfrac{\partial f_s}{\partial \sigma}:C':\varepsilon^e+\dfrac{\partial f_s}{\partial d_c}\right]\dot{d}_c \\ \left[\dfrac{\partial f_c}{\partial \sigma}:C:\dfrac{\partial g_s}{\partial \sigma}-H_{cs}\right]d\lambda^s+\left[\dfrac{\partial f_c}{\partial \sigma}:C:\dfrac{\partial g_c}{\partial \sigma}-H_c\right]d\lambda^c \\ \qquad =\dfrac{\partial f_c}{\partial \sigma}:C:d\varepsilon+\left[\dfrac{\partial f_c}{\partial \sigma}:C':\varepsilon^e+\dfrac{\partial f_c}{\partial d_c}\right]\dot{d}_c \end{cases} \tag{2-41}$$

$$H_s=\frac{\partial f_s}{\partial \alpha^p}\frac{\partial \alpha^p}{\partial \gamma^p}h_s$$

$$H_{sc}=\frac{\partial f_s}{\partial \alpha^p}\frac{\partial \alpha^p}{\partial \gamma^p}h_c$$

$$H_c=\frac{\partial f_c}{\partial \bar{\sigma}}\frac{\partial \bar{\sigma}}{\partial \varepsilon_v^c}tr\left(\frac{\partial g_c}{\partial \sigma}\right)-\frac{\partial f_c}{\partial \phi}(1-\phi)tr\left(\frac{\partial g_c}{\partial \sigma}\right)$$

$$H_{cs}=\frac{\partial f_c}{\partial \phi}(1-\phi)tr\left(\frac{\partial g_s}{\partial \sigma}\right)$$

In these relations, the two coefficients H_{sc} and H_{cs} represent the coupling effects between the hardening functions of the two plastic mechanisms. In general case, plastic shearing induced plastic compaction or dilation may affect plastic hardening of pore collapse mechanism. Inversely, pore collapse mechanism generates also plastic shear strains, which will affect plastic hardening of shearing mechanism. However, in some particular cases, a simplified version can be used. In the present work, based on the experimental results for similar porous materials (porous chalk), it seems that the hardening functions of the two plastic mechanisms for cementitious materials can be assumed to be independent each other. Thus, we take $H_{sc}=H_{cs}=0$.

2.3 Determination of Parameters

The parameters of the model have been determined from conventional laboratory tests (Yurtdas, 2006). The first series of tests were performed on sound cement paste, and the other one was on totally damaged cement by nitrate ammonium solution. Each series are composed of triaxial compression tests at different confining pressures and hydrostatic compression test.

Note that only a small number of tests are available for the studied cement paste. Ideally, more series are expected to more precisely determine the evolution of the leaching damage degree in different loading conditions and to evaluate possible uncertainties of experimental data. For instance, we do not have experimental data on mechanical properties of partially degraded material. Therefore, some extrapolation is assumed between the sound and fully degraded states.

2.3.1 Elastic Parameters

At the beginning of deviatoric loading, we can observe an elastic behaviour phase on the stress-strain curve. The initial elastic modulus of material can be calculated with the measurement of the axial deformation according to the current stress:

$$E = \frac{\Delta\sigma_{11}}{\Delta\varepsilon_{11}}$$

In some cases, it is generally difficult to capture this initial linear elastic phase. The elastic modulus can then be identified from cycles of unloading-recharging performed during the first stage of loading. Furthermore, for the most geomaterials, the elastic modulus generally depends on confining pressure, for example, the elastic modulus increases with the confining pressure. This increase is generally related to the closing of initial microcracks contained in the material. However, this variation is not significant for the cement paste studied. The average values of elastic parameters obtained in various triaxial compression tests are then used. The Poisson's ratio is calculated by comparing the variations of the lateral and radial strains in the elastic phase, that is to say:

$$\upsilon = -\frac{\Delta\varepsilon_2}{\Delta\varepsilon_1}$$

2.3.2 Parameters for deviatoric mechanism

The proposed model contains 6 parameters for the deviatoric plastic mechanism: two define the failure surface (n, C), three for the deviatoric plastic hardening law (α_0, B, β) and one determines the boundary between compressibility and dilatancy (η).

Parameters *n*, C

These two parameters can be obtained from peak stresses in triaxial compression tests with different confining pressures. Fig. 2-1 to Fig. 2-6 show the values of deviatoric stress at failure state (peak point of stress –strain curves). Putting the values of failure stress of each test in the plan (p, q), thus the nonlinear failure surface (curve) can be identified by 3 points (at least). An additional assumption is introduced here: the uniaxial tensile strength is equal to 1/10 of uniaxial compression strength. Fig. 2-14 shows the failure surfaces (lines) obtained for sound and fully damaged materials.

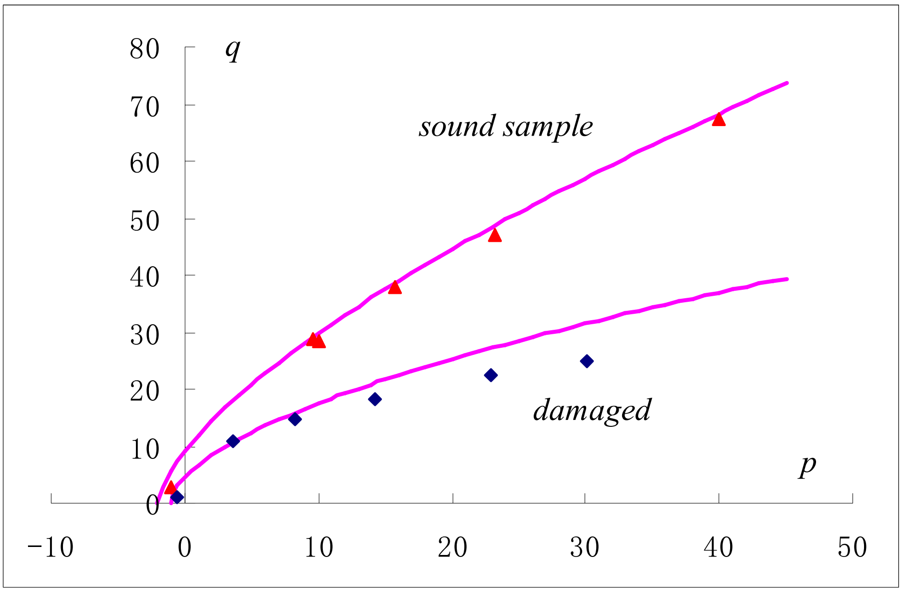

Figure 2-14: Failure surfaces for sound and fully degraded materials

Fig. 2-15(a) represents the sensitivity of failure surface to covertures coefficient n. Indeed, this parameter affects the internal friction angle of material; higher its value is, larger the failure opening surface is, corresponding to higher initial frictional angle. More significantly, when the value of n is higher, the dependency of failure surface on hydrostatic stress is more important. When $n=1$, one recovers the classical linear Drucker-Prager failure surface. The parameter C is related to the cohesion of material. In the Fig. 2-15(b), the influence of this parameter is presented.

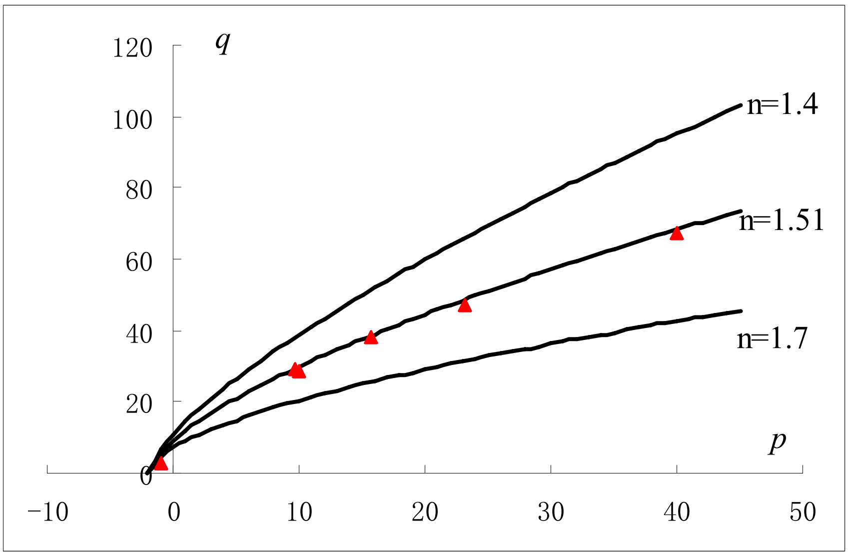

Figure 2-15(a): Influence of parameter n on failure surface

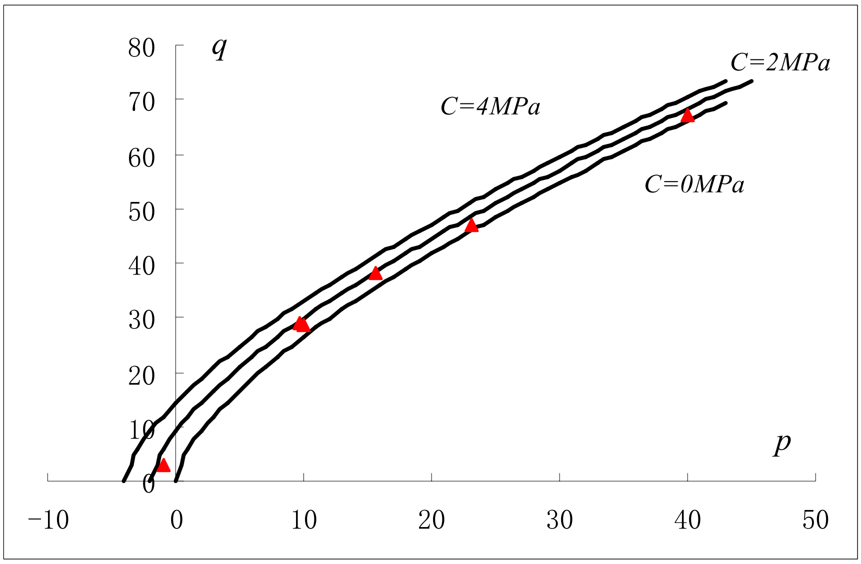

Figure 2-15(b): Influence of parameter C on failure surface

Parameters B, β, α_0

The parameter B controls the kinetics of plastic hardening, β makes it possible to take account of the influence of confining pressure on plastic hardening process and α_0 denotes the initial value of the plastic hardening. In order to determine the plastic hardening law, an iterative procedure is used. Normally, the experimental data of triaxial compression at low confining pressure is used to obtain the values of these parameters because the pore collapse mechanism is not activated in such cases. At first, neglect the influence of confining pressure and putting $\beta = 0$. According to Eq. (2-19) and experimental data, we draw the curve $\alpha - \gamma_s$ as shown in Fig. 2-16. We can see that the hyperbolic law can well describe this curve and then the values of B and α_0 can be deduced. Once B and α_0 are determined, for each test with different confining pressure, the hardening plastic law is finally obtained by the determination of β. Fig. 2-17 shows the relation between the normalizing coefficient χ_p and confining pressure using the value of parameter β.

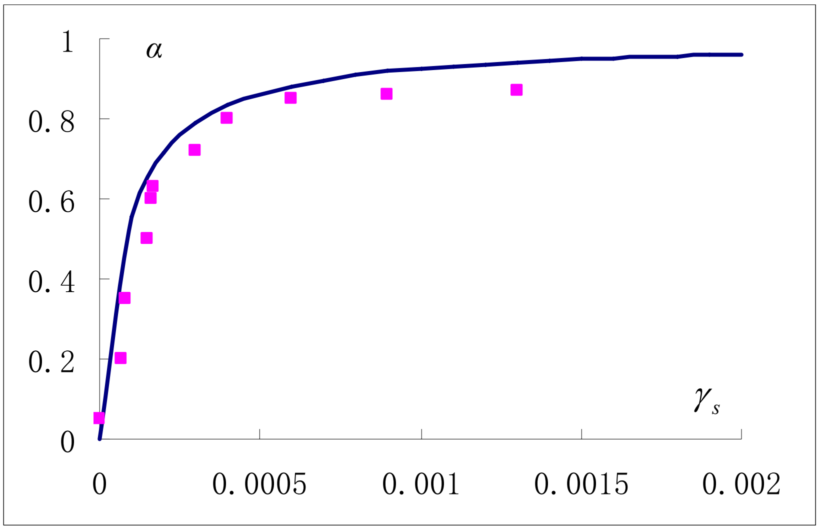

Figure 2-16: Evolution of hardening function α with plastic distortion variable γ_s

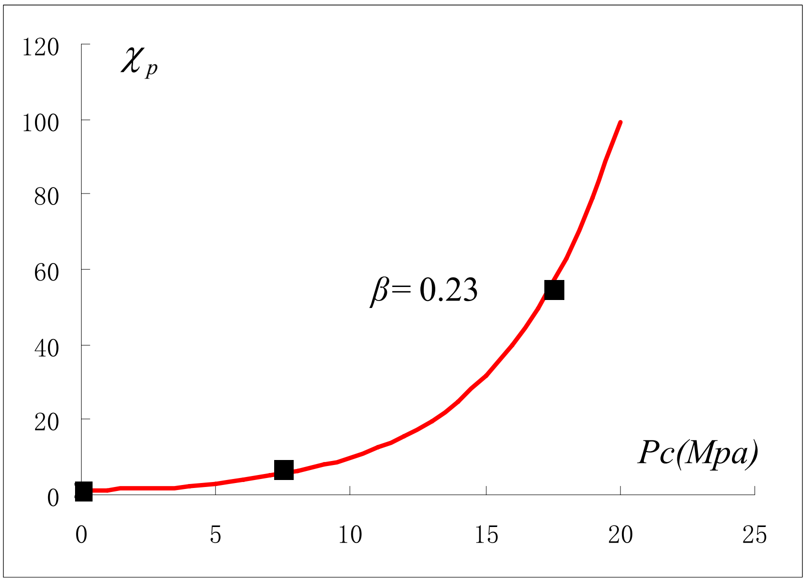

Figure 2-17: Variation of normalizing coefficient in deviatoric plastic hardening law and determination of parameter β

In order to determine the parameter η, which represents the slope of the boundary line between the zone of compressibility and that of dilatancy, it is first necessary to find the point of transition from volumetric strain curve in each triaxial test, as illustrated in Fig. 2-18. Then, we collect all the transition points in the $p-(q-C)$ plan (see Fig. 2-19), and easily deduce the value for η.

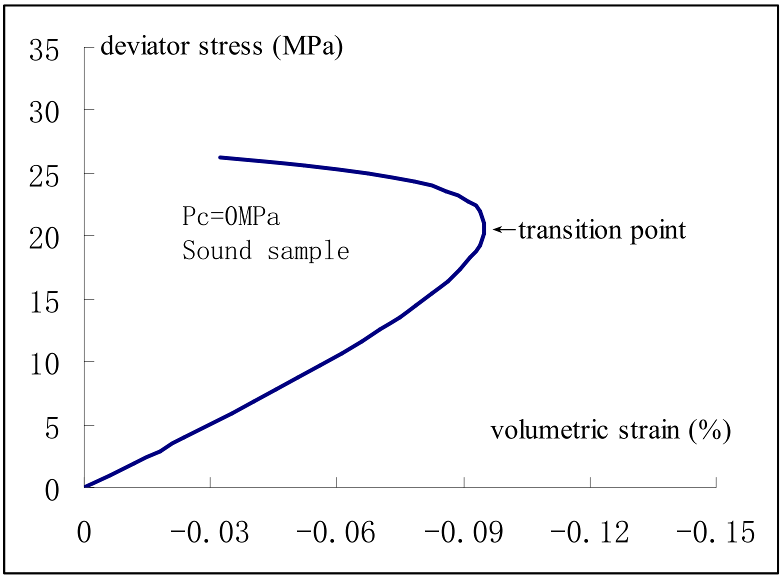

Figure 2-18: Determination of transition point between volumetric compressibility and dilatancy

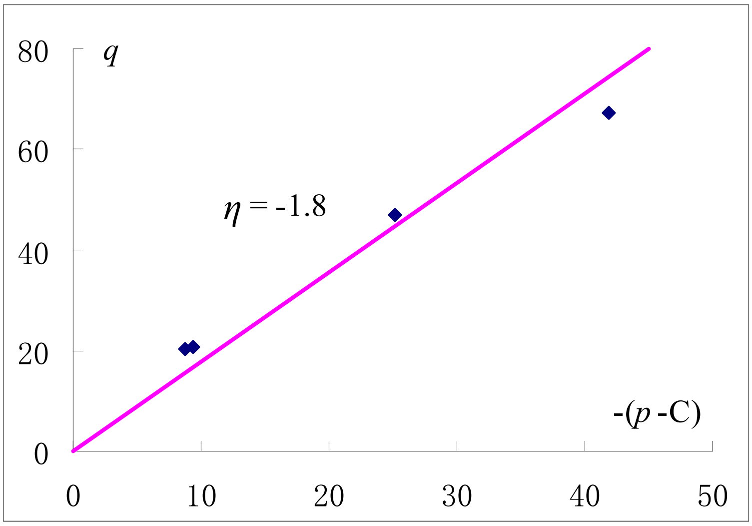

Figure 2-19: Transition line between dilatancy and compressibility η

2.3.3 Parameters for pore collapse mechanism

There are 4 parameters involved in the pore collapse mechanism. The parameter q_2 describes the geometrical form of the cap yield surface and the other three parameters a , m , b determine the pore collapse plastic hardening law.

Fig. 2-20 shows the choice of the parameter q_2 for chemically degraded sample.

This value is determined from the hydrostatic test and triaxial tests at high confining pressure (for instance $Pc = 10MPa$). Based on the experimental data, two experimental points can be obtained and the plastic yield surface can be identified from these points. In this figure, the influence of q_2 is illustrated: when this value increases, the corresponding plastic threshold in hydrostatic compression decreases.

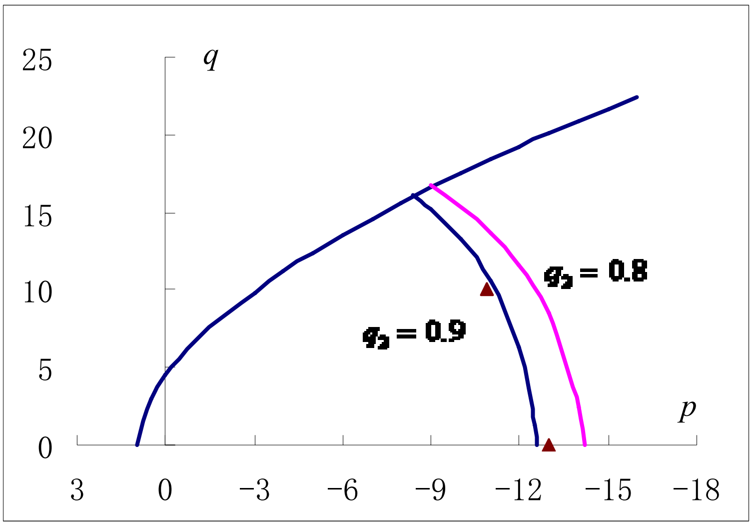

Figure 2-20: Determination of parameter q_2

The set of three parameters a, m, b determines the rate of pore collapse plastic strain. Fig. 2-21 shows the influence of each parameter on mechanical response under hydrostatic compression test.

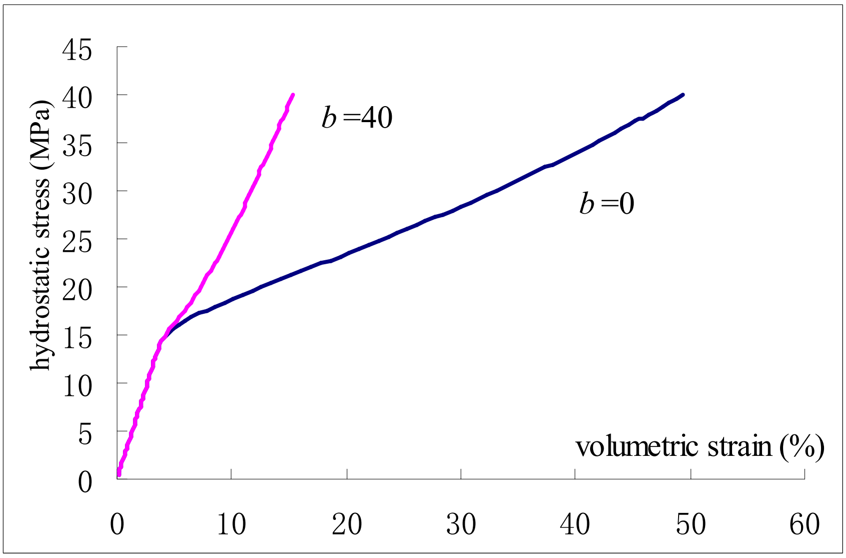

Figure 2-21(a): Influence of parameter b on hydrostatic stress – volumetric strain curve

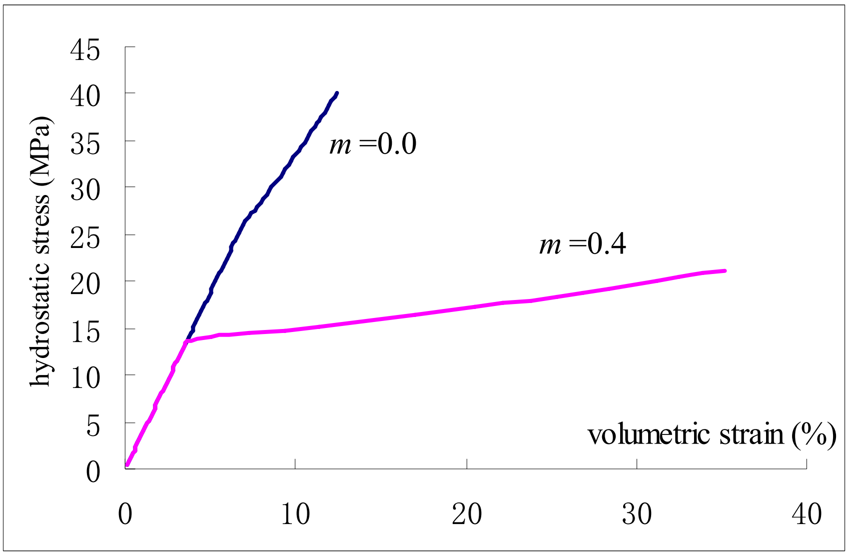

Figure 2-21(b): Influence of parameter m on hydrostatic stress – volumetric strain curve

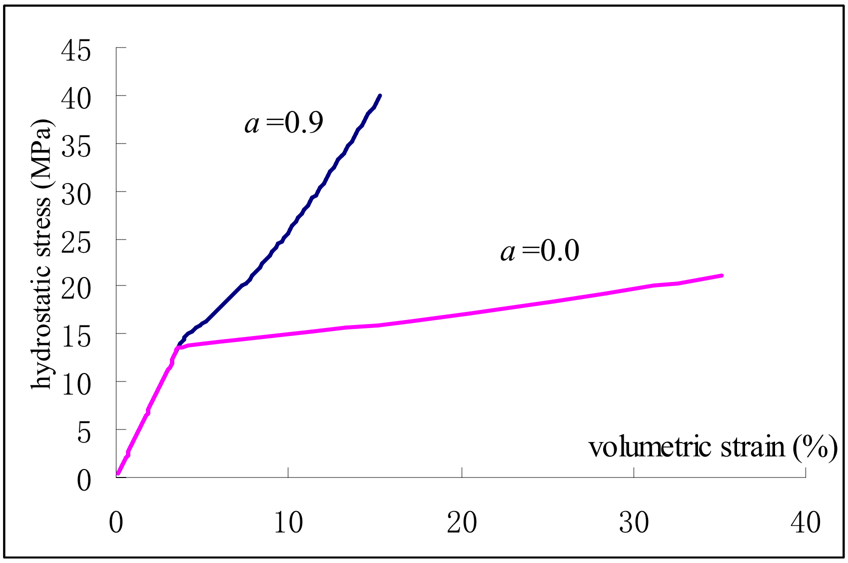

Figure 2-21(c): Influence of parameter a on hydrostatic stress – volumetric strain curve

2.3.4 Influences of chemical damage

Using the procedure presented in the previous section, all the parameters of elastoplastic model have been determined respectively for sound and fully degraded cements paste. Table 2-1 presents the typical values obtained.

Table 2-1: Typical values of model's parameters respectively for sound and fully degraded cements pastes

Parameters	Sound state	Degraded state
Initial Young's modulus $E\ (MPa)$	5000	2700
Initial Poisson's ratio υ	0.35	0.19
Plastic shear failure parameter n	1.51	1.73
Plastic shear failure parameter A	14	14
Plastic shear failure parameter $C\ (MPa)$	2.0	1.0
Plastic shear failure parameter B	8E-5	2E-4
Plastic shear failure parameter α_p	0.0	0.0
Plastic shear failure parameter β	0.23	0.23
Compressibility-dilatancy transition η	-1.8	-1.8
Initial pore collapse yield stress $\overline{\sigma}^0\ (MPa)$	70	32
Pore collapse yield function parameter q_2	0.9	0.9
Pore collapse yield function parameter b_0	180	40
Pore collapse yield function parameter a	0.9	0.9
Pore collapse yield function parameter m	0.4	0.4

One can clearly observe that the chemical damage affects not only elastic properties but also plastic behaviour. Using a fully phenomenological approach here, we try to capture the variations of main parameters as functions of chemical damage variable. Note that the damage value corresponding to fully degraded material is $d_c = 0.19$.

As before mentioned, the chemical damage affects the elastic bulk modulus and shear modulus through the following relations:

$$k(d_c) = \frac{k_0}{1+\alpha_1 d_c} \quad \text{and} \quad \mu(d_c) = \frac{\mu_0}{1+\alpha_2 d_c}$$

Using the values of elastic parameters obtained from sound and degraded samples, the values of α_1 and α_2 can be deduced.

Furthermore, comparing the values of parameters for plastic description between the sound and degraded materials, we can find that the following plastic parameters are affected by chemical damage and the following empirical relations are determined:

$$n = n_0 + \alpha_3 d_c,\quad B = \frac{B_0}{1-\alpha_4 d_c},\quad C = \frac{C_0}{1+\alpha_5 d_c},\quad \bar{\sigma}^0 = \frac{\bar{\sigma}_0^0}{1+\alpha_6 d_c},\quad b = \frac{b_0}{1+\alpha_7 d_c} \tag{2-42}$$

The values of all the parameters involved in these relations are given in Table 2-2:

Table 2-2: Values of parameters used for influence of chemical damage on elastic and plastic properties

Parameters	α_1	α_2	α_3	α_4	α_5	α_6	α_7
	14.9	3.35	1.21	3.16	5.26	6.25	18.42

2.4 Implementation of constitutive model and numerical Simulation

2.4.1 Implementation of constitutive model

The proposed elastoplastic model taking into account chemical degradation is implemented into the finite element code THMPASA developed at the LML. This code has been developed for numerical modeling of coupled thermo-hydro--mechanical evolution problems in saturated and unsaturated porous media.

In the context of FEM method, the nodal displacements, pore pressure, temperature and calcium concentration in fluid are taken as main unknowns. The loading path is divided into a number of steps (increments). At the loading step k, the governing equations are verified in the global system in weak form. The evolution of chemical damage is determined through a specific block in this code, devoted to numerical modeling of chemical diffusion process. This feature will be discussed in the next chapter.

The local integration of constitutive equations consists to update stress, plastic strain and internal variables according to loading history and current increments of displacements (strains), pore pressures, temperature and chemical damage.

At each material point (called Gauss integration point), local increments of strains, pore pressures, temperature and chemical damage are extracted from global system. Let i the current iteration number. At the beginning of the iteration, the set of state and internal variables are known: $\sigma^{(k,i-1)}$, $\varepsilon^{(k,i-1)}$, $\varepsilon^{e(k,i-1)}$, $d_c^{(k,i-1)}$, $\gamma^{s(k,i-1)}$ and $\varepsilon_v^{c(k,i-1)}$.

1. Given increments of total strain and chemical degradation so that $\varepsilon^{(k,i)} = \varepsilon^{(k,i-1)} + \Delta\varepsilon^{(k,i)}$ and $d_c^{(k,i)} = d_c^{(k,i-1)} + \Delta d_c^{(k,i)}$.
2. Update the elastic and plastic properties with the current value of chemical damage.
3. Assume an fully elastic behavior, perform the elastic prediction: $\Delta\hat{\sigma}^{(k,i)} = C(d^{(k,i)}) : \Delta\varepsilon^{(k,i)}$, $\hat{\sigma}^{(k,i)} = \sigma^{(k,i-1)} + \Delta\hat{\sigma}^{(k,i)}$. Check the yield functions $f_s(\hat{\sigma}^{(k,i)}, \gamma^{(k,i-1)}, d_c^{(k,i)})$ and $f_c(\hat{\sigma}^{(k,i)}, \gamma^{(k,i-1)}, d_c^{(k,i)})$. If $f_c<0$ and $f_s<0$, the elastic prediction is then taken as the reel solution. Then go to (6).
4. Else, calculate increments of plastic strains according to loading path using Eq. (2-30) or Eq. (2-39) or Eq. (2-41).
5. Update stress, strain and internal variables.
6. $\sigma^{(k,i)} = \hat{\sigma}^{(k,i)} - C(d_c^{(k,i)})(\Delta\varepsilon^{c(k,i)} + \Delta\varepsilon^{c(k,i)})$.
7. Exit and send back the updated values to global system.

2.4.2 Numerical Simulations

In this section, we present numerical simulations of laboratory tests performed on both sound and chemically degraded samples. As each sample is seen as the representative volume element of material testes, it is assumed a uniform distribution of stress, strain and chemical damage inside the sample. Therefore, only average responses of samples are discussed here. The model's parameters used in the simulations are given in Table 2-1. Note that the simulations presented here represent a first phase of validation of the proposed model.

Triaxial compression tests on sound sample are first studied. Fig. 2-22 to Fig. 2-24 show the comparisons between model's predictions and experimental data for various confining pressure. In an overall way, there is a good agreement between the simulations and test data. The proposed model correctly predicts the main features of mechanical behaviour of cement paste.

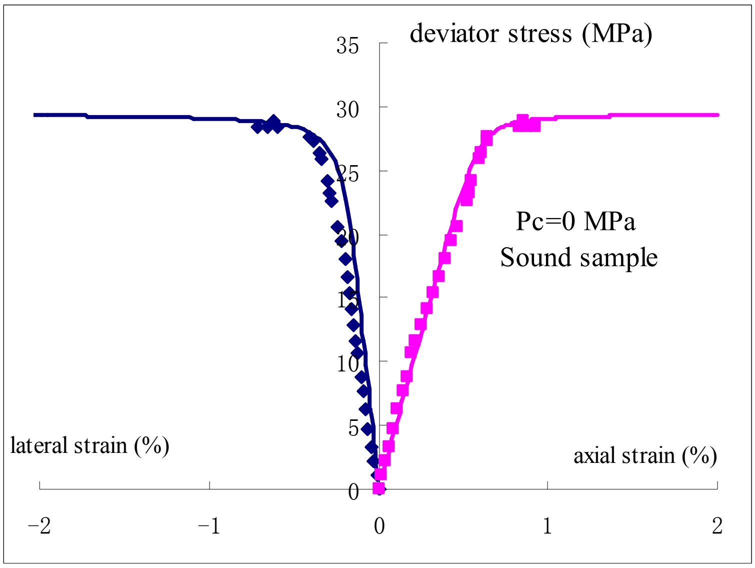

Figure 2-22: Comparisons between numerical simulations (continuous lines) and experimental data in triaxial compression test at $P_c = 0\text{MPa}$ on sound sample

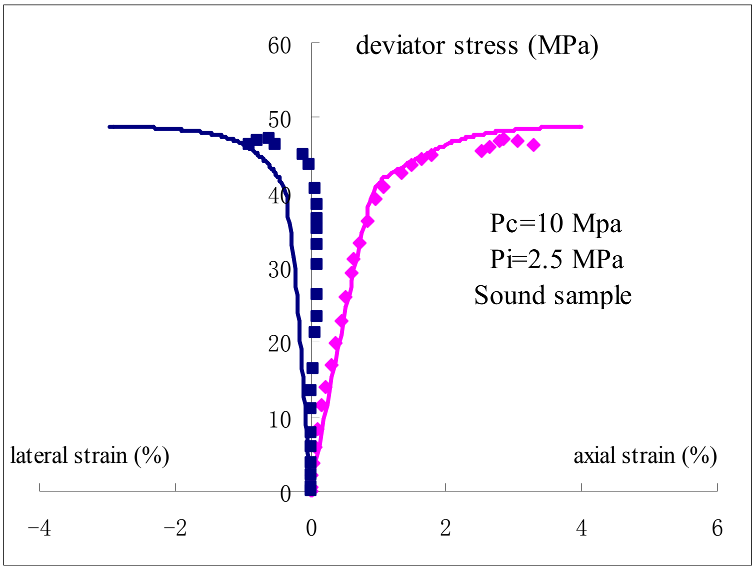

Figure 2-23: Comparisons between numerical simulations (continuous lines) and experimental data in triaxial compression test at $P_c = 10\text{MPa}$ and $P_i = 2.5\text{MPa}$ on sound sample

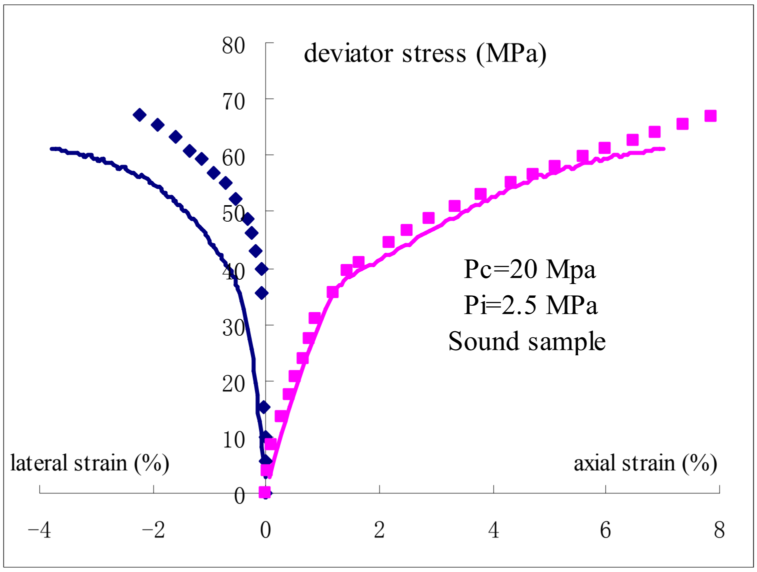

Figure 2-24: Comparisons between numerical simulations (continuous lines) and experimental data in triaxial compression test at $P_c = 20\text{MPa}$ and

$P_i = 2.5\text{MPa}$ on sound sample

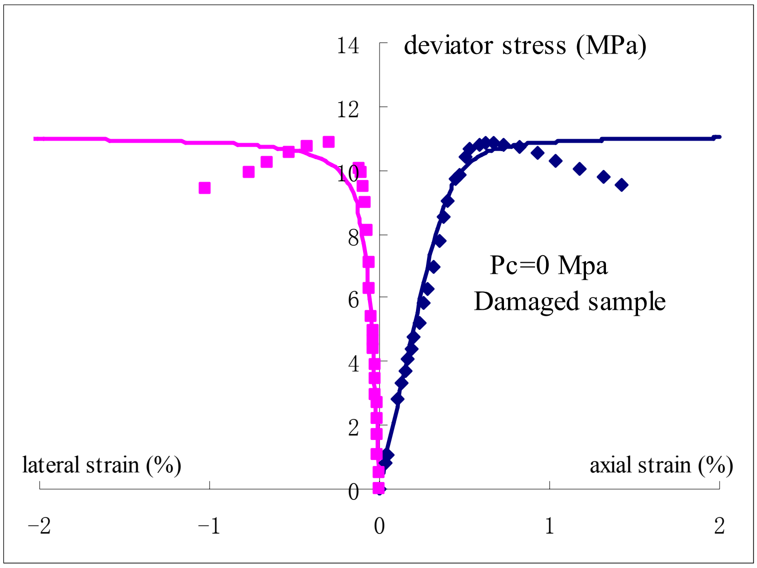

Figure 2-25: Comparisons between numerical simulations (continuous lines) and experimental data in triaxial compression test at $P_c = 0\text{MPa}$ on chemically degraded sample

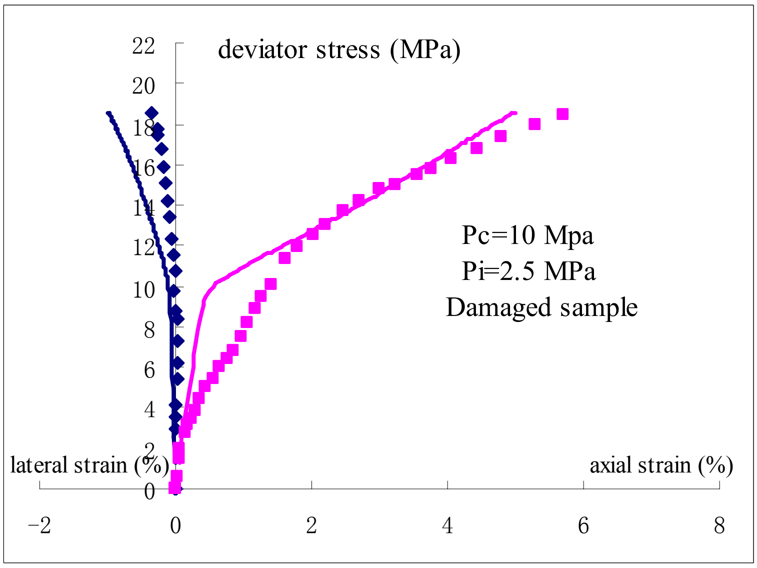

Figure 2-26: Comparisons between numerical simulations (continuous lines) and experimental data in triaxial compression test at $P_c = 10\text{MPa}$ and

$P_i = 2.5\text{MPa}$ on chemically degraded sample

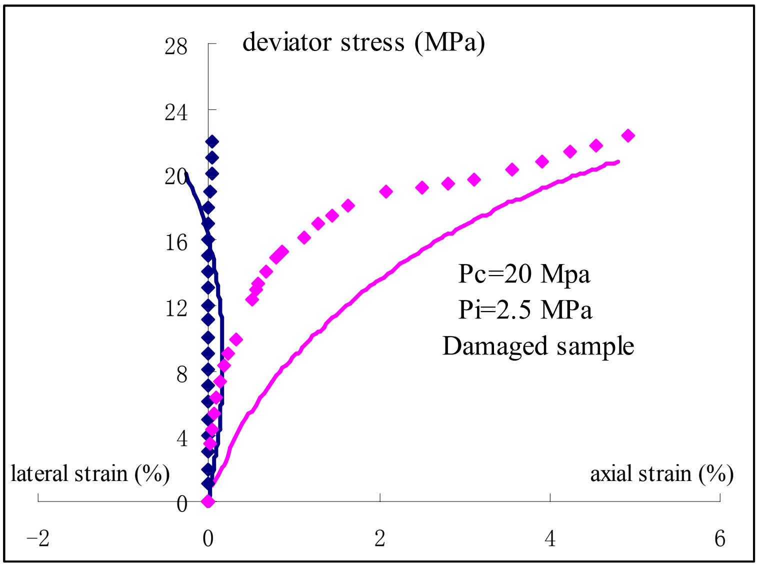

Figure 2-27: Comparisons between numerical simulations (continuous lines) and experimental data in triaxial compression test at $P_c = 20\text{MPa}$ and $P_i = 2.5\text{MPa}$ on chemically degraded sample

In Fig. 2-25 to Fig. 2-27, the simulations of triaxial compression tests on chemically degraded samples are presented. Again, one can also find a good agreement between the simulations and tests data. It seems that the proposed model corrects the mechanical responses of chemically degraded samples and the effect of chemical degradation of cement paste is well captured. Finally, we show the simulation of hydrostatic compression test on chemically degraded sample in Fig. 2-28. The response of cement paste in this loading path is also well described.

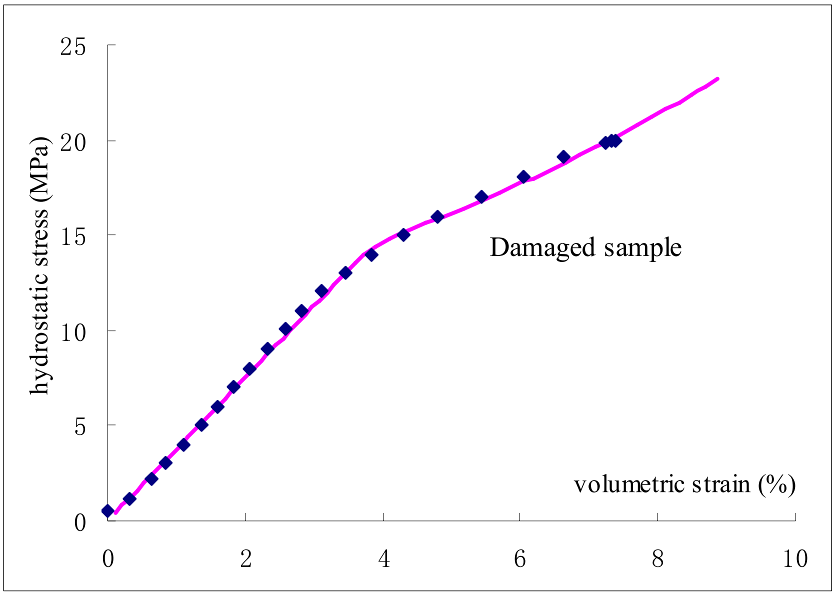

Figure 2-28: Comparisons between numerical simulations (continuous lines) and experimental data in hydrostatic compression test on chemically degraded sample

2.5. Conclusions

In this chapter, we have presented the formulation of an elastoplastic model for cement paste under compression-dominated stresses. Based on relevant experimental data performed both on sound and chemically degraded sample, two plastic mechanisms are identified: deviatoric mechanism and pore collapse mechanism. Compared the mechanical responses of cement paste between sound and degraded samples, the effects of chemical damage on mechanical behaviour of cement have been taken into account. Both elastic and plastic properties are affected by chemical damage. We have then proposed an identification procedure for the determination of model's parameters. The proposed model is implemented in a computer code using finite element method for coupled THM-C problems. We have applied the proposed model to simulate typical laboratory tests. It seems that the proposed model is able to describe the main features of mechanical behaviour of cement paste in sound and degraded states.

In the next chapter, we will deal with numerical modelling of chemical diffusion problem to determine the evolution of chemical damage.

Chapter 3: Coupling of chemical degradation process and mechanical response

3.1 Introduction

In the previous chapter, we have presented an elastoplastic model for cement paste taking into account effects of chemical degradation on elastic and plastic properties. However, the chemical damage was considered as given data for each loading step. Indeed, it is assumed that the damage evolution is fully governed by chemical dissolution and diffusion process. In this chapter, we will deal with the determination of chemical damage evolution.

3.2 Phenomenological chemistry model for calcium leaching

As mentioned in chapter 1, the calcium leaching of calcium from solid skeleton is the main mechanism of chemical degradation in cement paste affecting mechanical properties. The kinetics of chemical leaching is controlled by the diffusion of calcium ions in pore fluid. The chemical damage is directly related to the increase of porosity which may be determined by mass balance equation of calcium ion exchange.

3.2.1 Generalized diffusion equation

As before mentioned, at a natural (reference) state, the calcium concentration in pore fluid C_a^{++} is in equilibrium with that in solid skeleton C_a^{solid}. When the cement paste is in contact with aggressive fluid on its exterior boundary, the chemical equilibrium is broken. The calcium is dissolved from solid skeleton and is diffused inside pore fluid. The chemical dissolution and diffusion of calcium ions must verify the general mass balance equation. However some assumptions are necessary to simply modeling:

- all solid phases can be modeled using the concepts of thermodynamic equilibrium;
- the time required to dissolve solid calcium is very short compared to the diffusion time;
- The material is and remains saturated over time and isothermal conditions are preserved;
- The cement paste is considered as an isotropic porous medium.

Based on these assumptions, the mass balance equation reads:

$$\frac{\partial\left(\phi C_a^{++}\right)}{\partial t} = -\mathrm{div}\Phi_{C_a^{++}} + M^0_{C_a^{solid}\to C_a^{++}} \tag{3-1}$$

C_a^{++} is the calcium concentration of the pore solution, ϕ is the porosity, $\Phi_{C_a^{++}}$ is the flux of calcium ions. And $M^0_{C_a^{solid}\to C_a^{++}}$ describes the quantity of calcium dissolved in the liquid phase per unit of time which can be rewritten as:

$$M^0_{C_a^{solid}\to C_a^{++}} = -\frac{\partial C_a^{solid}}{\partial t} = -\frac{\partial C_a^{solid}}{\partial C_a^{++}}\cdot\frac{\partial C_a^{++}}{\partial t} \tag{3-2}$$

The flux of calcium ions is given by Fick's law:

$$\vec{\Phi}_{C_a^{++}} = -D_{C_a^{++}}.\vec{\nabla}(C_a^{++}) \tag{3-3}$$

where $D_{C_a^{++}}$ is the effective diffusion coefficient which can depend on calcium concentration in fluid, temperature and mechanical deformation of material (Gérard, 2000; Mainguy, 2000).

Introducing Eq. (3-2) and Eq. (3-3) into Eq. (3-1), one gets the generalized diffusion equation of calcium concentration in pore fluid:

$$\left[C_a^{++}\frac{\partial\phi}{\partial C_a^{++}}+\phi\left(C_a^{++}\right)+\frac{\partial C_a^{solid}}{\partial C_a^{++}}\right]\cdot\frac{\partial C_a^{++}}{\partial t}=\operatorname{div}\left[D(C_a^{++})\cdot\vec{\nabla}(C_a^{++})\right]\tag{3-4}$$

In the bracket, the first two terms correspond to effect of porosity change on calcium diffusion process and the third one is related to phase change of calcium ions. Generally, the effect related to the phase change, $\frac{\partial C_a^{solid}}{\partial C_a^{++}}$ is dominant compared to the other ones (Delagrave, 1997). Therefore, it is possible to simply the generalized diffusion equation by neglecting the first two terms in the bracket.

$$\frac{\partial C_a^{solid}}{\partial C_a^{++}}\cdot\frac{\partial C_a^{++}}{\partial t}=D(C_a^{++})\cdot\nabla^2\left(C_a^{++}\right)\tag{3-5}$$

where ∇^2 is the Laplace operator. This equation is a partial differential equation that describes the calcium ions diffusion process in pore fluid. Note that this diffusion equation is strongly non-linear in nature due to the dependency of diffusion coefficient on various factors and also to non linear phase change equation.

3.2.2 Phase change relation

In the generalized diffusion Eq. (3-5), the term $\frac{\partial C_a^{solid}}{\partial C_a^{++}}$ still needs to be determined. This term represents the derivative of calcium ions in solid skeleton with respect to calcium concentration in pore fluid. Therefore, it should be determined from the chemical equilibrium curve between C_a^{solid} and C_a^{++}. As mentioned in the chapter 1, this equilibrium curve should be determined from laboratory data. In this work, we have adopted the data obtained by Berner (1992) on cement paste, as shown in Fig. 3-1.

As already analyzed, this curve contains three phases of dissolution. In the first phase, the calcium content in solid skeleton decreases quickly corresponding to the dissolution of Portlandite. During the second phase, the dissolution rate is smaller than that in the first phase and we have essentially the dissolution of partial C-S-H and other hydrates. Finally, there is a sharp diminution of solid calcium until the complete dissolution of calcium in solid skeleton. To distinguish these three phases, two characteristic values of C_a^{++} are generally defined, respectively equal to 19 and 2 mol/m^3. These two characteristic values define the transition point between the three dissolution phases.

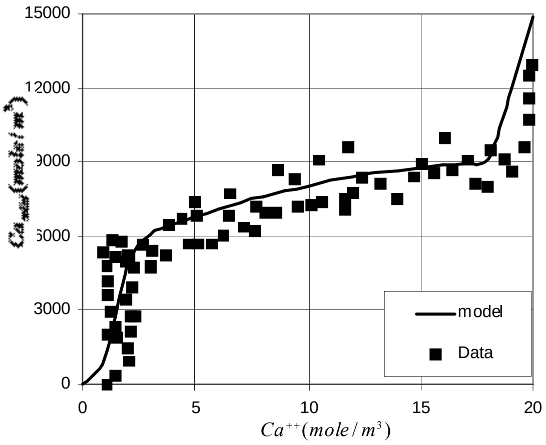

Figure 3-1: Chemical equilibrium curve between solid calcium C_a^{solid} and calcium concentration in pore fluid C_a^{++} : experimental data by Berner (1992) and phenomenological chemistry model by Gerard (1996)

Based on the experimental data given by Berner (1992), Gerard (1996) established a phenomenological chemistry model which describes the chemical equilibrium curve as follows:

$$C_a^{solid} = a - b(C_a^{++})^2 + cC_a^{++} - \left[\frac{e}{1+\left(\dfrac{C_a^{++}}{x_2}\right)^n} + \frac{f}{1+\left(\dfrac{C_a^{++}}{x_1}\right)^m} \right] \quad (3\text{-}6)$$

In this expression, a, b, c, e, f are the parameters of the empirical model. The values of these parameters only depend on the proportion of calcium in the cement paste. Gerard (1996) proposed to determine these parameters from the molar fraction of Portlandite (S_{por}) and the total calcium content of the hydrated cement past (S_{tot}); the following empirical relations have been proposed:

$$e = Spor \ , \qquad f = 0.565(Stot - Spor), \quad b = (Stot - Spor - f)/400 \ ,$$
$$c = (Stot - Spor - f)/20 + 20b \ , \quad a = Spor + f$$

m, n are two controlling parameters which can vary between 1 to 100. The parameters x_1, x_2 define the transition between three dissolution phases. As mentioned above, they are about 2 and $19\,\mathrm{mol/m^3}$. Fig. 3-1 shows the comparison between experimental data and mathematical description of equilibrium curve.

Using the empirical law (3-6), the derivative $\frac{\partial C_a^{solid}}{\partial C_a^{++}}$ can be easily deduced:

$$\frac{\partial C_a^{solid}}{\partial C_a^{++}} = -bC_a^{++} + c - \left[\frac{1}{x_2^n} \cdot \frac{e \cdot n \cdot C_a^{++(n-1)}}{\left(1 + \left(\frac{C_a^{++}}{x_2}\right)^n\right)^2} + \frac{1}{x_1^m} \cdot \frac{f \cdot m \cdot C_a^{++(m-1)}}{\left(1 + \left(\frac{C_a^{++}}{x_1}\right)^m\right)^2} \right] \tag{3-7}$$

3.2.3 Diffusion coefficient

According to the generalized diffusion equation, the diffusion coefficient is the main factor controlling the kinetics of diffusion of calcium concentration in pore fluid. A series of studies (Bentz and Garvoczi, 1992; Gérard, 1996) have shown that the diffusion coefficient depends on the volume fractions of various hydrate species, temperature, and possibly mechanical deformation. Under isothermal conditions and neglecting effect of mechanical deformation on diffusion process, we have adopted the following relations proposed in the phenomenological chemistry model by Gérard (1996):

$$D = D_s \left(\frac{D_0}{D_s} \right)^{\frac{\beta V_{por}^d + \alpha V_a^d}{V_{por}^i + V_a^i}}, \qquad \alpha = (1-\beta)\frac{V_{por}^i}{V_a^i} + 1, \qquad 0 < \beta < \frac{V_a^i + V_{por}^i}{V_{por}^i} \tag{3-8}$$

Where D_0 and D_s are respectively the initial (sound material) and asymptotic (fully degraded material) isotropic diffusion coefficients. V_{por} and V_a denote the volume fraction of Portlandite and that of all other hydrates respectively. The indices d and i indicate respectively the degraded and initial state. The departure of the Portlandite can be responsible for the opening of a macroporosity. Thus, this increases significantly the diffusivity of the porous medium. Because of this reason, the coefficient β is introduced to translate the scale effect that describes the contribution of the dissolution of Portlandite on the increase of the coefficient of diffusion. We have shown the effect of the parameter β on the variation of diffusion coefficient with calcium concentration (Fig. 3-2).

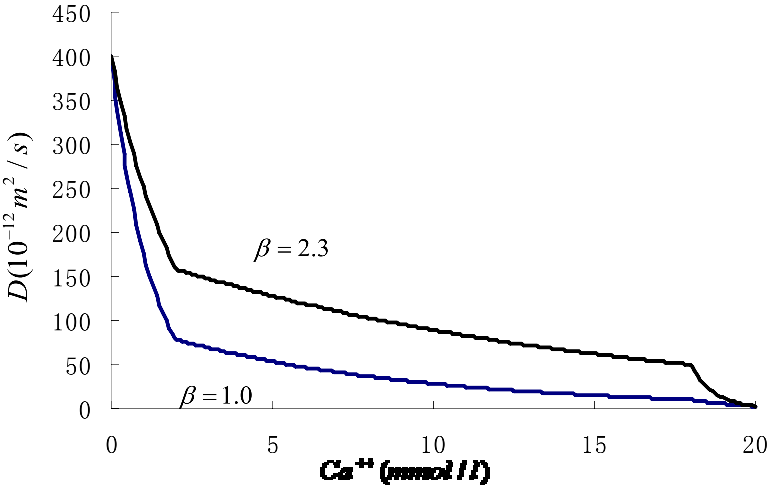

Figure 3-2: Effect of parameter β on the evolution of diffusion coefficient with calcium concentration in pore fluid

Further, as the chemical dissolution kinetics is controlled by diffusion process, it is obvious that the diffusion coefficient should depend on the chemical nature of fluid. Consider the pure water as a reference fluid and the corresponding diffusion coefficient as the reference value. The actual diffusion coefficient associated with another aggressive fluid can be obtained by multiplying the reference value by an appropriate amplification factor. Let λ_t be such a multiplier, the actual diffusion coefficient corresponding to a specific aggressive fluid is given by $\lambda_t D$. The determination of the multiplier is based on relevant experimental data in different dissolution conditions; for instance, comparing the diffusion kinetics between pure water and nitrate ammonium.

3.3 Numerical implementation

For the numerical solution of the generalized diffusion equation, a specific block is developed inside the finite element code THMPASA. At this first stage of modeling, influences of mechanical deformation and temperature are not taken into account. The chemical diffusion problem is then solved in an independent way.

Various methods could be used such as finite elements and finite differences method. For the reason of compatibility with the code THMPASA, we have used the finite element method (FEM) for the numerical solution of generalized diffusion equation.

Recalling the partially differential equation for diffusion of calcium ions in pore fluid:

$$f\left(C_a^{++}\right)\frac{\partial C_a^{++}}{\partial t}=D\left(C_a^{++}\right)\cdot\nabla^2\left(C_a^{++}\right) \tag{3-9}$$

In order to simply the notation, we will denote the calcium concentration by C. In the three dimensional Cartesian coordinate system, the diffusion equation is rewritten as:

$$f(C)\frac{\partial C}{\partial t}=D(C)\left[\frac{\partial}{\partial x}\frac{\partial C}{\partial x}+\frac{\partial}{\partial y}\frac{\partial C}{\partial y}+\frac{\partial}{\partial z}\frac{\partial C}{\partial z}\right] \tag{3-10}$$

In order to get physically admissible solution, we need to precise the boundary conditions associated with the specific problem. In general, there are three boundary kinds of conditions:

- prescribed values of the unknown at one part of boundary (Type 1):

  $$C=C_1(x,y,z,t) \qquad at \quad \Gamma_1$$

  Where C_1 is the given concentration value at the boundary

- no concentration diffusion (Type 2)

  $$\frac{\partial C}{\partial n}=0 \qquad at \qquad \Gamma_2$$

  where n is the outward unit normal to the boundary

- prescribed values of the normal derivative of concentration (Type 3)

  $$D\frac{\partial c}{\partial n}+\beta(C-C_a)=0 \qquad at \qquad \Gamma_3$$

  where β is the calcium exchange coefficient at the boundary.

3.3.1 Galerkin's residual method

As mentioned above, this partially differential equation is nonlinear. The numerical solution is based on step by step iterative procedure. The first stage consists in transforming the exact equation to integral weak form. Galerkin's Weighted Residual Method is largely used for this purpose. This method selects the weight functions in a special way: they are chosen from the base (sharp) functions.

After determined its weak form, the second step is the spatial discretization of geometrical domain which is divided into a finite number of elements. Inside each element, the concentration field is approximated as function of their nodal values by introducing sharp functions noted N_i, for instance:

$$C^e(x,y,z,t)=\sum_{i=1}^{m} N_i C_i^e = [N]\{C\}^e \tag{3-11}$$

where m is the number of nodal points. $[N]$ and $\{C\}$ are the column vectors which contain sharp functions and nodal values of calcium concentration:

$$[N]=[N_1 \quad N_2 \cdots N_m]$$
$$\{C\}^e=\begin{bmatrix} C_1^e & C_2^e \cdots C_m^e \end{bmatrix}^T$$

Applying the Galerkin's method to one individual element, we have:

$$\int_{\Omega^E} N_i \left[D\left(\frac{\partial}{\partial x}\frac{\partial C^e}{\partial x}+\frac{\partial}{\partial y}\frac{\partial C^e}{\partial y}+\frac{\partial}{\partial z}\frac{\partial C^e}{\partial z}\right)-f(C)\frac{\partial C^e}{\partial t}\right] d\Omega = 0 \quad \text{i=1,2…m} \tag{3-12}$$

The integration by parts leads to:

$$\int_{\Omega^e}\left[\frac{\partial N_i}{\partial x}(D\frac{\partial C^e}{\partial x})+\frac{\partial N_i}{\partial y}(D\frac{\partial C^e}{\partial y})+\frac{\partial N_i}{\partial z}(D\frac{\partial C^e}{\partial z})+f(C)N_i\frac{\partial C^e}{\partial t}\right]d\Omega$$
$$-\int_{\Gamma^e}DN_i\frac{\partial C^e}{\partial n}d\Gamma=0 \qquad i=1,2,\cdots m \qquad (3\text{-}13)$$

where Ω^e 、 Γ^e are defined as the geometrical domain and boundary surface of the current element. Considering three boundary conditions, we can deduce:

$$\int_{\Gamma^{e1+e2}}DN_i\frac{\partial C^e}{\partial n}=0 \quad , \quad \int_{\Gamma^{e3}}D\frac{\partial C^e}{\partial n}=\int_{\Gamma^{e3}}\beta(C_a-C) \qquad (3\text{-}14)$$

Combining Eq. (3-11) and Eq. (3-14), the integration form for each element is given by:

$$\int_{\Omega^e}D\left[\frac{\partial N_i}{\partial x}\cdot\frac{\partial[N]}{\partial x}+\frac{\partial N_i}{\partial y}\cdot\frac{\partial[N]}{\partial y}+\frac{\partial N_i}{\partial z}\cdot\frac{\partial[N]}{\partial z}\right]\{C\}^e\,d\Omega$$
$$+\int_{\Omega^e}f(C)N_i[N]\left\{\frac{\partial C}{\partial t}\right\}^e d\Omega-\int_{\Gamma_3}\beta N_i\left[C_a-[N]\{C\}^e\right]d\Gamma=0 \qquad (\text{i=1,2,…m}) \quad (3\text{-}15)$$

Assembly all the elements and using the matrix form, we have:

$$\int_{\Omega}D\left[\frac{\partial[N]^T}{\partial x}\cdot\frac{\partial[N]}{\partial x}+\frac{\partial[N]^T}{\partial y}\cdot\frac{\partial[N]}{\partial y}+\frac{\partial[N]^T}{\partial z}\cdot\frac{\partial[N]}{\partial z}\right]\{C\}^e\,d\Omega+$$
$$\int_{\Omega}f(C)[N]^T\left[[N]\{\dot{C}\}^e\,d\Omega\right]-\int_{\Gamma_3}\beta[N]^T\left[C_a-[N]\{C\}^e\right]d\Gamma=0 \qquad (3\text{-}16)$$

where $\{\dot{C}\}^e=\left\{\frac{\partial C}{\partial t}\right\}^e$

This equation can be expressed in matrix form:

$$[R]\{\dot{C}\}+[H]\{C\}=\{F\} \qquad (3\text{-}17)$$

where $R_{ij} = \sum r_{ij}^{e}$, $H_{ij} = \sum (h_{ij}^{e} + g_{ij}^{e})$, $F_{ij} = \sum f_{ij}^{e}$

and

$$r_{ij}^{e} = \int_{\Omega^e} f(C) N_i N_j \, dxdydz$$

$$h_{ij}^{e} = \int_{\Omega^e} D \left[\frac{\partial N_i}{\partial x} \cdot \frac{\partial N_j}{\partial x} + \frac{\partial N_i}{\partial y} \cdot \frac{\partial N_j}{\partial y} + \frac{\partial N_i}{\partial z} \cdot \frac{\partial N_j}{\partial z} \right] dxdydz$$

$$g_{ij}^{e} = \int_{\Gamma_3^e} \beta N_i N_j \, d\Gamma$$

$$f_{i}^{e} = \int_{\Gamma_3^e} \beta C_a N_i \, d\Gamma$$

3.3.2 Temporal discretization

The global system (3-17) to be solved contains time derivative of calcium concentration with time. For numerical solution, the total time interval is then divided into a number of incremental time interval noted by Δt. The time derivative $\dot{C}$ should be approximated by a discrete form. In this work, a finite difference method is used time discretization. If the time interval is small enough, we can draw an assumption that the derivative of concentration $\{\dot{C}\}$ varies linearly, we have:

$$\dot{C}(t - \Delta t + \tau) = \dot{C}_{t-\Delta t} + \frac{\dot{C}_t - \dot{C}_{t-\Delta t}}{\Delta t} \tau \tag{3-18}$$

The integration for above equation leads to

$$C(t - \Delta t + \tau) = \dot{C}_{t-\Delta t} \tau + \frac{\dot{C}_t - \dot{C}_{t-\Delta t}}{\Delta t} \cdot \frac{\tau^2}{2} + G \tag{3-19}$$

If $\tau = 0$, $C(t - \Delta t + \tau) = C_{t-\Delta t}$, one gets $G = C_{t-\Delta t}$. When we choose $\tau = \Delta t$, Eq. (3-19) becomes

$$C_t = C(t) = \dot{C}_{t-\Delta t}\Delta t + \frac{\dot{C}_t - \dot{C}_{t-\Delta t}}{\Delta t}\cdot\frac{\Delta t^2}{2} + C_{t-\Delta t} \tag{3-20}$$

Some arrangements lead to:

$$\left\{\dot{C}\right\}_t = -\left\{\dot{C}\right\}_{t-\Delta t} + \frac{2}{\Delta t}(\{C\}_t - \{C\}_{t-\Delta t}) \tag{3-21}$$

Introducing the time discretization into the global diffusion system (3-17), one obtains:

$$\begin{aligned}\left[[R_n]^{-1}[H_n] + \frac{2}{\Delta t}I\right]\{C_n\} + \left[[R_{n-1}]^{-1}[H_{n-1}] - \frac{2}{\Delta t}I\right]\{C_{n-1}\} \\ = [R_n]^{-1}\cdot\{F\}_n + [R_{n-1}]^{-1}[F]_{n-1}\end{aligned} \tag{3-22}$$

If the time increment is very small, we can suppose that $[R_n]$ is nearly the same as $[R_{n-1}]$, therefore, the simplification for Eq. (3-22) is:

$$([H] + \frac{2[R]}{\Delta t})\{C\}_n + ([H] - \frac{2[R]}{\Delta t})\{C\}_{n-1} = \{F\}_n + [F]_{n-1} \tag{3-23}$$

This system of linear equations can be solved by classical methods. The initial condition is that we know the values of concentration at the $(n-1)^{th}$ time step. At first we assume that the concentration at n^{th} step $\{C\}_n$ is the same as $n-1$ time step; then, using the average value of the n and $n-1$ time step, the matrix $[H]$, $[R]$ can be determined. Also $\{F\}_n$ and $[F]_{n-1}$ are given. After the inversion of the system, the new $\{C\}_n$ can be obtained; at last, comparing the new and old values of $\{C\}_n$, if the absolute error is smaller than 10^{-3}, we think the convergence is obtained; otherwise, updates the old value of n step in place of new value, and return to second step.

3.3.3 Verification

In this section, two important things are focused in our goal. The first is that the convergence of the numerical solution, the second is whether the diffusion model is agreed with the experimental data.

Convergence:

In the criteria of convergence, the time increment must allow the condition $\Delta t \leq \dfrac{2\Delta l^2 \cdot f(C)}{3D(C)}$. For example, consider the uniaxial sample (bar) of 20cm length subjected to deionized water at its left boundary, as shown in Fig. 3-3. Taking the diffusion multiplier coefficient $\lambda_t = 1$.

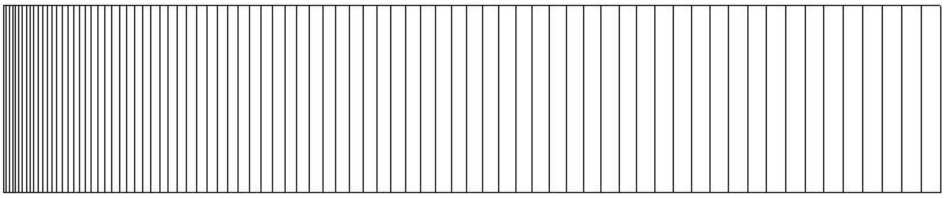

Figure 3-3 Mesh of a 1D simulation to calculate the calcium leaching

Fixed time interval $t = 1\text{day}$:

In this case, we study influences of mesh size. 1-D simulations have been performed using different finite element meshes as shown in Table 3-1.

Table 3-1: Different cases used in 1D simulation

Size of the element $N°1$(mm)	0.001	0.001	0.001	0.01	0.01	0.01	0.05	0.1
Geometrical increase ratio	1.01	1.02	1.03	1.00	1.01	1.02	1.00	1.00
Total Number of elements	300	200	150	200	310	188	200	100

Case Number	1	2	3	4	5	6	7	8

In Fig. 3-4, we show the variation of calcium concentration along with the axis of bar for the different cases studied. One can see that for the size between 0.001mm and 0.01mm, the mesh size has negligible influences on numerical results. However, if the is increased up to 0.05mm, the numerical result is significantly different with those using small sizes. Therefore, preliminary studies should be necessary in order to take an optimal choice of mesh size in view of numerical accuracy and computing time.

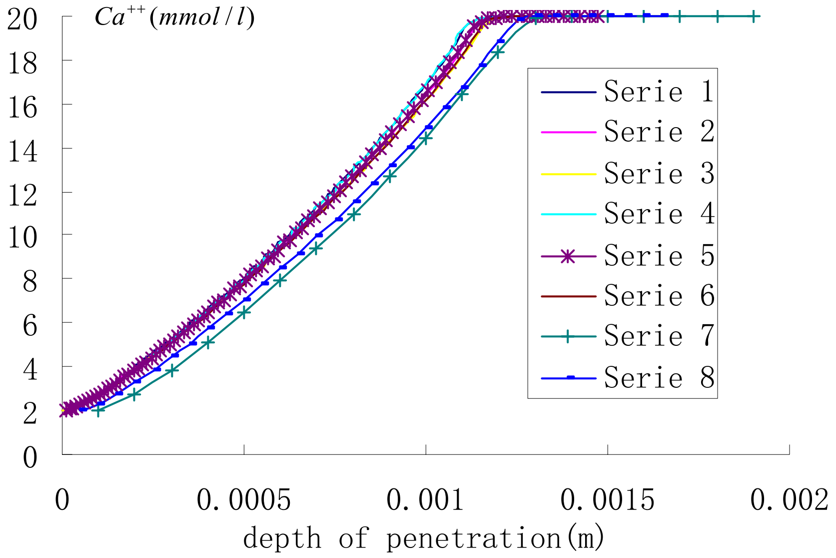

Figure 3-4 C_a^{++} distribution along one dimensional bar for a given period of chemical leaching with different mesh sizes

<u>Fixed mesh size</u> (0.01mm):

Based on the above result, we choose the size of the first element to be 0.01mm and a geometrical ratio as 1.02. The objective now is to study influences of time increment. Table 4-2 shows the series of numerical simulations using different time increments.

Table 4-2: different time increments used in numerical simulations

Time increment (day)	0.05	0.1	0.2	0.5	1	2	4
Case Number	1	2	3	4	5	6	7

The comparisons of numerical results between different cases are shown in Fig. 3-5. One can see that the differences between different cases are very small. However, it appears that with larger time increment, the obtained concentration profile may contain some local irregular variations, as shown in Fig. 3-6 for the case $N°7$. As a conclusion, the numerical results seem to be stable when the time increment is smaller than 1 day.

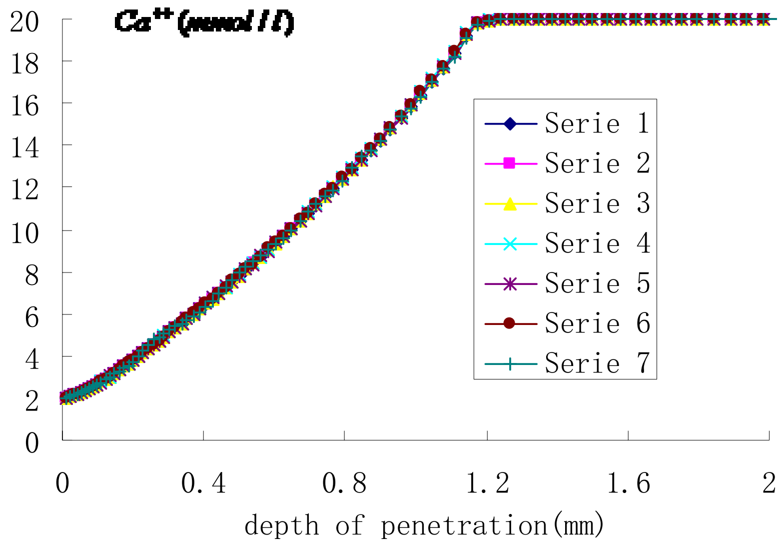

Figure 3-5 C_a^{++} distribution along the axis of bar at a given instance with different time increments

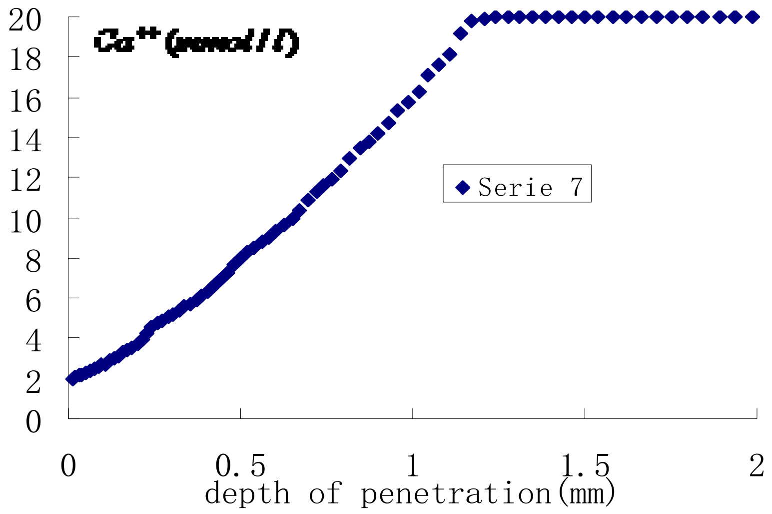

Figure 3-6: C_a^{++} distribution along the axis of bar at a given instance in the case $N°7$

In order to determiner the diffusion process, the essential material characters and model's parameters are wanted. In the work of Le Bellégo (2000), she has obtained a series of data for mortar. Also, Kuhl (2004) has also achieved some parameters for cementitious materials. In their researches, we find that for the calcium content and Portlandite content and there volume ratio, these two studies have some difference but vary in a limit range. In our study, we use the parameters obtained by Le Bellégo due to the lack of the experimental data. Therefore, the material and model parameters used in the leaching process are given in Table 3-3.

Table 3-3: Parameters of phenomenological chemistry model

$S_{tot} = 15278 mole/m^3$	$n = 70$	$\beta = 2.3$
$S_{por} = 4427 mole/m^3$	$m = 5$	$V_{por} = 0.18$
$x_1 = 2$	$D_0 = 3*10^{-12} m^2/s$	$V_{C-S-H} = 0.40$
$x_2 = 19$	$D_s = 400*10^{-12} m^2/s$	$V_{Aft+Afm} = 0.14$

In the work of Gérard, several calculations have carried on such as the numerical simulations of immersion in deionised water. Using the same parameters, we precede this calculation with the simplified Eq. (3-23). The numerical result shows that the leaching depth for deionised water condition after 3 months is about 1.71mm. This result is very similar to the result obtained by Gérard and the difference is within 2 percent. This means that the numerical implementation can well describe the Gérard's model. On the other hand, the experimental depth of calcium leaching after 3 months of immersion in deionised water is about 0.5-2.7 mm due to the different corposant of materials (Gérard, 2002). Thus, it is conformed that the numerical result has a good accuracy to the average value for the experimental.

The second comparison is applied in the ammonium nitrate condition. The mortar samples are immerged in nitrate ammonium solution with a concentration of $6\,\mathrm{mol/l}$ and measure the degraded depth at 28, 56, and 98 days of leaching. The numerical results obtained at correspond days are given together with the corresponding experimental values in Table 3-4. In this case, we determined the multiple coefficient as $\lambda_t = 60$ with the relation $\lambda_t = t_0/t$. t_0 represents the time in deionised water and t as the actual condition to arrive the same degradation depth.

Table 3-4: Chemical leaching depth at 28, 56, and 98 days

Period	Simulation (mm)	Experiments (mm) (Gérard, 2002)	Differences
28 days	8.73	8.93	-2.2
56 days	12.94	12.61	+2.6
98 days	17.38	13.5	-4.3

In this part, we discuss the two possibly problems during the simulation, and finally, we draw the conclusion that the diffusion model can well describe the leaching process not only in deionised water condition but also in acid condition, and the numerical methods are well formulated which can be well used in the following simulation of chemo-mechanical coupling process.

3.4 Simulations of coupled chemical-mechanical tests

The coupled chemical mechanical tests have been performed in LML in collaboration with TOTAL Company (Yurtdaz et at. 2006). Each coupled test is realized in the following steps:

- A sound sample is placed in the triaxial cell.
- The given confining pressure is applied; for instance $Pc = 5MPa$.
- The deviatoric stress (that is equal to 50 % of the failure stress) is applied.
- The nitrate of ammonium (or H_2S) is injected with $Pi = 2.5MPa$ at the inlet point and the pore pressure at the outlet point is equal to 0 MPa.

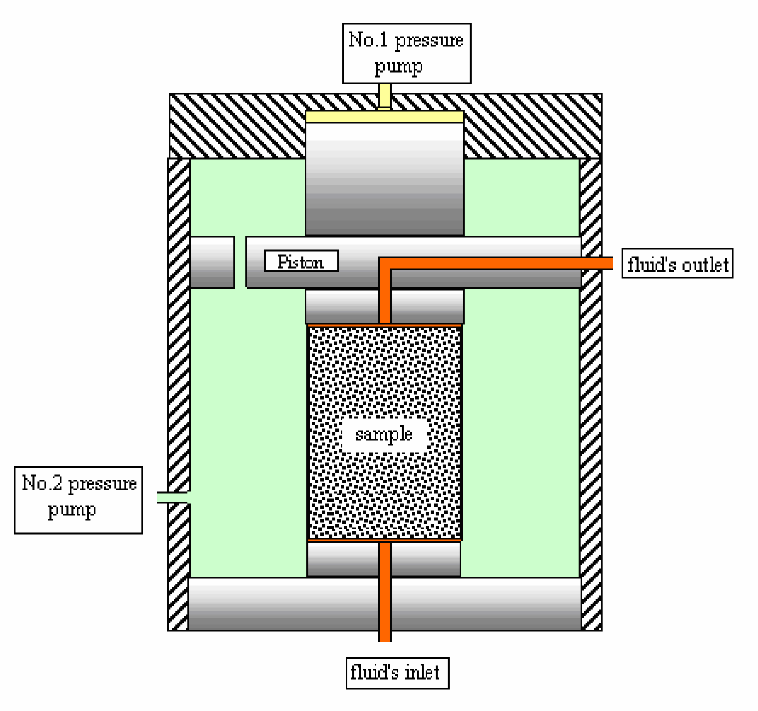

Figure 3-7: Illustration of testing device (Yurtdaz et at. 2006)

Fig. 3-7 shows an illustration of the experimental device. In this figure, three pumps are equipped in the experimental system: one for the deviatoric stress (No.1) and one for the confining pressure (No.2); in addition, the third pumps is used to inject the liquid from the bottom surface.

The emphasis of this study is on the mechanical responses during the triaxial loading with chemical degradation. In each test, we measure the evolution of average axial strain in function of time. Based on the experimental results, two tendencies of evolution have been observed. The first is that along with the chemical leaching, the deformation increases steadily and the sample will keep stable while the other shows that with the increasing of time, the deformation increases more and more till the failure of the sample.

Fig. 3-8 shows the numerical simulation and the experimental data for the test with the confining pressure $Pc = 10MPa$ and nitrate solution (NH_4NO_3). Fig. 3-9 shows the numerical simulation and the experimental data for the test under the confining pressure $Pc = 5MPa$ and with the aggressive solution (H_2S). The mechanical responses obviously depend on the level of applied deviatoric stress during chemical degradation. In the analyses in the Chapter 2, we have found that at $Pc = 10MPa$, the maximum resistance at total chemical damaged state is superior to 50% of the failure stress of the sound material. Therefore, the evolution of axial strain in this test tends toward a stationary state without accelerated failure by chemical degradation. However, in the simulation for $Pc = 5MPa$, the maximum resistance of the chemical damaged material is inferior to 50% of the failure stress of the sound material. Hence, we observe that a clear acceleration of the axial deformation occurs leading the rupture of the sample. In Fig.3-10, the distributions of calcium concentration along the axis of sample are given for different instances. We can observe progressive propagation of chemical degradation front inside the sample.

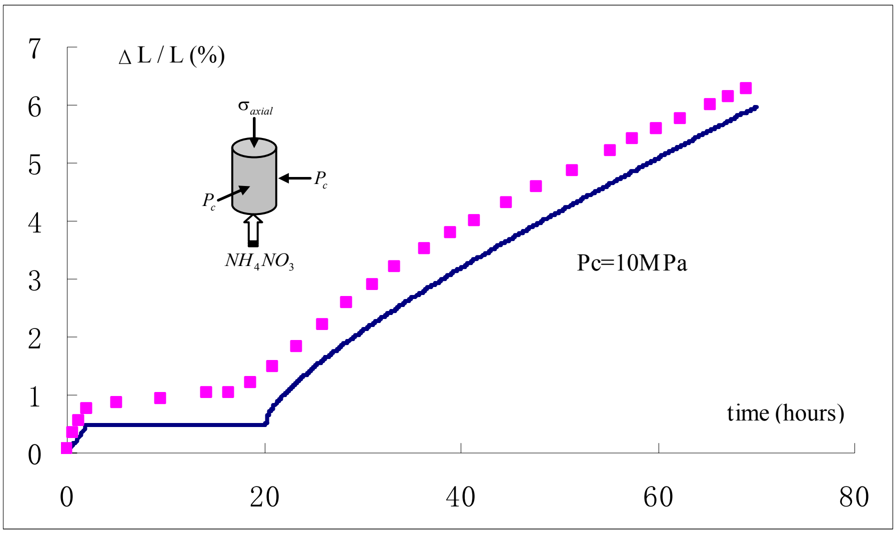

Figure 3-8: Evolution of the total axial strain with time for the test under Pc=10MPa and with NH_4NO_3: comparison between the numerical simulation and the experiment

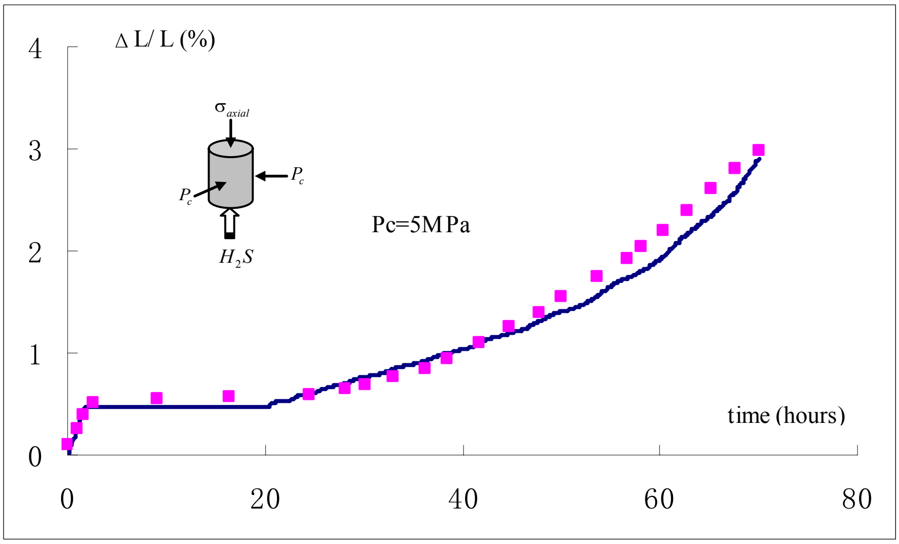

Figure 3-9: Evolution of the total axial strain with time for the test under Pc=5MP and with H_2S: comparison between the numerical simulation and the experiment

Comparing the numerical simulations and experimental data for two tests, we can consider that the proposed elastoplastic model with chemical degradation can well describe the coupled chemical-mechanical tests.

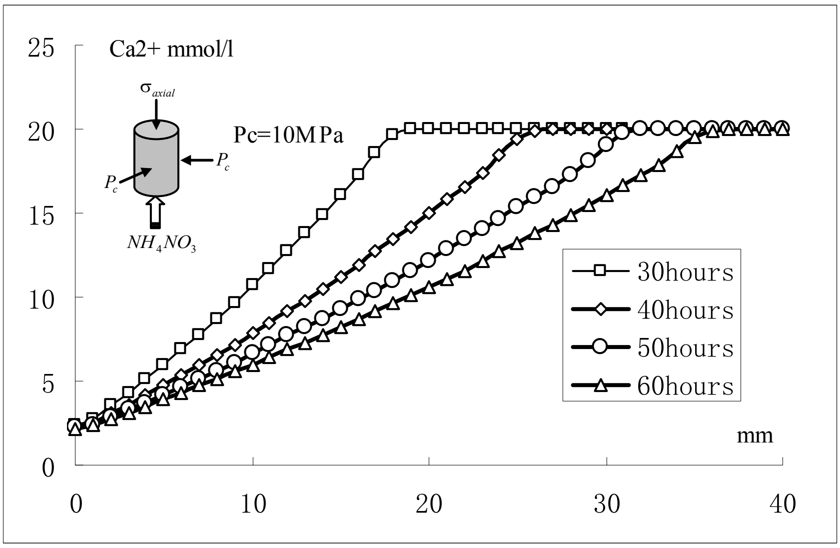

Figure 3-10: Distribution of C_a^{++} calculated for different periods at Pc=10MPa with NH_4NO_3

3.5 Conclusion

In this chapter, we have addressed the numerical solution of chemical diffusion process. The kinetics of chemical damage is directly related to this diffusion process. A phenomenological chemistry model is adopted to determine phase change in the dissolution of calcium ions and variation of diffusion coefficient with modifications of different phases. A specific computer block is developed for the numerical solution using finite element method. The numerical stability of solution is tested. Finally, the proposed model is applied to the modelling of coupled chemical-mechanical tests seen as small structure. There is a good agreement between numerical simulations and experimental data.

Chapter 4: Mechanical behavior of cement paste subjected to mechanical damage and chemical degradation

4.1 Introduction

This thesis focuses on the effects of the chemical degradation on mechanical behavior of cement paste. In Chapter 2, we have addressed the coupling between elastoplastic behavior and chemical degradation of cement paste under high compressive stresses by neglecting mechanical damage due to microcracks. In chapter 3, the evolution of chemical damage has been determined through the chemical leaching process, which is governed by the generalized diffusion equation. We have applied finite element method to obtain numerical solutions of chemical leaching process.

In this chapter, we will extend the previous work by considering mechanical damage by microcracks in cement-based material under low compressive stress and tensile stress. Indeed, in civil engineering structures, the cementitious materials should be loaded not only in compression-dominant conditions, but also in other loading conditions such as very low confining pressure, tensile stresses. In these cases, experimental data show that mechanical damage due to growth of microcracks will be an essential mechanism of deformation and failure in cement-based materials (Schlangen, 1992). Therefore, in order to make the constitutive model to be able to predict mechanical responses in such loading conditions, in this chapter, we propose an extension of the model to include mechanical damage mechanism. However, the emphasis of this work remains on the modeling of chemical degradation effects on mechanical behavior of cement paste under compressive stresses; the description of mechanical damage is reduced as simple as possible. Some qualitative comparisons with experimental data will be presented at the end of this chapter.

4.2 Description of mechanical damage

In according to extensive experimental data (Mahboubi, 2005), the cement-based materials exhibit brittle mechanical behavior in triaxial compression tests with low confining pressures. This brittle response is generally represented by a peak value of deviatoric stress followed by a material softening phase. On the microscopic level, we can observe nucleation and propagation of inter granular and intra- matrix microcracks. The propagation of microcracks is essentially dominated by tensile and shearing modes. The chemical damage affects not only elastic properties but also plastic properties and flow properties such as permeability (Perlot, 2006). The rate of damage evolution decreases when the confining pressure increases. When this one becomes high enough, the mechanical damage by microcracks become secondary and we obtain a ductile elastoplastic behavior as that studied in chapter 2 (see Fig. 2-3). In this chapter, we discuss the description of mechanical damage evolution and its coupling with elastoplastic behavior. Therefore, taking into mechanical damage, the free energy function reads:

$$\Psi\left(\varepsilon^{e},\gamma^{p},d_{m},d_{c}\right)=\frac{1}{2}\left[k\left(d_{c},d_{m}\right)\left(\varepsilon_{v}^{e}\right)^{2}+2\mu\left(d_{c},d_{m}\right)e_{ij}^{e}e_{ij}^{e}\right]+\Psi_{p}\left(\gamma_{p},d_{m},d_{c}\right)\qquad(4\text{-}1)$$

As observed in many experimental data, the induced mechanical damage affects elastic properties of materials. Considering the case with small density of microcracks and without interaction between microcracks, we adopt here the results issued from the dilute scheme in micromechanical analysis of elastic cracked materials (Mura, 1987). Further, the elastic properties of damaged material are generally different when microcracks are open or closure. For instance, the compressibility modulus of damaged material can be restored when the microcracks are closed. These so-called unilateral effects should be taken into account. The effective elastic parameters of chemically and mechanically damage materials may be expressed as follows:

$$k\left(d_m,d_c\right)=\frac{1-\alpha_3 H(\varepsilon_v)d_m}{1+\alpha_1 d_c}k_0 \quad \text{and} \quad \mu\left(d_m,d_c\right)=\frac{1-\alpha_4 d_m}{1+\alpha_2 d_c}\mu_0 \tag{4-2}$$

$H(.)$ is the Heaviside function. The values of parameters α_3 and α_4 which can be determined from experimental data show progressive degradation of elastic properties with mechanical damage evolution. The conjugate force associated with the mechanical damage variable is defined by

$$Y_{dm}=-\frac{\partial \Psi^e}{\partial d_m}=\frac{1}{2}\left[\frac{k_0}{1+\alpha_1 d_c}\left\langle \varepsilon_v^e\right\rangle+2\frac{\mu_0}{1+\alpha_2 d_c}e_{ij}^e e_{ij}^e\right]-\frac{\partial \Psi_p}{\partial d_m} \tag{4-3}$$

The bracket $\langle x\rangle$ denotes $\langle x\rangle=0$ if $x\leq 0$ and $\langle x\rangle=x$ if $x\geq 0$. In the framework of thermodynamics, the damage evolution law is determined through a dissipation potential, which is a function of the conjugate damage force. We can see that the conjugate damage force independently depends on elastic and plastic strains.

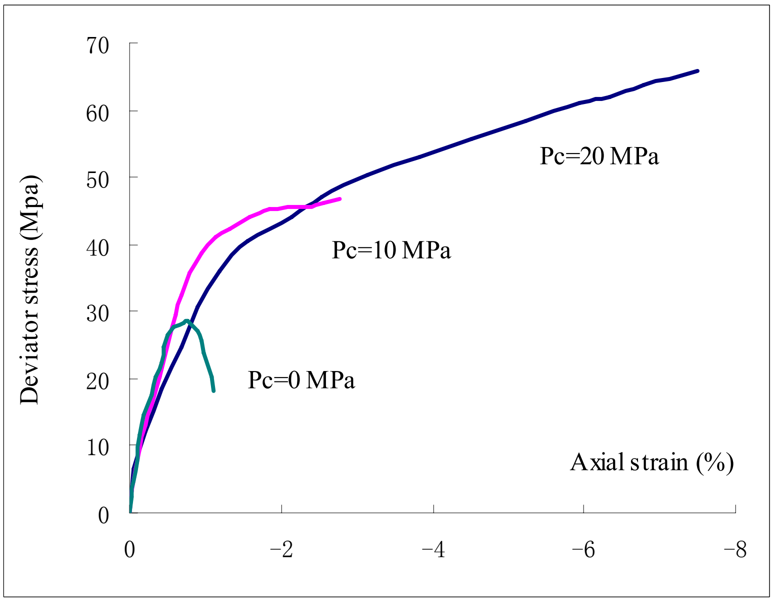

Figure 4-1(a): Result of triaxial tests on cement paste: axial strain - deviator stress curves (Yurtdas et al., 2006)

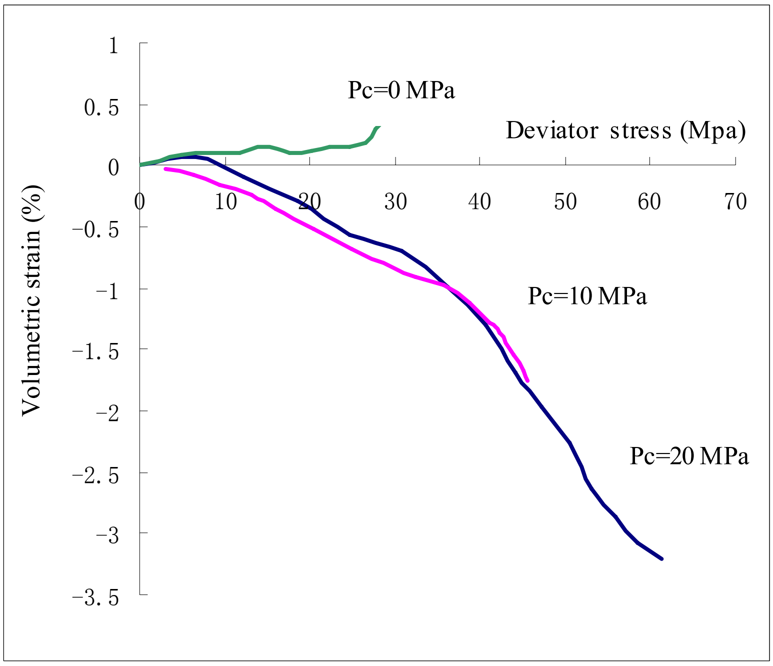

Figure 4-1(b): Result of triaxial tests on cement paste: deviator stress - volumetric strain curves (Yurtdas et al., 2006)

Mechanical damage criteria

Fig. 4-1 shows the experimental results of the cement paste in compression at different confining pressures. These curves show the transition from quasi brittle to ductile behavior of material when the confining pressure increases. In Fig. 4-1(a), we can observe that at low confining pressures, the material softening appears due to increase of mechanical damage evolution; in parallel, the volumetric strain under low confining pressure is dominated by dilation. From this phenomenon, in a first approximation, we can assume that the mechanical damage is related to volumetric dilation of material. For the sake of simplicity, we neglect the influence of shear strains on mechanical damage evolution and assume that this one only depends on total volumetric strain. The following measure of damage force is defined:

$$\xi_d = \frac{1}{2}\left[\frac{k_0}{1+\alpha_1 d_c}\langle\varepsilon_v\rangle^2\right] \Big/ \chi_d \tag{4-4}$$

According to experimental data for typical cement-based materials as shown in chapter 2 and in Fig. 4-1, the mechanical behavior of concrete strongly depends on confining pressure. In order to take into account this pressure dependency, we introduce the normalizing coefficient χ_d, which is expressed as a function of the effective mean stress:

$$\chi_d = \left(\frac{\langle 3I \rangle + f_c}{f_c} \right)^{B_1} \tag{4-5}$$

The coefficient f_c denotes the uniaxial compression strength of material of sound state, and B_1 is the parameter of model which controls the rate of the ductile response. Based on the damage criterion proposed by Mazars (1984) for concrete, the following function is proposed:

$$f_d = A_2 - A_2 \exp\left[B_2 \left(\xi_d - \xi_d^0 \right) \right] - d_m = 0 \tag{4-6}$$

The parameter A_2 defines a critical value of damage corresponding to residual strength of damaged material; B_2 is controlling the kinetics of damage evolution; and ξ_d^0 defines the initial threshold of damage force. Note that the mechanical response of frictional materials line cement paste is generally dissymmetric under compression and tension. For instance, the evolution of damage is higher in tension than in compression. In order to capture this dissymmetry, two different damage laws are used respectively in compressive and tensile conditions:

$$\begin{aligned} d_{mc} &= A_{2c} - A_{2c} \exp\left[B_{2c} \left(\xi_d - \xi_{dc}^0 \right) \right] \\ d_{mt} &= A_{2t} - A_{2t} \exp\left[B_{2t} \left(\xi_d - \xi_{dt}^0 \right) \right] \end{aligned} \tag{4-7}$$

The effective damage variable is determined as:

$$d_m = \alpha_t d_{mt} + \left(1 - \alpha_t \right) d_{mc} \tag{4-8}$$

where d_{mt} and d_{mc} are the components of mechanical damage in tensile and compressive conditions. The parameter α_t specifies the loading condition and depends on loading path. It varies between 0 (full compression) and 1 (full tension). In the model of Mazars (1984), a continuous evolution law of α_t was proposed as a function of applied stresses. However, for the sake of simplicity, a simpler version is used here. Only two extreme values are considered; full compression ($\alpha_t = 0$) and full tension ($\alpha_t = 1$). In transition criterion use is the following: when one of three principal stresses becomes tensile; the tensile condition is considered. Else we are in compression condition.

4.3 Influence of mechanical damage on plastic flow

As we presented in chapter 2, the present model contains two types of plastic mechanisms, the first is the plastic shearing mechanism that is dominant at low confining pressure and the second is the pore collapse that determines the evolution of plastic strain at high confining pressure. Further, the brittle behavior related to mechanical damage occurs only at low confining pressures. Therefore, we assume that the mechanical damage affects the deviatoric plastic mechanism only.

Due to the growth of microcracks generating mechanical damage, material bounds in solid skeleton are progressive destroyed. There is redistribution of local stresses in sound material areas. Generally, plastic flow rate is intensified in damaged material. This is equivalent to introduce degradation effect by mechanical damage in plastic hardening law determined in chapter 2. Thus based on typical experimental data, the plastic hardening function of damaged material is expressed by:

$$\alpha = (1 - d_m)\left[\alpha^0 + (1 - \alpha^0)\frac{\gamma_s}{B + \gamma_s}\right] \tag{4-9}$$

Further, according to the same physical raison, the parameter C, which represents the material cohesion (hydrostatic tension strength) of material, generally decreases with induced damage. The following simple relation is proposed:

$$C = C_0 \left(1 - d_m\right) \tag{4-10}$$

4.4 Parameter identification and numerical simulations

The model's parameters can be determined from uniaxial tension and compression tests. Typical values of parameters obtained are shown in Table 4-1.

Table 4-1: Typical values of parameters of mechanical damage evolution

Parameters	α_3	α_4	B_1	ξ_{dc}^0	B_{2c}	A_{2c}
Chemically sound material- compression	1.0	1.0	2.0	3000	5E-6	0.4
Chemical degraded material-compression	1.0	1.0	2.0	3000	5E-6	0.2
Chemically sound material- tension	1.0	1.0	2.0	300	5E-5	0.9
Chemically degraded material- tension	1.0	1.0	2.0	300	5E-5	0.7

Fig. 4-2 shows the simulation of uniaxial compression tests, respectively for chemically sound and degraded materials. We can see that the proposed model is able to correctly predict brittle behavior of cement paste including material softening under low confining pressure conditions. And at higher confining pressures, the damage rate progressively vanishes and only plastic deformation is active. We recover the same predictions as those presented in chapter 2.

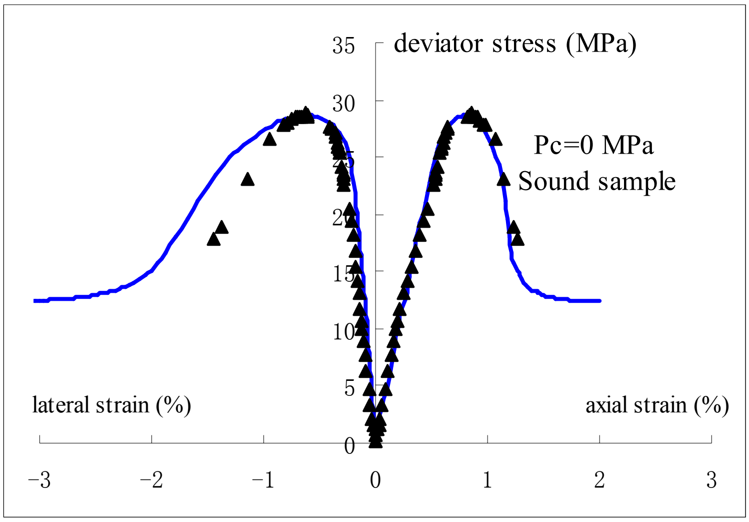

Figure 4-2(a): Comparisons between numerical simulations and experimental data in uniaxial compression test on chemically sound sample

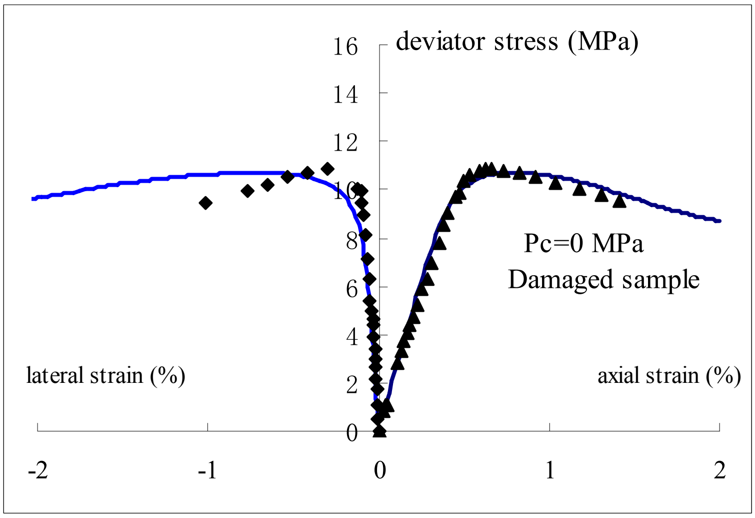

Figure 4-2(b): Comparisons between numerical simulations and experimental data in uniaxial compression test on chemically degraded sample

Note that the damage evolution rate is also affected by chemical degradation. For instance, the parameter A_{2c} is variable with chemical damage state. In our study, this value is 0.4 for chemically sound state, while decreases to 0.2 in fully chemically degraded material. This means that the chemical degraded material has a more ductile behavior (with smaller chemical damage evolution rate) than the sound material. However, from the experimental data, it seems that the ratio between the residual stress and peak stress is almost constant in chemically sound and degraded materials.

This suggests that the material softening behavior is fully controlled by mechanical damage.

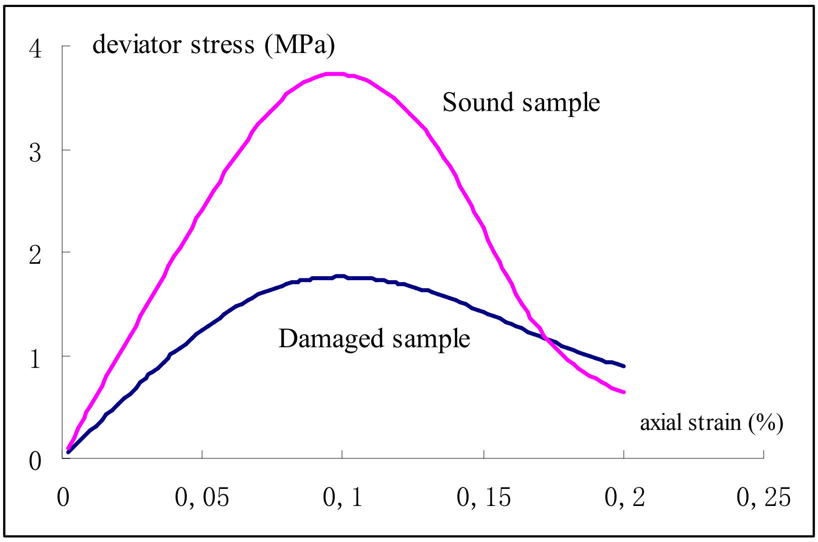

Figure 4-3: Simulation of uniaxial traction test on sound sample and chemically degraded sample

4.5 Simulation of 3 points bending tests subjected to chemical degradation

In this section, a simple example of application of the proposed model is presented. It consists of three point bending tests of beam largely performed in civil engineering to investigate basic responses of concrete structures. A series of tests have been realized on mortar samples by Le Bellégo (2000). The principle of the tests is to perform a preliminary phase to generate chemical degradation state in the specimens, followed by mechanical loading. With these tests, it is possible to investigate mechanical responses of beam at different chemical degradation state.

Inspired by the tests performed by Le Bellégo (2000) on the mortar, we propose to realize numerical modeling of cement paste beam subjected to three point bending and chemical degradation. The considered beam has a size of 40mm*80mm* 320mm as shown in Fig. 4-4. The beam is subjected to chemical degradation by ammonium nitrate solution at its bottom surface. However, the lateral and top surfaces of the beam are protected from chemical degradation. The chemical degradation process is activated for different durations, for instance 7 days, 14 day, 28 day etc. At each chosen time, the beam is extracted from the chemical solution, and is loaded mechanically. Fig. 4-4 shows the illustration of three point bending configuration of the beam with chemical attack condition. The LVDT placed at the centre of the beam is used to measure the displacement along y axis.

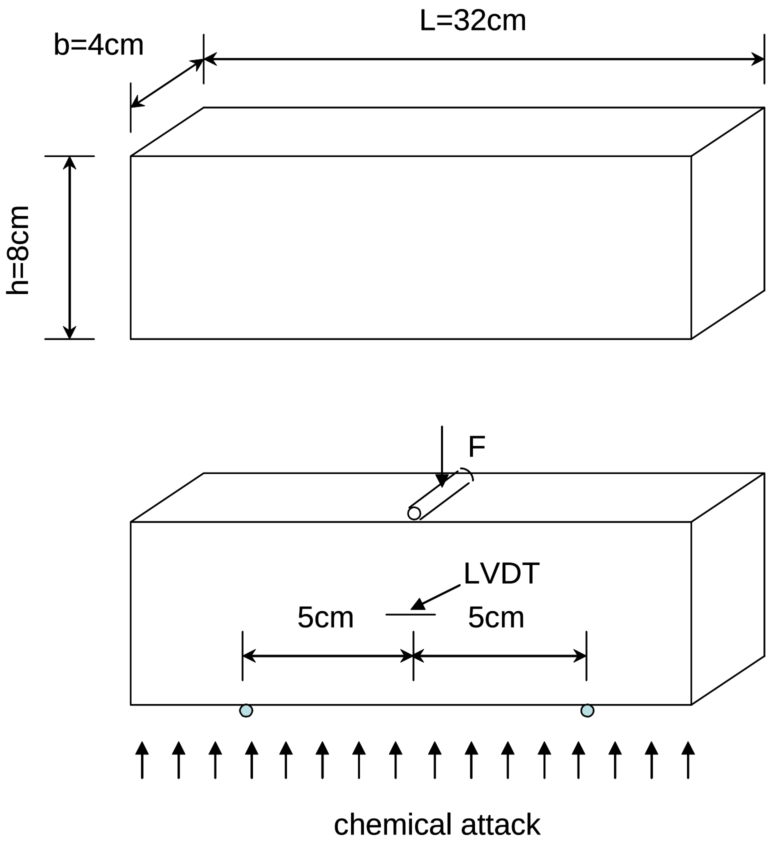

Figure 4-4: Illustration of 3 point bending test with chemical degradation

4.5.1 Mesh, boundary and initial conditions

The mesh used for chemical and mechanical modeling is shown in Fig. 4-5. Making use of the symmetry of the problem, only half of the beam is meshed and four-node element is used in this mesh. The initial conditions are that:

- The x-displacement is fixed at surface AB ;

- The y-displacement is fixed at point E;
- The concentration of ammonium nitrate is $6mmol/l$ at surface BC;
- There is no normal flux of calcium concentration at the surfaces AB, CD and AD.

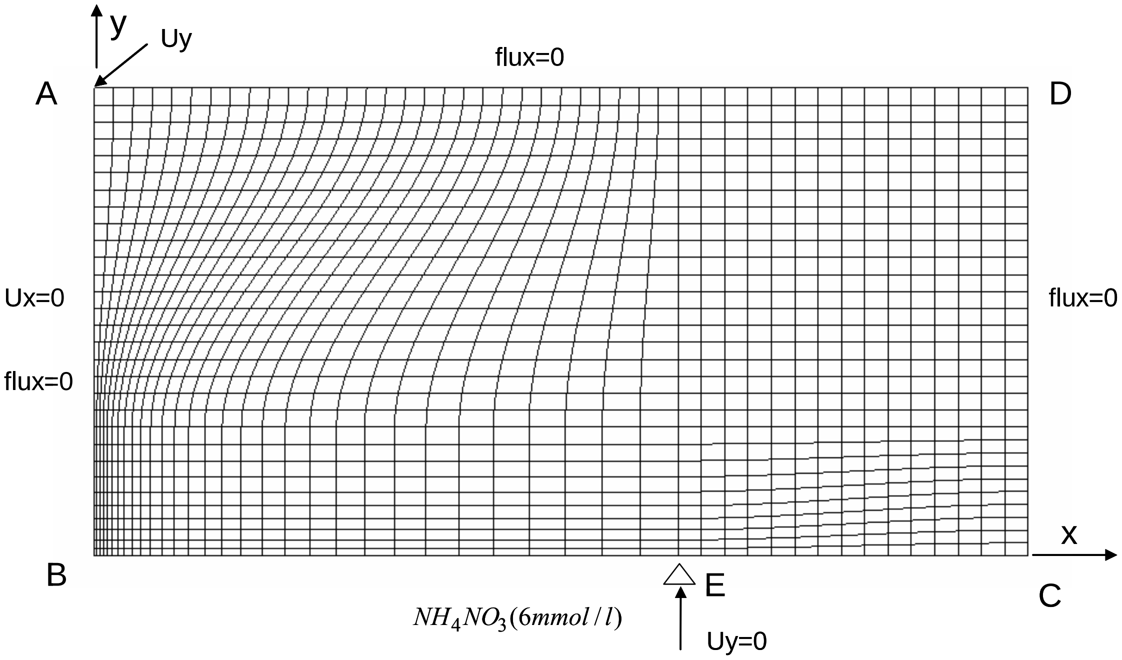

Figure 4-5: FEM mesh and boundary conditions used for chemical and mechanical modeling of cement paste beam

4.5.2 Chemical leaching calculation

The result of chemical degradation is the calcium concentration distribution in the beam (see Fig. 4-6). The simulation predicts that the location of the chemical leaching front is at 9mm from the bottom of the beam after 7 days of chemical attack.

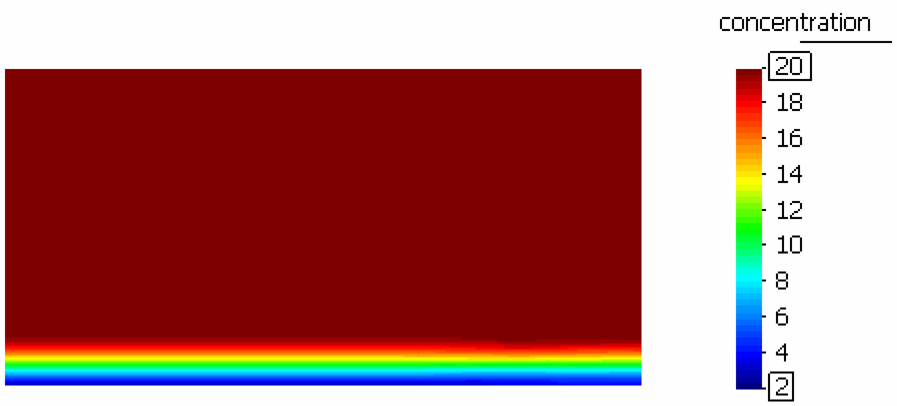

Figure 4-6: Distribution of C_a^{++} as a function of depth in the beam after 7 days of leaching by ammonium nitrate solution

4.5.3 Mechanical simulation and comparison

Based on the simulation of chemical leaching, the beam becomes a heterogeneous porous medium composed of material zones with different levels of chemical degradation. Appropriate elastic, plastic and damage parameters can be determined at each material point. In the mechanical loading, the vertical force is applied to the middle of the top surface (Point A). Fig. 4-7 shows the simulation of force-displacement curve in partially chemically degraded beam (see Fig. 4-6).

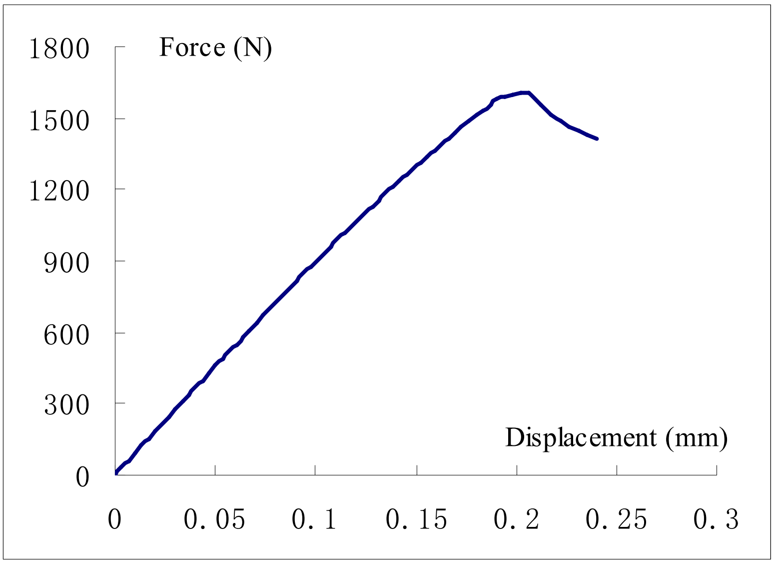

Figure 4-7: Deflection – force curve of the beam after 7 days of chemical

leaching

Fig. 4-8 shows the evolution of the mechanical damage at different steps of mechanical loading. We can observe that the evolution of mechanical damage contains two phases: at first, the damage evolves in the bottom zone affected by chemical degradation; then along with the increasing of the mechanical loading, the damage extends quickly to the centre of the beam and finally the beam will fail in form of the crossing fissure. This failure pattern given by the simulation is compatible with many experimental observations (Pihlajavaara, 1974; Le Bellégo, 2003; Zhang, 2003).

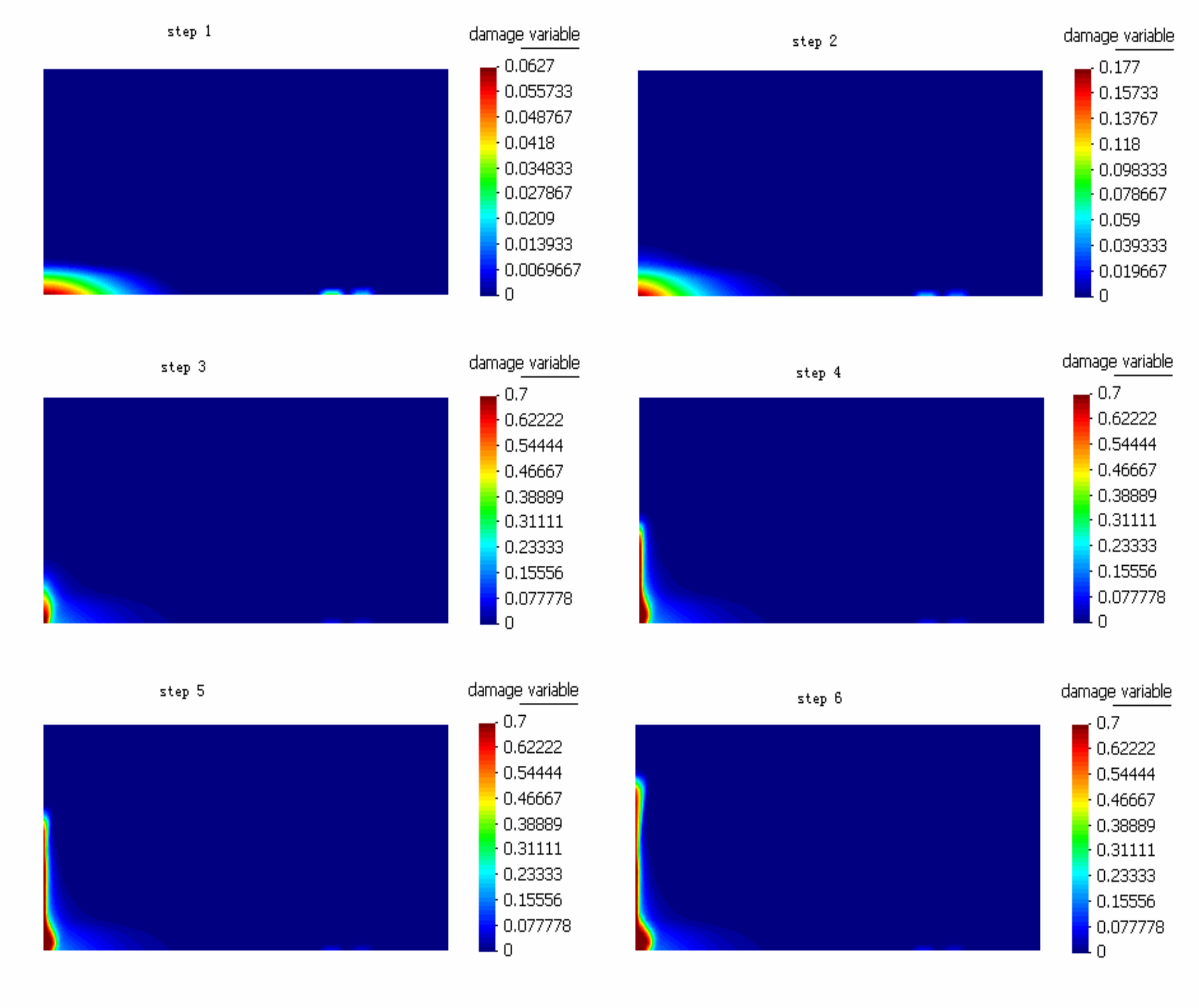

Figure 4-8: Evolution of mechanical damage at different loading steps

A series of simulations have been performed with different chemical leaching time. Fig. 4-9 shows the load-deflection curves for various cases. From this figure, several remarks can be drawn:

- The maximal force is highly dependent on the chemical degradation state, and also the higher the leaching depth is, the lower the stiffness is.
- Accompanying the increasing of chemical damage, the deflection at peak grows but the increasing amplitude is quite small; the plastic deformation plays an important role in mechanical behavior.

Certainly, because of the limit of present model and the lack of relevant data for the determination of model's parameters, these simulations can only partly describe the response of actual responses, mainly at the pre-peak phase.

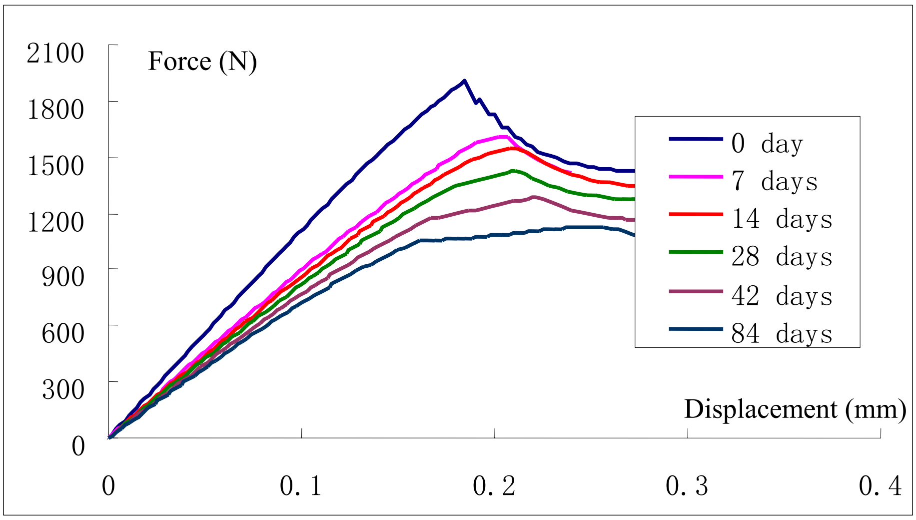

Figure 4-9: Deflection-force curves of beam at different chemical degradation periods

In the experimental studies performed by Le Bellégo (2000) on mortar beams, the loss of apparent stiffness and the decrease of maximal load have been observed during the chemical degradation process. However, the deflection at peak state is almost independent of chemical degradation state. Mortar and cement are widely used in many engineering applications. Their basic mechanical behaviors are quite similar.

The chemical degradation due to dissolution of calcium ions is nearly the same in the two materials. However, some differences still exist; the behavior of mortar is generally more brittle than that of cement paste.

In order to make qualitative comparison between the present numerical simulations and experimental data obtained by Le Bellégo (2000), we have calculated the ratio of peak force diminution by chemical degradation as a function of degradation time, as shown in Fig. 4-10. We can observe that the general trends are very similar in two materials. The peak force in 3 point bending tests decreases with chemical degradation.

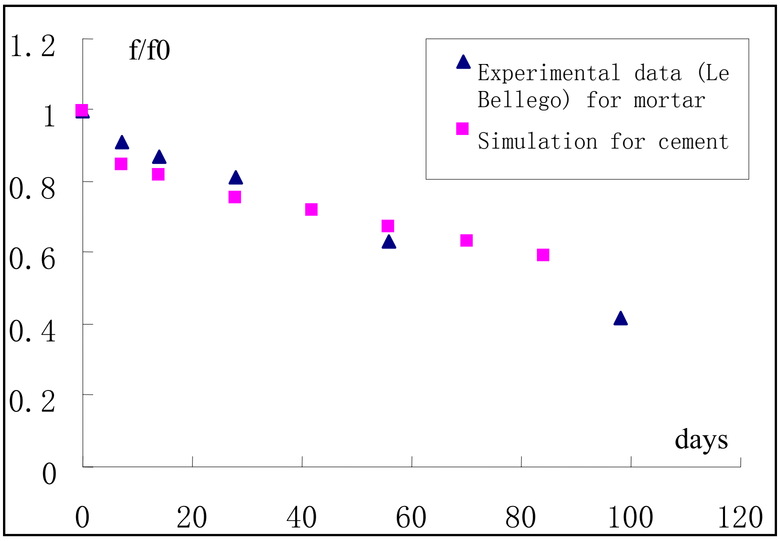

Figure 4-10: Variation of peak force ratio as a function chemical degradation time

4.6 Conclusion

We have proposed an extension of chemo-mechanical model to include mechanical damage by microcracks. This makes the model to be able to describe mechanical behavior of cement paste under low confining pressure and tension. Even if the description of mechanical damage is quite simple, the proposed model is still able to capture main features of behavior observed in most cement-based material. An example of application of the proposed model to typical engineering structures is presented. We have studied the case of 3 point bending of a beam subjected to chemical degradation. The effects of chemical degradation on mechanical responses of the beam have been investigated. In a qualitative way, the results obtained by numerical simulations are in agreement with experimental data obtained on similar materials.

Conclusion & Perspective

We have presented in this thesis a systematic modeling procedure for mechanical properties of cement-based materials under mechanical loading and chemical leaching. This procedure consists of four part, they are: summary of the present research in the related domains; the analyses of the experimental results carried out at LML; the presentation of the constitutive law and the coupling with chemical damage; the numerical simulation of mechanical responses both at material level and at structural level. According to the practice, these aspects are written by four chapters.

In the first chapter, the phenomenological observation and characteristic introduction of cementitious materials have been presented and they are used as the basic framework for the present study. In this framework, the leaching phenomena, the mechanical properties due to calcium leaching are qualitatively stated. Several focuses in this coupling process has been mentioned. In the following chapter, based on the experimental data, the plastic mechanisms can be summarized and constitutive law for sound material and chemically damaged material has been introduced by the same formula. This referred to the chemical degradation at the different states. Therefore, a damage variable called 'the chemical damage' is introduced in the present model and the coupling process within mechanical loading and chemical loading has been realized in the following chapter. In chapter 3, we dealt with the evolution of the chemical damage by generalized diffusion equation, and their numerical solutions have been obtained by the finite element method. At the end of this chapter, the proposed constitutive law with chemical damage has been applied to the time-dependent simulation of chemical-mechanical coupling tests. Finally, we extended the model to tensile condition and the mechanical damage has been discussed in chapter 4. Consequently, a simple application of three points blending test has been performed.

Based on our study, we can draw some conclusions as following:

- The microstructural analysis showed that the dissolution front existed during calcium leaching process. We used the pH indicator like phenolphthalein to obtain this front which distinguished the transition between the sound zone and the chemically degraded zone.
- As a consequence, the front modeling for calcium leaching was used to describe the evolution of the porosity. In our study, the Gérard's model was applied directly and the numerical solutions described its agreement with the experimental data.
- The porosity is an important factor which is mainly affected by calcium leaching. In our study, the increase of porosity due to chemical leaching was defined as the chemical damage. In the time-dependant simulation of chemical-mechanical coupling test, the present constitutive model can well manifest its influence at different damage states.
- Chemical leached cement sample and sound cement sample were tested in triaxial compression tests and hydrostatic tests. The samples at two state showed the same mechanical properties: a brittle behaviour occurred by material softening phase in post peak at low confining pressure; two plastic mechanism were obviously observed, they are the plastic shearing mechanism that is dominant at low confining pressure and the pore collapse that determines the evolution of plastic strain at high confining pressure. Due to the different chemically damaged degree, the evolution of each plastic is different. The general trend is that the more chemical damage is, the more plastic produced. The main focus of this work is to obtain an elastoplastic model with chemical damage. In this model, the main plastic mechanisms have been well explicated.
- The simplified mechanical damage criterion by microcracks under low compressive stress and tensile stress has been introduced in the present model at the end of this thesis. The applications showed that this extension can predict mechanical responses in tensile loading conditions and qualitative comparison between the present numerical simulations and experimental data of three points bending tests revealed the similar trends.

The experimental and constitutive model presented in this thesis exposed an area of future scientific interest and industrial importance. The following are possible extensions for future research:

- For constitutive law: at the end of this thesis, the mechanical damage has been discussed. Actually, this is also a complex process and more attractions can be emphasized in this part. At the same time, with the development of measure, the more and more quantitative experimental investigations can be performed in the future, and the evolution of calcium leaching and mechanical response can be clarified more precisely, these will lead to improvement of current modeling and new theoretical development.
- For applications, this study may be motivated in part of geological sequestration residual acid gas and fluids. The degradation predictions are particularly useful during the lifetime to estimate security risks. The more factors such as creep, temperature, freezing should be considered simultaneously in the future.

Bibliography

[1] Abou-Mesalam M. M., 2002. Leaching behavior of some radionuclides from cement matrix incorporating exhausted polymeric resins. Journal of Radioanalytical and Nuclear Chemistry 1, 123–128

[2] Adenot F., 1992. Durabilité du béton: caractérisation et modélisation des processus physiaues et chimiques de dégradation du ciment. Thèse de Doctorat, Université d'Orléans, France

[3] Adenot F., 1992. Modelling of the corrosion of the cement paste by deionized water. Cement and concrete research, 22(04),489-495

[4] Bangert F., Kuhl D., Meschke G., 2001. Finite element simulation of chemo-mechanical damage under cyclic loading conditions. In: de Borst R., Mazars J., Pijaudier-Cabot G. and van Mier (Eds.). Fracture mechanics of concrete structures. Balkema Publishers, Lisse, 145-152

[5] Bangert F., Grasberger S., Kuhl D., Meschke G., 2003. Environmentally induced deterioration of concrete: physical motivation and numerical modeling. Engineering Fracture Mechanics 70, 891–910

[6] Baroghel-Bouny V., Mainguy M., Lassabatere T. and Coussy O., 1999. Characterization and identification of equilibrium and transfer moisture properties for ordinary and high-performance cementitious materials. Cement and Concrete Research 8, 1225-1238

[7] Bary B., Bournaze J.-P. and Bourdarot E., 2000. Poro-damage approach applied to hydro-fracture analysis of concrete. Journal of Engineering Mechanics 9, 937-943

[8] Bentz D.P., Garboczi E.J., 1992. Modelling the leaching of calcium hydroxide from cement paste: effects on pore space percolation and diffusivity. Materials and Structures 25, 523-533

[9] Bernard O., Ulm F.-J. and Germaine J.T., 2003. Volume and deviator creep of calcium-leached cement-based materials. Cement and Concrete Research 33, 1127-1136

[10] Berner U,. 1988. Modelling the incongruent dissolution of hydrated cement minerals. Radiochimica Acta 44-45, 387-393

[11] Berner U,. 1992. Evolution of pore water chemistry during degradation of cement in a radioactive waste reposity environment. Wsater management 12, 201-219

[12] Biot M.A., 1941. General theory of three dimensional consolidation. J. Appl. Phys. 12, 155-164

[13] Biot M.A., 1955. Theory of elasticity and consolidation for a porous anisotropic solid. J.Appl. Phys. 26,182-185

[14] Biot M.A. and Willis D.G., 1957. The elastic coefficients of the theory of consolidation. J.Appl. Mech. 28, 594-601

[15] Biot M.A., 1973. Non linear and semi-linear rheology of porous solid. J. of Geophy. Res.,

78(23), 4924-4937

[16] Boudon-Cussac D., Hild F., and Pijaudier-Cabot G., 1999. Tensile Damage in Concrete: Analysis of Experimental Technique. J. Engrg. Mech., Volume 125, Issue 8, pp. 906-913

[17] Buil M., Revertegat E., Ollivier J.P., 1992. Modelling cement attack by pure water. In ASTM STP-1123, Gilliam T.M. and Wiles C.C.(Eds.), American Society for Testing and Materials, West Conshohocken, USA

[18] Carde C., François R., Torrenti J.-M., 1996. Leaching of both calcium hydroxide and C–S–H from cement paste: modelling the mechanical behavior. Cement and Concrete Research 22, 1257–1268.

[19] Carde C., Escadeillas G., François R., 1997. Use of ammonium nitrate solution to simulate and accelerate the leaching of cement pastes due to deionized water. Magazine of Concrete Reacher 49, 295-301

[20] Carde C., François R., Ollivier J.P., 1997. Microstructural changes and mechanical effects due to the leaching of calcium hydroxide from cement paste. In: Scrivener K., Young J.(Eds.), Mechanics of Chemical Degradation of Cement-Based Systems. Champman&Hall, London, 30-37

[21] Carde C., François R., 1997. Effect on the leaching of calcium hydroxide from cement paste on mechanical properties. Cement and Concrete Research 27, 539–550.

[22] Carde C. and François R., 1999. Modelling the loss of strength and porosity increase due to the leaching of cement pastes. Cement & Concrete Composites 21, 181-188

[23] Cheng A.H.-D., 1997, Material coefficients of anisotropic poroelasticity. Int. J. Rck Mech. Min. Sci., 34(2), 199-205

[24] Chen J.J., Thomas J J., Taylor H F.W., Jennings H.M., 2004. Solubility and structure of calcium silicate hydrate. Cement and Concrete Research 34, 1499–1519

[25] Constantinides G.. and Ulm F.-J., 2004. The effect of two types of C-S-H on the elasticity of cement-based materials: Results from nanoindentation and micromechanical modeling. Cement and Concrete Research 34, 67-80

[26] Constantinides G., 2006. PhD. Thesis, Department of Civil and Environmental Engineering, Massachusetts Institute of Technology

[27] Coussy O., 1991. Mécanique des milieux poreux, Editions Technip, Paris

[28] Coussy O., 1995. Mechanics of porous continua. Wiley, New York

[29] Coussy O., Ulm F.-J., 2001. Elements of durability mechanics of concrete structures. In: Ulm F.-J., Bazant Z.P., Wittmann F.(Eds.), Creep, Shrinkage and Durability Mechanics of Concrete and other Quasi-Brittle Materials. Elsevier Science, Amsterdam, 3993-4009

[30] Cristescu N., 1994. A procedure to determine non-associated constitutive equations for geomaterials. International Journal of Plasticity 10, 103-131

[31] Da C, 2005. Modélisation du comportement hydromécanique d'un mortier sous compression et desiccation. Thèse d'Etat, Université de Lille 1

[32] Delagrave A., Study of ingress mechanisms of chloride ions in ordinary and high performance concretes, Ph.D. Thesis, Laval University, Quebec City, Canada, 1996

[33] Delagrave A., Pigeon M., Marchand J. and Revertégat E., 1996. Influence of chloride ions and ph level on the durability of high performance cement paste. Cement and Concrete Research 26, 749-760

[34] DeJong M.J. and Ulm F.-J., 2007. The nanogranular behavior of C-S-H at elevated temperatures (up to 700 °C). Cement and Concrete Research 37, 1-12

[35] Delagrave A., Gérard B., Marchand J., 1997. Modelling the calcium leaching mechanisms in hydrated cement pastes. In: Scrivener K., Young J.(Eds.), Mechanics of Chemical Degradation of Cement-Based Systems. Chapman & Hall, London, 30-37

[36] Dhir R.K., Hewlett P.C., Dyer T.D., 1999. Chemical profiles of cement pastes exposed to a chloride solution spray. Cement and Concrete Research 29, 667–672

[37] Diez P., Arroyo M., Huerta A., 2002. Adaptive simulation of the coupled chemo-mechanical concrete degradation. In: Mang H., Rammerstorfer F., Eberhardsteiner J.(Eds.), Proceedings of the Fifth World Congress on Computational Mechanics, WCCM Ⅴ, Vienna University of Technology, Vienna

[38] Faucon P., Le Bescop P., Adenot F., Bonville P., Jacquinot J. F., Pineau F. and Felix B., 1996. Leaching of cement: Study of the surface layer. Cement and Concrete Research 26, 1707-1715

[39] Faucon P., Adenot F., Jacquinot J. F., Petit J. C., Cabrillac R. and Jorda M., 1998. Long-term behaviour of cement pastes used for nuclear waste disposal: review of physico-chemical mechanisms of water degradation. Cement and Concrete Research 28, 847-857

[40] Feldman R.F. and Beaudoin J.J., 1974. Microstructure and strength of hydrated cement. Proc of the 6th International Symposium on the chemistry of cement, Moscou.

[41] Fredrich J.T., Evans B., Wong. T.F., 1989. Micromechanics of the brittle to plastic transition in Carrara marbe. J.of Geophys.Res.94, 4129-4145

[42] Fujita T., Sugiyama D., Swanton S.W., Myatt B.J., 2003. Observation and characterization of colloids derived from leached cement hydrates. Journal of Contaminant Hydrology 61, 3–16

[43] Galleé C., Peycelon H. and Le Bescop P., 2004. Effect of an accelerated chemical degradation on water permeability and pore structure of cementbased materials. Advances in Cement Research 3, 105–114

[44] Gérard B., 1996. Contribution des couplages mécanique-chimie-transfert dans la tenue à long terme des ouvrages de stockage de déchet radioactifs. Thèse de Docdorat, E.N.S.de Cachan et Université de Laval

[45] Gérard B., Pijaudier-Cabot G. and Laborderie C., 1998. Coupled diffusion-damage modelling and the implications on failure due to strain localisation. International Journal of Solids and Structures 35, 4107-4120

[46] Gérard B. and Marchand J.,2000. Influence of cracking on the diffusion properties of cement-based materials: Part I: Influence of continuous cracks on the steady-state regime. Cement and Concrete Research 30, 37-43

[47] Gérard B., 2000. Hydrolysis of cement-based materials: a review. In: Setzer M.(Eds.), Pore Solution in Hardened Cement Paste. Aedificatio Publishers, Freiburg, 271-304

[48] Gérard B., Le Bellego C., Bernard O., 2002. Simplified modelling of calcium leaching of concrete in various environments. Materials and Structures 35, 632–640

[49] Guillon E., Moranville M, Kamali S., 2006. Characterization of the mechanical damage of a chemically degraded cement paste. Materials and Structures 39, 401–409

[50] Gurson A.L, 1977. Continnum theory of ductile rupture by void nucleation and growth: part 1-yield criterion and flow rules for porous ductile media. Transactions of the ASME 99, 2-15

[51] Haga K., Sutou S., Hironaga M., Tanaka S., Nagasaki S., Cement and Concrete Research 35 , 1764–1775

[52] Hayakawa K. and M urakami S., 1997. Thermodynamical modelling of elastic-plastic damage and experimental validation of damage potential. Int J. Damage Mechanics 6, 333-363

[53] Heukamp F., Ulm F.-J., Germaine J. , 2001A. Mechanical properties of calcium leached cement paste: triaxial stress states and the influence of pore pressure. Cement and Concrete Research 31, 767-774

[54] Heukamp F., Mainguy M., Ulm F,-J., 2001b. Beyond the crack size criterion: the effect of a fracture on calcium leaching depletion of cementitous materials. In: de Borst R., Mazar J., Pijaudier-Cabot G., van Mier J. (Eds.), Fracture Mechanics of Concrete Structures. Balkema Publishers, Lisse, 215-221

[55] Heukamp F.H, Ulm F.-J, Germaine J.T, 2003. Poroplastic properties of calcium-leached cement-based materials. Cement and Concrete Research 33, 1155–1173

[56] Heukamp F., 2003. Chemomechanics of calcium leaching of cement-based materials at different scales : the role of CH-dissolution and C-S-H degradation on strength and durability performance of materials and structures, PhD. Thesis. Department of Civil and Environmental Engineering, Massachusetts Institute of Technology

[57] Hohberga I., de Grootb G.J., van der Veenc A.M.H., Wassing W., 2000. Development of a leaching protocol for concrete. Waste Management 20, 177-184

[58] Homand S. and Shao J.F., 2000. Mechanical behavior of a porous chalk and water/chalk interaction, Part I: Experimental study. Oil & Gas Science and Technology 55, 591-598

[59] Hueckel T., 1997. Chemo-Plasticity of clay subjected to stress and flow of a single contaminant. International Journal for Numerical and Analytical Methods in Geomechanics 21, 43-72

[60] Hill R., 1958. A general theory of uniqueness and stability in elastic-plastic solids. J. Mech.

Phys. Solids 6, 239-249

[61] Imran I., 1994. Applications of non-associated plasticity in modelling the mechanical response of concrete. PhD. Thesis, Department of Civil Engineering, University of Toronto, Canada

[62] Israel D., Macphee D.E., Lachowski E. E., 1997. Acid attack on pore-reduced cements. Journal of Materials Science 32, 4109-4116

[63] Jia Y., 2006. Contribution à la modélisation thermo-hydro-mécanique des roches partiallement saturées: application au stockage des déchets radioactifs. Thèse d'Etat, Université de Lille 1

[64] Ju J. W ., 1989 . On energy based coupled elastoplastic damage theories : constitutive modeling and computational aspects. Int. J. Solids Structures 25(7), 803-833

[65] Kamali S., Gérard B., Moranville M., 2003. Modelling the leaching kinetics of cement-based materials—influence of materials and environment. Cement & Concrete Composites 25, 451–458

[66] Kearsley E. P. and. Wainwright P. J, 2001. Porosity and permeability of foamed concrete. Cement and Concrete Research 31, 805-812

[67] Khazraei R., 1996. Experimental study and modelling of damage in brittle rocks. Doctoral Thesis, University of Lille

[68] Krajcinovic D., 1996. Damage Mechanics. Elsevier Science, Amsterdam

[69] Kuhl D., Bangert F., Mescheke G., 2000. An extension of damage theory to coupled chemo-mechanical processes. European Congress on Computional Methods in Applied Science and Engineering ECCOMAS 2000, Barcelona, 11-14 September 2000

[70] Kuhl D., Bangert F., Mescheke G., 2004. Coupled chemo-mechanical deterioration of cementitious materials, Part Ⅰ: Modeling. International Journal of Solids and Structures 41, 15-40

[71] Kuhl D., Bangert F., Mescheke G., 2004. Coupled chemo-mechanical deterioration of cementitious materials, Part Ⅱ: Numerical methods and simulations. International Journal of Solids and Structures 41, 41-67

[72] Le Bellégo C., Gérard B., and Pijaudier-Cabot G., 2000. Chemo-mechanical effects in mortar beams subjected to water hydrolysis. Journal of Engineering Mechanics 3, 266-272

[73] Le Bellégo C., Gérard B., Pijaudier-Cabot G., 2001a. Mechanical analysis of concrete structures submitted to aggressive water attack. In: de Borst R., Mazar J., Pijaudier-Cabot G., van Mier J.(Eds.), Fracture Mechanics of Concrete Structure. Balkema Publishers, Liser, 239-246

[74] Le Bellégo C., Gérard B., Pijaudier-Cabot G., Dubé J.-F., Molez L. 2003. Coupled mechanical and chemical damage in calcium leached cementitious structures. Journal of Engineering Mechanics, 129(3), 333-341

[75] Leblond J.B. and Perrin G., 1996. Introduction à la mécanique de la rupture ductile des

métaux. Lecture notes (in French), Ecole Polytechnique, Paris

[76] Lemaitre J., Chaboche J.L., 1990. Mechanics of solid materials. Cambridge University Press, Cambridge, U.K

[77] Li N., Zhu Y.M., Su B. and Gunter S., 2003. A chemical damage model of sandstone in acid solution. International Journal of Rock Mechanics and Mining Sciences 40, 243-249

[78] Liu Z. Boukpeti N., Li X., Collin F., Radu J.-P., Heuckel T. and Charlier R. , 2005. Modelling chemo-hydro-mechanical behaviour of unsaturated clays: a feasibility study. International Journal of Numerical and Analytical Methods in Geomechanics 29, 919-940

[79] Lubarda V.A and Krajcinovic D., 1995. Some fundamental issues in rate theory of damaged elastoplasticity. Int. J. of Plasticity 11(7), 763-798

[80] Lydzba D. and Shao J.F., 1999, Study of poroelasticity material coefficients as response of microstructure, Mechanics of Cohesive-Frictional Material 5, 149-171

[81] Lydzba D. and Shao J.F., 1999. Study of poroelasticity material coefficients as response of microstructure. Mechanics of Cohesive-Frictional Material, 5(2), 149-171

[82] Lydaba D. and Shao J.F., 2002, Stress equivalence principle for saturated porous media, C.R. Mécanique 330, 297-303

[83] Lydzba D. and Shao J.F., 2002. Stress equivalence principle for saturated porous media. C.R. Mécanique 330, 297-303

[84] Mahboubi A. and Ajorloo A., 2005. Experimental study of the mechanical behavior of plastic concrete in triaxial compression. Cement and Concrete Research, Volume 35, Issue 2, :412-419

[85] Mainguy M., 1999. Modèle de diffusion non-linéaires en milieux. Applications à la dissolution et au séchage des matériaux cimentaires. Ph.D. thesis, L'Ecole Nationale des Ponts et Chaussées

[86] Mainguy M. Tognazzi C. Torrenti J.M., Adenot F., 2000. Modelling of leaching in pure cement paste and mortar. Cement and Concrete Research 30, 83-90

[87] Mainguy M., Coussy O., 2000. Propagation fronts during calcium leaching and chloride penetration. Journal of Engineering Mechanics 126, 250-257

[88] Mainguy M., Ulm F.-J., 2000. Coupled diffusion-dissolution around a fracture channel: the solute congestion phenomenon. International Journal for Transport in Porous Media 6, 1-19

[89] Mainguy M., Ulm F. -J. and Heukamp F. H., 2001. Similarity properties of demineralization and degradation of cracked porous materials. International Journal of Solids and Structures 38, 7079-7100

[90] Marchand J., Bentz D.P., Samson E. and Maltais Y., 2000. Influence of Calcium Hydroxide Dissolution on the Transport Properties of Hydrated Cement Systems. Materials Science of Concrete, 113-129

[91] Mohamad-Hussein A. and Shao J.F., 2007. Modelling of elastoplastic behaviour with non local damage in concrete under compression. Computers and Structures 85(23-24),

1757-1768

[92] Mura, T., 1987. Micromechanics of defects in solids, 2nd edition. Martinus Nijhoff Publ., The Hague, Boston.

[93] Nguyen V.H., Colina H., Torrenti J.M.,., Boulay C., Nedjar B., 2007. Chemo-mechanical coupling behaviour of leached concrete. Nuclear Engineering and Design, doi:10.1016 /j.nucengdes.2007.02.013

[94] Nemat-Nasser, S., Hori, M., 1993. Micromechanics: overall properties of heterogeneous materials. North-Holland, Amsterdam, The Netherlands.

[95] Neville A.M., 1995. Properties of Concrete, 4th Edition, Longman Group Limited, Essex, England.

[96] Paterson, M. S., 1978. Experimental Rock Deformation -- The Brittle Field. Springer-Verlag, Berlin.

[97] Perlot C., Verdier J., Carcassès M., 2006. Influence of cement type on transport properties and chemical degradation: Application to nuclear waste storage. Materials and Structures 39, 511-523

[98] Perrin G. and Leblond J. B., 1990. Analytical study of a hollow sphere made of plastic porous material and subjected to hydrostatic tension-application to some problems in ductile fracture of metals. International Journal of Plasticity 6, pp. 677-699.

[99] Perrin G. and Leblond J.B., 2000. Accelerated void growth in porous ductile solids containing two populations of cavities. International Journal of Plasticity 16, 91-120

[100] Pietruseczak S., Jiang J. and Mirza F.A., 1988. An elastoplastic constitutive model for concrete. Int. J. Solid and Structures 24(7), 705-722

[101] Pietruszczak S., Lydzba D. and Shao J. F., 2006. Modelling of deformation response and chemo–mechanical coupling in chalk. Int. J. Numer. Anal. Meth. Geomech, 30:997–1018

[102] Pihlajavaara S.E. 1974. A review of some of the main results of a research on the ageing phenomena of concrete, effect of moisture conditions on strength, shrinkage and creep of mature concrete. Cement and Concrete Research, 4, pp. 761-771.

[103] Pijaudier-Cabot G., Gérard B., Molez L., 1998a. Damage mechanics of concrete structures subjected to mechanical and environmental actions. In: de Borst R., Bicanic N., Mang H., Meschke G.(Eds.), Computational Modelling of Concrete Structures. Balkema, Rotterdam, 559-566

[104] Pijaudier-Cabot G., Gérard B., Burlion N., Molez L., 1998b. Localisation of damage in quasi-brittle materials and influence of chemically activated damage. In: de Borst R., van de Giessen E.(Eds.), Material Instabilities in Solids. John Wiley & Sons, Chicester, 441-456

[105] Rothwell M., Anstice H. M. and Pearson G. J., 1998. The uptake and release of fluoride by ion-leaching cements after exposure to toothpaste. Journal of Dentistry 26, 591-597

[106] Sakr K., Sayed M.S., and Hafez N., 1997. Comparison studies between cement and cement-kaolinite properties for incorporation of low-level radioactive wastes. Cement and

Concrete Research 27, 1919-1926

[107] Salari M.R., Saeb S., William K.J., Patchet S.J., Carrasco R.C., 2004. A coupled elastoplastic damage model for geomaterials.

[108] Schlangen E., van Mier J.G.M., 1992. Experimental and numerical analysis of micromechanisms of fracture of cement-based composites. Cement & Concrete Composites 14 , pp. 105-118

[109] Shao J. F., 1987. Etude du comportement d'une craie blanche très poreuse et modélisation. Thèse de doctorat, Université de Lille 1

[110] Shao J.F., Giraud A., 2002. Comportement poromécanique des roche saturées. Lois incrémentales viscoplasticité et endommagement, Modèle de comportement des sols et des roches. Hermes Editions, 175-201

[111] Shao J.F., Jia Y., Kondo D., Chiarelli A.S., 2006. A coupled elastoplastic damage model for semi-brittle materials and extension to unsaturated conditions. Mechanics of Materials 38, 218-232

[112] Singh U.K., Digby P.J., 1989a. A continuum damage model in the progressive failure of brittle rocks. Int. J. Solids Struct. 25, 647-663

[113] Siruguet K. and Leblond J.B., 2004. Effect of void locking by inclusions upon the plastic behavior of porous ductile solids—I: theoretical modeling and numerical study of void growth. International Journal of Plasticity 20, pp. 225-254.

[114] Siruguet K. and Leblond J.B., 2004. Effect of void locking by inclusions upon the plastic behavior of porous ductile solids—part II: theoretical modeling and numerical study of void coalescence. International Journal of Plasticity 20, pp. 255-268.

[115] Terrien M., 1980. Emission acoustique et comportement mécanique post-critique d'un béton sollicité en traction. Bulletin de liaison de Pont et Chaussées, 105, pp. 65-72.

[116] Tognazzi C., 1998. Couplages fissuration – dégradation chimique dans les matériaux cimentaires: caractérisation. Thèse de doctorat de l'INSA de Toulouse.

[117] Torrenti J.-M., Mainguy M., Adenot F., Tognazzi C., 1998. Modelling of leaching in concrete. In: de Borst R., Bicanic N., Mang H., Meschke G.(Eds.), Computational Modelling of Concrete Structure. Balkema, Rotterdam, 559-566

[118] Ulm F.-J., Torrenti J.-M, Adenot F., 1999. Chemoporoplasticity of calcium leaching in concrete. Journal of Engineering Mechanics 125, 1200-1211

[119] Ulm F.-J., Rossi P., Schaller I., and Chauvel D., 1999. Durability scaling of cracking in hpc structures subject to hygromechanical gradients. Journal of Structural Engineering 6, 693-702

[120] Ulm F.-J., Coussy O., Li K.F. and Catherine L., 2000. Thermo-chemo-mechanics of ASR expansion in concrete structures. Journal of Engineering Mechanics 3, 233-242

[121] Ulm F.-J., Heukamp F., Germaine J., 2001. Durability mechanics of calcium leaching in concrete and beyond. In: de Borst R., Mazars J., Pijaudier-Cabot G., van Mier J.(Eds.),

Fracture Mechanics of Concrete Structures. Balkma Publishers, Lisse, 133-143

[122] Ulm F.-J., Lemarchand E., Heukamp H.F, 2003. Elements of chemomechanics of calcium leaching of cement-based materials at different scales. Engineering Fracture Mechanics 70, 871–889

[123] Wang K.J, Nelsen D.E. and Nixon W.A., 2006. Damaging effects of deicing chemicals on concrete materials. Cement & Concrete Composites 28, 173–188

[124] Wawersik W.R., Fairhurst C., 1970. A study of brittle rock fracture in laboratory compression experiments. Int. J. Rock Mech. Min. Sci. 7, 561-575

[125] Xie S.Y., 2005. Contribution à l'étude du comportement mécanique d'une roche poreuse. Thèse d'Etat, Université de Lille 1

[126] Yokozeki K., Watanabe K., Sakata N., Otsuki N., 2004. Modeling of leaching from cementitious materials used in underground environment. Applied Clay Science 26, 293–308

[127] Yurtdas I., Xie S., Secq J., Burlion N., Shao J.-F., Sibai M., 2006. Etude expérimentale du couplage entre le comportement thermo-hydro-mécanique et la dégradation chimique d'une pâte de ciment pétrolière. Rapport (LML-MGC-03-03/A) pour TOTAL

[128] Zhang, J., Liu, Q., 2003. Determination of concrete fracture parameters from a three-point bending test. Tsinghua Science and Technology 8 (6), pp. 726-733.

[129] Zohdi T.I., Kachanov M., Sevostianov I., 2002. On the perfectly plastic flow in porous material. International Journal of Plasticity 18, 1649-1659